UNIVERSITY OF CRETE

DEPARTMENT OF MATERIALS SCIENCE AND TECHNOLOGY

SYNTHESIS AND CHARACTERIZATION OF HYPERBRANCHED POLYMERS OF 2-(DIMETHYLAMINO)ETHYL METHACRYLATE VIA SELF CONDENSING VINYL COPOLYMERIZATION

MASTER THESIS

PANAGIOTIS G. FALIREAS

FOUNDATION FOR RESEARCH AND TECHNOLOGY

INSTITUTE OF ELECTRONIC STRUCTURE AND LASER

POLYMER GROUP

HERAKLION, MAY 2010

ΠΑΝΕΠΙΣΤΗΜΙΟ ΚΡΗΤΗΣ

ΤΜΗΜΑ ΕΠΙΣΤΗΜΗΣ ΚΑΙ ΤΕΧΝΟΛΟΓΙΑΣ ΥΛΙΚΩΝ

ΣΥΝΘΕΣΗ ΚΑΙ ΧΑΡΑΚΤΗΡΙΣΜΟΣ ΥΠΕΡΔΙΑΚΛΑΔΙΣΜΕΝΩΝ ΠΟΛΥΜΕΡΩΝ ΜΕΘΑΚΡΥΛΙΚΟΥ (2-ΔΙΜΑΙΘΥΛΟΑΜΙΝΟ)ΑΙΘΥΛΕΣΤΕΡΑ ΜΕΣΩ ΒΙΝΥΛΙΚΟΥ ΠΟΛΥΜΕΡΙΣΜΟΥ ΑΥΤΟΣΥΜΠΥΚΝΩΣΗΣ

ΜΕΤΑΠΤΥΧΙΑΚΗ ΕΡΓΑΣΙΑ

ΠΑΝΑΓΙΩΤΗΣ ΦΑΛΗΡΕΑΣ

ΙΔΡΥΜΑ ΤΕΧΝΟΛΟΓΙΑΣ ΚΑΙ ΕΡΕΥΝΑΣ

ΙΝΣΤΙΤΟΥΤΟ ΗΛΕΚΤΡΟΝΙΑΚΗΣ ΔΟΜΗΣ ΚΑΙ LASER

ΤΜΗΜΑ ΠΟΛΥΜΕΡΩΝ

ΗΡΑΚΛΕΙΟ, ΜΑΙΟΣ 2010

Abstract

We report the synthesis of randomly branched (arborescent) ionizable polymers by self – condensing vinyl copolymerization (SCVCP) of an acrylic inimer 2-(2-methyl-1-triethylsiloxy-1-propenyloxy)ethyl methacrylate (MTSHEMA) with 2-(dimethylamino)ethyl methacrylate (DMAEMA) via group transfer polymerization (GTP). The influence of the comonomer ratio, γ=[DMAEMA]/[MTSHEMA] and the monomer concentration in the polymerization on the polymer characteristic were investigated. In addition, we prepared hyperbranched polymers of a lower degree of branching by the slow addition of the comonomer mixture (inimer and monomer) to a monofunctional GTP initiator, 1-methoxy-1-(trimethylsilyloxy)-2-methyl-1-propene (MTS). Finally the addition of 2-(trimethylsilyloxy)ethyl methacrylate (TMSHEMA) to living PDMAEMA hyperbranched precursors core yielded "hyperstar" polymers comprising a hyperbranched core and linear polymer chains in the shell.

The absolute molecular weights of the polymers were measured by GPC equipped with a refractive index, a viscosity and a low angle laser light scattering detectors. Depending on the comonomer ratio, γ=[DMAEMA]/[MTSHEMA], and the monomer concentration in the polymerization hyperbranched PDMAEMAs and hyperstar polymers with number-average molecular weights between 6,000 and 650,000 $gmol^{-1}$ were obtained. The addition of a monofunctional initiator in the polymerization led to a considerable narrowing of the molecular weight distribution of the polymers, in particular for high MTS contents. The Mark-Houwink exponents of these hyperbranched polymers were significantly lower ($0.2 < \alpha < 0.5$) compared to that of a linear PDMAEMA ($\alpha = 0.6$) thus verifying the branched polymer structure. ^{1}H NMR spectroscopy indicated that very high comonomer conversions were obtained in most cases, however it could not be used to calculate the degree of branching of these polymers. The hydrodynamic size of the hyperbranched polymers in organic solvents were determined by dynamic light scattering while capillary viscosity measurements were used to calculate their intrinsic viscosities in organic media. The pH and temperature responsive behavior of the hyperbranched PDMAEMAs in aqueous solution were investigated by potentiometric titrations and dynamic light scattering respectively. Finally, melt rheology measurements were carried out in order to investigate the rheological response of the polymers. Dynamic

spectra revealed that the hyperbranched polymers are not entangled and follow a dynamic scaling based on a Rouse-like behaviour.

Περίληψη

Στη παρούσα εργασία πραγματοποιήθηκε η σύνθεση τυχαίων διακλαδισμένων (δενδροειδών) πολυμερών με τη μέθοδο του βινυλικού συμπολυμερισμού αυτοσυμπύκνωσης (SCVCP) του ακρυλικού μονομερούς-εκκινητή μεθακρυλικού 2 -(2-μέθυλο-1-τριέθυλοσιλοξυ-1-προπενυλόξυ) αιθυλεστέρα (MTSHEMA) και του μεθακρυλικού (2-διμεθυλοάμινο) αιθυλεστέρα (DMAEMA) μέσω πολυμερισμού μεταφοράς ομάδας (GTP). Μελετήθηκε η επίδραση του λόγου του μονομερούς προς το μονομερές-εκκινητή γ=[DMAEMA]/[MTSHEMA] καθώς και η συγκέντρωση του μονομερούς στο πολυμερισμό στα χαρακτηριστικά του πολυμερούς. Επιπλέον, συντέθηκαν υπερδιακλαδιζόμενα πολυμερή χαμηλότερου βαθμού διακλάδωσης υπό την αργή προσθήκη μίγματος μονομερούς-εκκινητή και μονομερούς σε μονοδραστικό GTP εκκινητή, 1-μεθοξυ-1-τριμεθυλοσιλοξυ-2-μεθυλο-1-προπένιο (MTS). Τέλος, η προσθήκη του μεθακρυλικού 2-(τριμέθυλοσιλοξύ) αιθυλεστέρα (TMSHEMA) σε υπεραδιακλαδισμένο ζωντανό πρόδρομο PDMAEMA πυρήνα απέδωσε υπεραδικλαδισμένα πολυμερή αστεροειδούς μορφής (hyperstars) τα οποία αποτελούνται από ένα διακλαδισμένο πυρήνα και γραμμικές αλυσίδες του πολυμερούς στο εξωτερικό περίβλημα.

Τα απόλυτα μοριακά βάρη των πολυμερών μετρήθηκαν με χρωματογραφία αποκλεισμού μεγεθών (GPC). Ανάλογα με το λόγο γ καθώς και τη συγκέντρωση του μονομερούς στο πολυμερισμό τα μέσα κατά αριθμό απόλυτα μοριακά βάρη των υπερδιακλαδισμένων πολυμερών PDMAEMAs και πολυμερών hyperstar υπολογίστηκαν μεταξύ 6.000 και 650.000 $gmol^{-1}$. Η προσθήκη ενός μονοδραστικού εκκινητή κατά τον πολυμερισμό οδήγησε σε σημαντική μείωση της κατανομής του μοριακού βάρους των πολυμερών, ιδιαίτερα για υψηλές συγκεντρώσεις MTS. Οι εκθέτες Mark-Houwink των υπερδιακλαδισμένων πολυμερών υπολογίστηκαν χαμηλότεροι ($0,2 < \alpha < 0,5$) συγκριτικά με αυτή ενός γραμμικού πολυμερούς PDMAEMA ($\alpha = 0,6$) επιβεβαιώνοντας της διακλαδισμένη δομή αυτών των πολυμερών. Με τη χρήση φασματοσκοπίας ^1H NMR, υπολογίστηκαν υψηλές αποδόσεις πολυμερισμού στις περισσότερες περιπτώσεις ωστόσο δεν ήταν δυνατός ο υπολογισμός του βαθμού διακλάδωσης μέσω αυτής της τεχνικής. Το υδροδυναμικό μέγεθος των υπερδιακλαδισμένων πολυμερών σε οργανικούς διαλύτες καθορίστηκαν με δυναμική σκέδαση φωτός, ενώ μετρήσεις ιξωδομετρίας χρησιμοποιήθηκαν για τον

υπολογισμό του εσωτερικού ιξώδους σε οργανικούς διαλύτες. Η εξάρτησης της συμπεριφοράς από το pH και τη θερμοκρασία των υπερδιακλαδισμένων PDMAEMAs σε υδατικό διάλυμα, ερευνήθηκαν με ποτενσιομετρική τιτλοδότηση και δυναμική σκέδαση φωτός αντίστοιχα. Τέλος, μετρήσεις ρεολογίας πραγματοποιήθηκαν προκειμένου να διερευνηθεί η ρεολογική απόκριση των πολυμερών. Τα αποτελέσματα των μετρήσεων έδειξαν την απουσία εναγκαλιασμών και ακολουθούν τη συμπεριφορά Rouse.

Contents

page

Chapter 1

Introduction

In the past decade the field of arborescent polymers has attracted particular attention using a large variety of synthetic approaches for their preparation, while the fundamental studies on structure and properties of these unique materials and their possible applications has been reported [1-4]. The development of various controlled/living polymerization techniques provided the possibility to synthesize a wide variety of these architectures, e.g. stars, brush-like chains, centipedes, dendritic (hyperbranched and arborescent) structures, self-assembling block copolymers and supramolecular structures. A branched polymer comprises of more than one backbone chains; that is, it is a nonlinear polymer [5] and it is characterized by the presence of branch points (junction points), atoms or small groups from which more than two long chains emanate) and by the presence of more than two chain-end groups. The interest in branched polymers arose from the fact that branching in polymers is a useful structural variable that can be used advantageously to modify the processing characteristics and properties of polymers such as crystallinity, melting point, physical properties, viscoelastic properties, solution and melt viscosities [6, 7].

1.1 Highly branched polymers

1.1.1 Hyperbranched polymers

Hyperbranched polymers (HBPs) (**Figure 1a**) are defined as polymer systems containing a large number of branching points connected by relatively short polymer chains in their molecular structure [8]. Their structure is not uniform (as in the case of dendritic polymers discussed below) and the individual molecules can have different molecular weights and degrees of branching. Due to their usual broad molecular weight distribution and to the occasionally occurring side reactions during their synthesis, such polymers are complex product mixtures of non regular molecular structures. On the other hand, they exhibit a lower viscosity in bulk and in solution

compared to their linear analogues of similar molecular weight (a property also typical for dendrimers). HBPs can be prepared in one-step or in several reaction steps. In some applications, HBPs replace dendrimers, because of their similar properties combined with a much lower price. The large number of functional end-groups offers the possibility for further modification of the HBPs which can be attractive for certain applications.

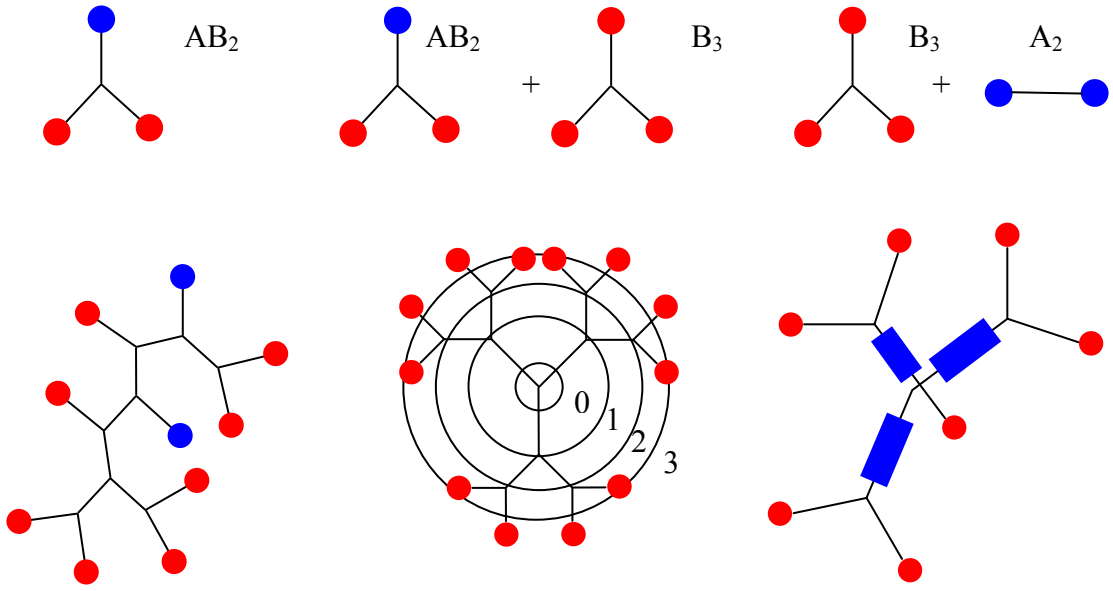

a) Hyperbranched polymer b) Dendrimer c) Highly branched

Figure 1. Schematic representation of hyperbranched (a), dendrimer (b), and highly - branched (c) polymers.

1.1.2 Dendrimers

Dendrimers (**Figure 1,b**) are similar to HBPs, but they possess a strictly regular branched structure [9, 10], so that they are sometimes referred to as structurally perfect hyperbranched polymers. Dendrimers have a high concentration of functional end-groups on their surface for a given molecular weight and volume. They are often prepared by a step-by-step reaction during which subsequent monomer layers, called generations, are attached to the surface functional groups, often using the protection-deprotection technique. The core molecule is referred to as “generation

0". Each successive repeat unit along all branches forms the next generation until the terminating generation.

1.1.3 Highly branched functional polymers

A third type of branched polymers similar to those described earlier, are highly branched functional polymers (**Figure 1c**). They are formed from A_{fA} and B_{fB} monomers where f_A and f_B denote the functionalities [8]. For alternating reaction (A+B →AB) in A_{fA} + B_{fB} systems, the reaction under stoichiometric conditions leads to gelation [11]. To avoid gelation it is possible to stop the polymerization by precipitation or to deactivate one of the two types of functional groups before reaching the critical gelation point. Alternatively, off-stoichiometric systems can be used. For this type of reactions, the critical molar ratio (CMR) to avoid gelation should be calculated or determined experimentally. The value of CMR depends mostly on the functionality of the components, but also on the reactivity of the functional groups, which are involved in bond formation. Comparing this synthesis with the classical polycondensation reaction of an AB_f monomer, it was found that the structure of the HBPs prepared by both methods are similar. The advantages of the B_3 + A_2 system are the lower price of the initial materials (reagents) and the wide range of accessible architecture of the end groups.

1.2 Synthetic approaches to hyperbranched polymers

The synthetic routes used for the preparation of the HBPs can be divided into two groups:

The first group includes single monomer reactions, (i.e.: the polycondensation of AB_f monomer or AB_f monomer plus core monomer, self-condensing vinyl polymerizations, ring opening reactions and addition reactions).

The second group involves the reaction of two monomers. This category includes the classical reaction of A_{fA} with B_{fB}, which in the case of an extreme difference in the group reactivities leads to the in situ formation of an AB_2 intermediate which further polymerizes to form the HBP. In that special case, the classical hyperbranched polymers "cross" with highly-branched off stoichiometric

polymers, however, with some distinct differences in structure development during the formation process.

1.2.1 Polycondensation of AB_f monomers

The most common route for the synthesis of HBPs is the polycondensation of AB_f monomers, which involves the typical features of a step growth reaction of multifunctional monomers and of the formed oligomers, but without the possibility of crosslinking (and hence gelation). As a result, hyperbranched molecules are obtained, which contain one focal group (A group), and dendritic, linear and terminal units (depending on the reactivity of the "A" group).

Through polycondensation of AB_f monomers, hyperbranched polyesters, polyureas, polycarbosilanes, polyamides, and polyethers have been successfully synthesized, [12, 13]. AB_2, AB_3 [14], AB_4, AB_5, and even AB_6 [15] monomers have been used to synthesize hyperbranched polymers. However, AB_2 monomers dominate in the synthetic approaches to hyperbranched products and the structural variety of these polymers is very broad. Among the AB_2 based polymers, polyester structures are favoured due to the availability of suitable monomers.

During the syntheses of HBPs, side reactions and intramolecular reactions such as cyclization are often observed. It was found [16] that cyclization reactions, which reduce the polymer molecular weight and molecular weight distribution, depend strongly on the monomer structure.

1.2.2 Self – condensing ring-opening polymerization

This method was proposed by Suzuki in 1992 [17] and is known as "multi-branching" polymerization. Branching units are generated during the ring opening reaction, while the starting AB monomers do not contain branching points. The polymerization is initiated by the addition of an appropriate initiator to generate active sites, which may allow for control over the molecular weight and molecular weight distribution of the resulting polymers. By this synthetic approach, hyperbranched etheramides [18], oxetanes [19, 20] and lactones [21] have been reported in the literature. These examples demonstate the trend in the synthesis of HBPs towards the exploration of new reaction types and the integration of chain growth mechanisms.

Reasons for this are the strive for better control on the structure and the polydispersity of HBPs.

1.2.3 Self – condensing vinyl polymerization (SCVP)

Frechét and coworkers proposed in 1995 a new method for the synthesis of HBPs from vinyl monomers known as "self – condensing vinyl polymerization" (SCVP) [22]. This reaction involves the use of a vinyl initiator-monomer (later called "inimer") of AB* type, in which A is a vinyl group and B* is a group capable of initiating the polymerization of the vinyl groups. **Figure 2a** shows the initial steps in SCVP. In order to initiate the polymerization, the B* group is activated. Upon activation of the B* groups, the polymerization starts by the addition of the B* group to the double bond of another AB* inimer, resulting in the formation of a dimer, A-b-A*B*. The asterisk indicates that a structural group can add monomer; it can be either in its active or dormant form. Lowercase letters indicate that the group has been consumed and can no longer participate in the polymerization. The resulting dimer has two active sites A* (propagating) and B* (initiating), for possible chain growth besides the vinyl group. Addition of a third monomer unit at either site results in the formation of the trimer which can now grow in the three directions.

The addition of a conventional monomer M to the polymerization leads to highly branched polymers allowing a better control of the molecular weight distribution and the degree of branching. The self-condensing vinyl copolymerization (SCVCP) method is a facile approach to obtain functional branched polymers, because different types of functional groups can be incorporated into a polymer, depending on the chemical nature of the comonomers. In addition, the chain architecture can be easily modified by a suitable choice of the comonomer ratio in the feed. Because the number of linear units is higher, the degree of branching of the copolymers is lower than that of SCVP homopolymers. SCVCP can be initiated in two ways (**Figure 2b**). First by the addition of the active B* group of an AB* inimer to the vinyl group A of another AB* inimer forming a dimer with two active sites, A* and B*. Second, by the addition of a B* group to the vinyl group of monomer M forming a dimer with one active site, M*. Both the initiating B* group and the newly created propagating centres A* and M* can react with a vinyl group in the system. Thus we have three different types of active centers, A*, B* and M* in the dimer,

which can react with double bonds A (inimer and macromolecules; each macromolecule contains strictly one double bond) and monomer M. SCVP has been applied to various types of living polymerization methods i.e. cationic [1, 23, 24], ATRP [25-27], nitroxide-mediated radical polymerization [24], ring opening polymerization [17] and also group transfer polymerization [28]. The latest polymerization technique combined with SCVP was used for the synthesis of the HBPs in the present study.

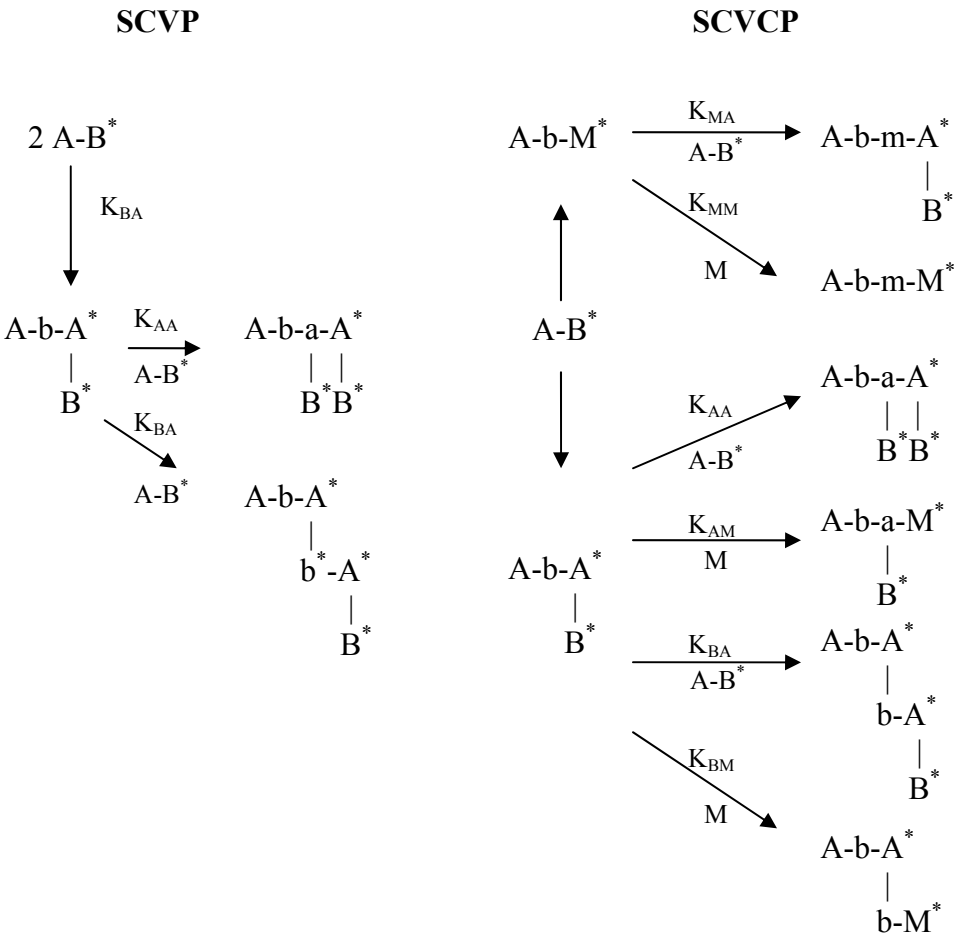

Figure 2. Initial steps in SCVP and SCVCP. Capital letters indicate vinyl groups (A and M) and active centers (A*, B*, M*), while lowercase letters represent the reacted groups (a, b and m)

1.2.3.1 Group transfer polymerization

Group transfer polymerization (GTP) was discovered in 1983 by Webster and co-workers in the research laboratories of DuPont as a versatile method for the synthesis of functional (meth)acrylic polymers [29-34]. It employs a silyl ketene acetal initator for the "living" polymerization of a variety of alkylated methacrylates. Initiation involves the Michael-type addition of the monomer to the silyl ketene acetal initator. The monomer adduct thus formed, adds rapidly more monomer in a repetitive Michael-type addition process to afford the desired polymer. The term GTP was adopted to indicate that the silyl group of the silyl ketene acetal initiator system has been transferred to the terminal moiety of the propagating polymer and subsequently to the monomer that is undergoing addition. Each transfer of the silyl group to the monomer regenerates a silyl ketene acetal group at the end of the propagating chain. Silyl ketene acetals are relatively stable species and require activation by a catalyst in order to initiate the polymerization of α, β-unsaturated monomers. Numerous catalysts for GTP polymerizations have been examined and these studies have revealed that bifluorides and bioxyanions such as tris(dimethylamino) sulfonium bifluoride ($TASHF_2$) and tetra-*n*-butyl ammonium bibenzoate (TBABB), respectively, afford optimum polymerization characteristics. The polymerization mechanism has been extensively investigated and, to date, a definitive mechanism is yet to receive universal acceptance. Several mechanisms have been proposed to rationalize the polymerization characteristics, including associative and dissosiative pathways.

In the dissociative route (**Figure 3**) the nucleophilic catalyst complexes with the silyl ketene acetal end group and in a reversible cleavage step generates a reactive enolate anion that adds monomer.

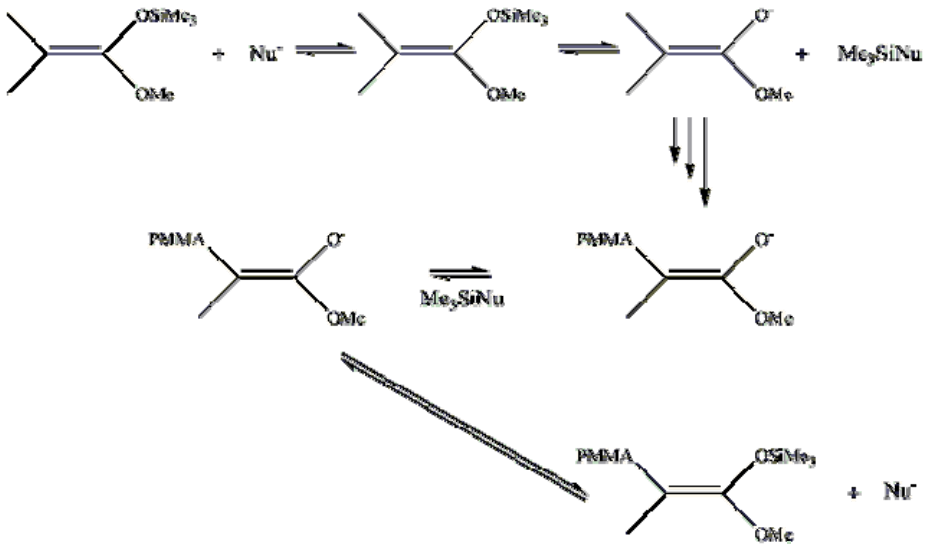

Figure 3. Dissociative process of GTP

The enolate end groups are then capped by R_3SiNu to regenerate the silyl ketene acetal ends. Since controlled polymer molecular weights and narrow molecular weights distribution are obtained at low catalyst concentrations, the equilibrium generating the enolate chain ends must be much faster compared to the rate of polymerization

In the associative mechanism (**Figure 4**) the silyl ketene acetal group is activated by complexation with the catalyst for the addition to monomer. The silyl group transfers to the incoming monomer and remains on the same polymer chain during the polymerization. The well-documented silyl end-group exchange would be occurring by some unknown process. The equilibrium rate for the catalyst complex formation must be fast to ensure control over the macromolecular characteristics.

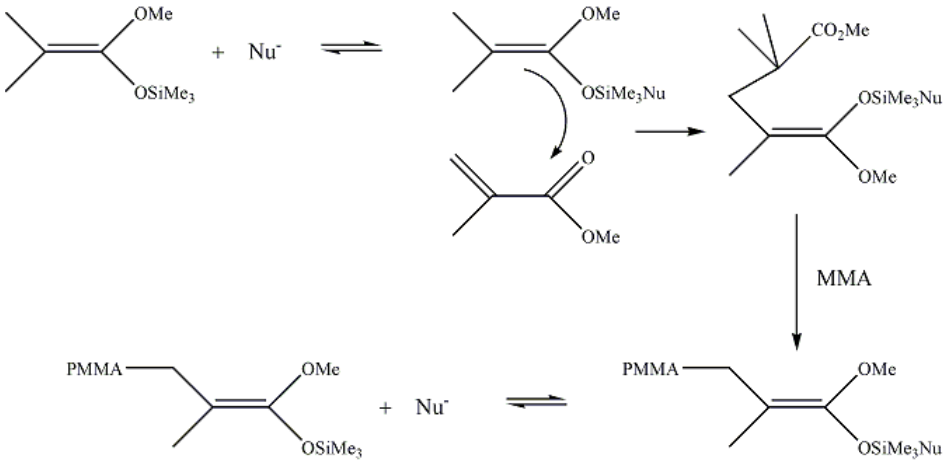

Figure 4. Associative process of GTP

GTP has been shown to be robust and compatible with numerous α,β-unsaturated monomers including acrylates, ketones, lactones, and polyunsaturated esters such as ethyl sorbate. In addition, GTP is suitable for use in a wide range of reaction solvents of varying polarity. Finally, although GTP demonstrates the fundamental characteristics of a "living" polymerization, namely narrow molecular weight distribution ($M_w/M_n < 1.1$), control over the polymer molecular weight derived from the monomer/initiator stoichiometry, and the ability to construct block copolymers, the technique is not foolproof and is inhibited by the presence of moisture and inherent termination reactions such as isomerization and back-biting.

1.3 Applications of hyperbranched polymers

HBPs are attractive for many applications because of the low viscosity of their solutions and melts, in many cases also for their good solubility, the large number of functional groups and their good processability. Their high functionality could be sometimes a disadvantage, because it leads to fast gelation during the synthesis of crosslinked products. The HBPs are a cheap alternative to dendrimers for applications that necessitate high functionality, but do not require the high structural precision of dendrimers. The polarity and functionality of HBPs can be modified by partial substitution of the reactive groups. The most common applications of HBPs are shown in **Figure 5,** and some of them will be described below.

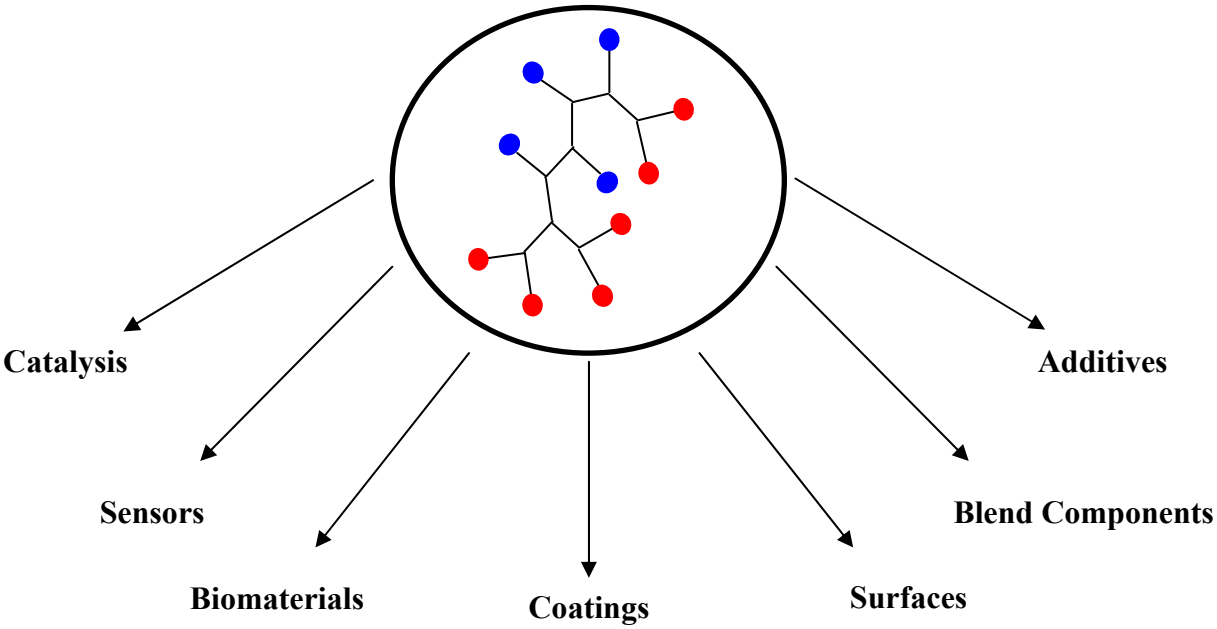

Figure 5. Applications of hyperbranched polymers.

1.3.1 HBPs in biomaterials

The perfectly branched dendrimers were applied in medicine as drug carrier molecules. Nowdays, they are partially replaced by well-defined hyperbranched polymers with multifunctional terminal groups. As carriers, hyperbranched macromolecules can offer their interior or peripheral functional groups to covalently fix bio-objects. Hyperbranched aromatic polyamides, synthesized by self condensation of AB_2 monomers or by polycondensation of reactant pairs are used as enzyme-supporting materials and have great potential to serve as supports for protein immobilization [35]. Suitable hyperbranched polymers can be also applied in medicine as biodegradable scaffolds [2].

1.3.2 HBPs in blends

HBPs can act as rheology control agents for polymers. Hyperbranched polyphenylene blended with linear polystyrene reduces the viscosity of the latter at higher temperatures and improves its thermal stability [36]. Another effect that was

observed was a change in the mechanical properties of polystyrene, an increase of its initial modulus after blending and was attributed to weak physical cross-linking of polystyrene through aryl–aryl interactions. Blends of hyperbranched polyesters with linear polymers such as polyesters, polyamides and polycarbonates were investigated [37], using a variety of functional HBPs bearing hydroxy and acetoxy (protected hydroxy) terminal groups. For comparative purposes, blends involving polyvinylphenol and polyacetoxystyrene instead of the hydroxyl and acetoxy functionalized HBPs were also studied. The results obtained for both the thermal and the phase behavior of these blends revealed, that the hydroxy-terminated hyperbranched polyesters exhibited similar characteristics to polyvinylphenol blended with linear polymers, such as bisphenol A polycarbonate and poly(butylene adipate). These results suggest that hydrogen bonding is the dominant factor in blends of this type rather than the polymer architecture of the additive.

1.3.3 HBPs as dispersants of actives

Hyperbranched polyesters or polyethers modified by alkyl chain termination of their functional groups show an amphiphilic character and can be used as carrier molecules for physically encapsulated organic molecules. For example, a modified hyperbranched polyester was used as a dye carrier in polyolefine blends [38]. The addition of the loaded HBP cause a homogenous distribution of the dye in the matrix and also a reduction in melt viscosity. The fact that alkyl modified hyperbrnached polyesters [39] or polyethers show amphiphilic character and can act as carrier molecules for physically enclosed organic molecules (for example, organic dyes) opens many news applications fields.

1.3.4 HBPs and surfaces

The modification of surfaces and thin polymer films dominates recent activities in the field of polymer science. Therefore HBPs have been studied lately on surfaces. This covers the field of the visualization of single dendritic macromolecules in order to obtain information on their shape and size [9, 40, 41], but also the use of dendrimers as carriers for metal ions [42], to change surface adhesion by dendrimer grafting [43] or studies on thin films (monolayers, self-assemblies) of dendrimers with

electrical, catalytic, or sensing properties [44]. The properties of random HBPs on surfaces have not been studied extensively, but it is expected to attract rapid attention in the near future. One example is the study of the surface morphology and friction of thin films of hyperbranched perfluorinated polymers as a function of the length of the perfluoroalkyl chains, by AFM [45]. Arborescent surface grafted poly(acrylic acid) has been also explored by Crooks [46] and Bergbreiter [47] for different applications. Their interest covers surface patterning, biocompatibility, ion binding ability, and sensing properties.

1.3.5 Other applications of HBPs

During the last years, experiments using HBPs as optical components have been described in the literature. Another area of intense investigation is the use of HBPs as a new class of ion-conducting materials. Hawker and coworkers were the first to synthesize hyperbranched poly(ether-esters) containing linear ethylene glycol units and tested them as novel electrolytes or ion-conducting elastomers. HBPs have been also studied as templating agents for nanoporosities in organosilicates. The investigated polymers were hyperbranched polyesters synthesised via the ring-opening polymerisation of an a-caprolactone derivative [48]. Hyperbranched polythiophenes [2] were described as light–harvesting molecules. A gradient of conjugation lengths exists in an enhanced single conjugated hyperbranched macromolecule, resulting in a light harvesting effect, and thus in enhanced light emission or in an intramolecular energy transfer from the less conjugated units to the longest conjugated fragments. The conjugation lengths increase upon increasing the molecular weight of the polymer. Finally, a modified hyperbranched polyester resin carrying hydroxyl functional groups was cross linked by UV light and was studied as a barrier against oxygen and water permeation [49]. The above examples show the potential of hyperbranched polymers for their broad use in many different technological fields.

1.4 The aim of this work

The aim of this work is the synthesis and characterization of functional HBPs polymers via SCVCP using 2-(dimethylamino)ethyl methacrylate (DMAEMA) as the

monomer. A series of HBPs were prepared by the combination of GTP and SCVP. First, the appropriate inimer (MTSHEMA) was synthesized and was used for the preparation of HBPs at different comonomer ratios γ ($\gamma=\frac{\text{monomer}}{\text{inimer}}$). The molecular characteristics of the polymers were studied by multi detector GPC equipped with a viscosity and low angle light scattering detector. The effect of the comonomer ratio γ on the degree of branching, the polymer molecular weight, the molecular weight distribution and the size of the polymers was investigated. In addition the intrinsic viscosities of the HBP polymers were compared to those with linear analogues in order to prove the compact structure of the branched polymers. We also show that the addition of 2-trimethylsilyloxyethyl methacrylate (TMSHEMA) to a living PDMAEMA hyperbranched precursor leads to hyperstar polymers with a hyperbranched core and linear polymer chain in the shell. PDMAEMA itself exhibits a dual pH and temperature responsive behaviour. The temperature sensitivity results from the (dimethylamino) groups and leads to a lower critical solution temperature (LCST) at around 50 ^{o}C. The pH responsive character is attributed to the reversible protonation/deprotonation process of the tertiary amine groups. Dynamic light scattering and potentiometric titrations were used to characterize the temperature and pH responsive behaviour of the HBPs, respectively. Finally, melt rheology measurements were carried out in order to investigate the rheological response of the HBPs.

Chapter 2

2.1 Experimental Section

2.1.1 Materials

All chemicals used are commercially available and were purchased from Aldrich, Germany. Ethylene glycol dimethacrylate (EGDMA) and triethylsilane (TES) were used for the inimer synthesis in the presence of chlorotris(triphenylphosphine) rhodium as the catalyst. The chemical formulas and names of the monomers, 2-(dimethylamino)ethyl methacrylate (DMAEMA) and 2-(trimethylsilyloxy)ethyl methacrylate (TMSHEMA), EGDMA and TES are shown in **Figure 1**. The polymerization catalyst was tetrabutylammonium bibenzoate (TBABB) and it was synthesized in-house by the method of Dicker et al [50], whereas THF served as the polymerization solvent. The monomers were passed through basic alumina columns and were stirred overnight over calcium hydride to remove the last traces of moisture and protonic impurities. This was done in the presence of an added free radical inhibitor, 2,2-diphenyl-1-picrylhydrazyl hydrate (DPPH), to avoid thermal polymerization. The monomers and the inimer were freshly distilled prior to the polymerization. The dried catalyst powder was stored in a round-bottom flask under vacuum until use. All glassware was dried overnight at 120 °C and assembled hot under dynamic vacuum prior to use.

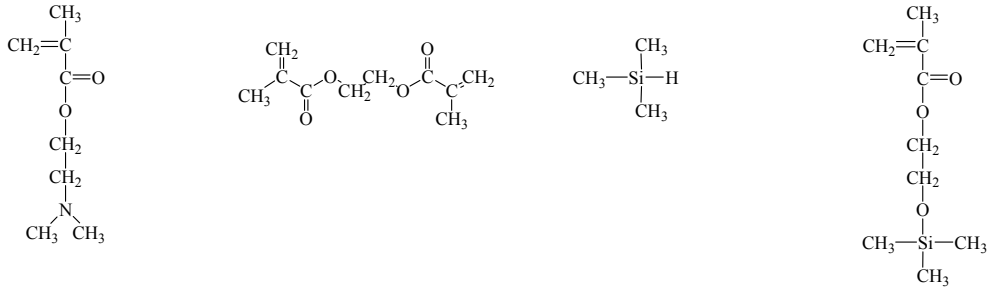

2-(Dimethylamino)ethyl methacrylate (DMAEMA) | Ethylene glycol dimethacrylate (EGDMA) | Triethylsilane (TES) | 2-(Trimethylsilyloxy)ethyl methacrylate (TMSHEMA)

Figure 1. Chemical structures and names of DMAEMA, EGDMA, TES and TMSHEMA

2.1.2 Synthesis of 2-(2-Methyl-1-triethylsiloxy-1-propenyloxy)ethyl methacrylate (MTSHEMA)

MTSHEMA was prepared by hydrosilylation of ethylene glycol dimethacrylate with triethylsilane catalyzed by chlorotris(triphenylphosphine)rhodium (**Figure 2**), following the procedure described by Ojima et al. [51]. To a degassed flask, ethylene glycol dimethacrylate (75.6 gr, 381mmol), triethylsilane (18.9 gr, 162 mmol) and chlorotris(triphenylphosphine)rhodium (14 mg, 15.1 μmol) were added under a dry nitrogen atmosphere. The mixture was stirred for 3h at 60 ^{o}C. Next, the unreacted ethylene glycol dimethacrylate was removed by distillation and the residual MTSHEMA was purified by distillation under high vacuum.

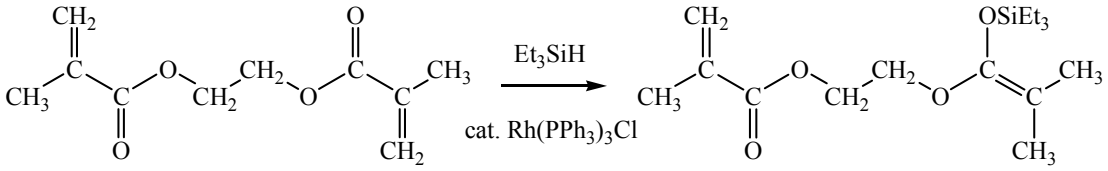

Figure 2. Synthetic procedure followed for the preparation of MTSHEMA

2.1.3 Homopolymerization of MTSHEMA

After its synthesis the polymerization of MTSHEMA was carried out in order to test the functionality of the inimer and obtain a PMTSHEMA hyperbranched polymer. The polymerization was performed at room temperature as following. Under inert conditions 1 ml of a 0.1 wt % TBABB solution in THF was added to 2.4 gr (7.76 mmol) of MTSHEMA in 12 ml THF under vigorous stirring, which triggered the polymerization. The polymerization exotherm was monitored with an external digital thermometer giving an exotherm which abated within 5 min. The polymerization was quenched with a few drops of methanol. Finally, the solvent was evaporated and the residue dried under vacuum at room temperature.

2.1.4 Copolymerization of MTSHEMA with 2-(dimethylamino)ethyl methacrylate

Polymerizations were carried out at room temperature at a constant TBABB and MTSHEMA concentration, while the concentration of DMAEMA was varied systematically. In a typical experiment, the polymerization was iniated by the addition of 0.25 mL of a 0.1 w/v % TBABB solution in THF to a mixture of MTSHEMA (0.30 gr, 0.95 mmol) and DMAEMA (1.65 gr, 10.5 mmol) in 9 ml THF (20 v/v % monomer concentration). The polymerization exotherm was monitored with an external digital thermometer and was used to follow the progress of the polymerization. For all comonomer ratios, $\gamma = \frac{[\text{DMAEMA}]}{[\text{MTSHEMA}]}$, full conversion of both comonomers was reached after ~20 min polymerization time. The polymerization was quenched with a few drops of methanol. The solution was stirred at room temperature for two hours and then precipitated in an excess of hexane. Finally, the polymer was collected and dried under vacuum at room temperature. The yield was > 98% with M_n = 6,300 and M_w/M_n = 1.8 (GPC, universal calibration).The comonomer ratio $\gamma = \frac{[\text{DMAEMA}]}{[\text{MTSHEMA}]}$, was varied from 11 to 80 by changing the concentration of the monomer at a constant inimer concentration. The influence of the monomer concentration $c_{pol.} = \frac{[\text{monomer}]}{[\text{solvent}]}$ on the polymer characteristics was also investigated for the same ratio γ.

2.1.5 Copolymerization of MTSHEMA with DMAEMA in the presence of monofunctional initiator

For the synthesis of the hyperbranched polymers prepared in this work 1-methoxy-3-(trimethylsilyloxy)-2-methyl-1-propene (MTS) was used as a monofunctional initiator. Polymerizations were performed at room temperature in different ratios of the comonomer MTSHEMA and DMAEMA to the monofunctional initiator, μ. A mixture of MTSHEMA (0.63 gr, 2 mmol) and DMAEMA (9 gr, 57 mmol) and a solution of TBABB in THF were added simultaneously under vigorous stirring to a solution of MTS (0.34 gr, 1.97 mmol) in 9 ml THF. The polymerization exotherm was monitored with an external digital thermometer and was used to follow

the progress of the polymerization. For all experiments, full conversion of both comonomers was reached after ~ 20 mins. The conversion was > 98% with M_n = 6,400 grmol^{-1} and M_w/M_n= 1.3 (GPC, universal calibration). The polymerization was quenched with a few drops of methanol. The solution was stirred at room temperature for two hours and then precipitated in an excess of hexane. Finally, the polymer was collected and dried under vacuum at room temperature.

2.1.6 Synthesis of hyperstar polymers

The preparation of the hyperbranched precursor was achieved by adding 0.25 mL of a 0.1 w/v % TBABB solution in THF to a mixture of MTSHEMA (0.30 gr, 0.95 mmol) and DMAEMA (1.65 gr, 10.5 mmol) in 9 ml THF. After the polymerization exotherm abated, TMSHEMA (1.2 gr, 5mmol) was added under vigorous stirring. The second exotherm verified the success of the polymerization. Finally the polymerization was quenched with a few drops of methanol. The solution was stirred at room temperature for two hours and then precipitated in an excess of hexane. Finally, the polymer was collected and dried under vacuum at room temperature.

2.1.7 Synthesis of linear PDMAEMA homopolymers

Linear PDMAEMA homopolymers with molecular weights from 2,000 gr mol^{-1} to 240,000 gr mol^{-1} were also synthesized using group transfer polymerization. A typical procedure is detailed below. To a round flask, kept under a dry nitrogen atmosphere and sealed with a rubber septum, containing ~ 5 mg TBABB (10 μmol) and a stirring bar, were added via a glass syringe 170 ml THF followed by 8.4 ml of freshly distilled DMAEMA (7.85 gr, 50 mmol). Next 0.1 ml 1-methoxy-3-(trimethylsilyloxy)-2-methyl-1-propene (MTS) was added under stirring which triggered the polymerization and caused an exotherm from 25 to 35 ^{o}C within 2 min. The polymerization mixture became viscous as manifested by the decelerated motion of the stirring bar. Similarly, PDMAEMA homopolymers of different molecular weights were prepared by varying the amount of added MTS at a constant amount of DMAEMA. These homopolymers were used as reference samples in the solution and melt viscosity studies.

2.2 Experimental techniques

2.2.1 Size exclusion chromatography

The linear and branched polymers obtained by the SCVCP of MTSHEMA with DMAEMA were characterized by conventional GPC (in house) and a multidetector GPC equipped with a viscosity and low angle laser light scattering detector using THF as the eluent. The latter measurements were carried out at the Research Center at Jülich under the supervision of Dr. Allgaier.

The actual molecular weight of a branched polymer of a given molecular weight differs significantly from that of a linear sample of the same molecular weight. This is due to the compact structure of the HBPs which leads to a larger retention volume for the branched polymers compared to that of a linear sample with the same actual molecular weight. Therefore, GPC with a mass-sensitive on-line detector, such as the viscosity detector using the universal calibration principle [52-54], is required for the determination of the precise molecular weights of branched polymers.

2.2.1.1 Basic principles

Size exclusion chromatography (SEC), also known as gel permeation chromatography (GPC), is a polymer separation method which allows determination of the polymer molecular weight and molecular weight distribution [55, 56]. Porath and Flodin [57] were the first to report that polymers can be separated by their size dependent degree of solute penetration through a packed porous material. The term gel permeation chromatography was defined by Moore [58], who developed rigid cross-linked polystyrene gels with a range of pore sizes, suitable for separation of synthetic polymers in organic media. GPC is extremely valuable for both analytic and preparative work with a wide variety of systems ranging from low to very high polymer molecular weights. The method can be also applied to a wide variety of solvents and polymers, depending on the type of gel used.

In a GPC experiment, a pump circulates solvent through a series of columns filled with porous beads (**Figure 3**). Often the beads are solvent swollen polymer gel particles. The beads are intentionally made with a variety of pores sizes that span the range of the sizes of the macromolecules to be separated. A small volume of a dilute

polymer solution in the same solvent is injected into the flowing solvent stream entering the columns. As the polymer solution passes thought the columns, the largest polymers are excluded from all but the largest pores, and elute from the column first. Progressively, smaller polymers can explore the smaller pores and therefore, larger volumes of the column and consequently elute later. Thus, the separation of molecules in GPC occurs by polymer size rather than polymer mass.

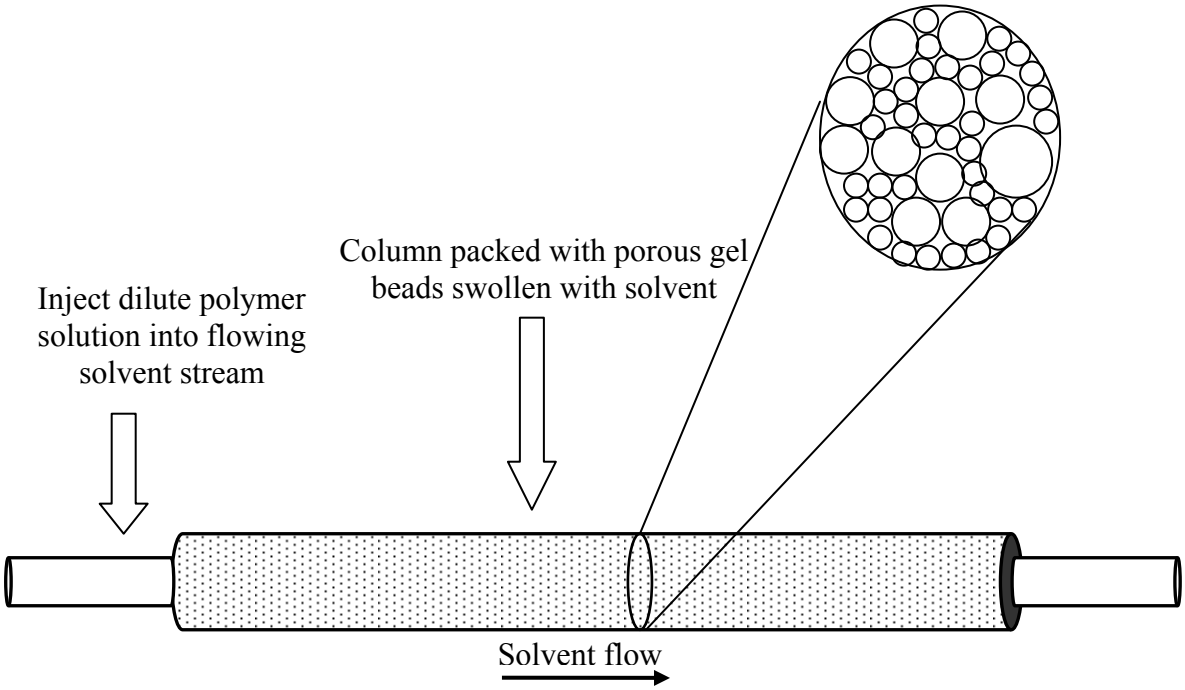

Figure 3. Schematic view of a separation column

After separation the solution passes through a variety of detectors, depending on the information required for a particular sample. Common detectors include a differential refractometer, absorption spectrophotometric detection (such as ultraviolet and infrared), light scattering photometer (for measuring the M_w of the eluent) and viscometer (for measuring the intrinsic viscosity of the eluent). With proper calibration, using narrow molar mass distribution standards, GPC can in principle determine the full molar mass distribution, including high-order averages.

The two main calibration techniques used in GPC are the conventional calibration and the universal calibration.

2.2.1.2 Conventional calibration

This technique uses a series of narrow molecular weight polymer standards of known molecular weights in order to establish a calibration curve. More precisely the calibration curve is established experimentally by relating the peak-retention volume (or time) to molecular weight for a series of known narrow molecular weight distribution standards (**Figure 4**). Polymer fractions of narrow molecular weight distribution elute as sharp peaks with the retention volume varying with the differences in molecular weight. In the presence of sufficient narrow fractions of the same polymer type, calibration curves can be accurately determined. This is the simplest method, but it is generally restricted in its utility owing to the lack of availability of many different polymer standard types.

The left-hand edge of **Figure 4** represents the point of injection. The retention volume V_0 is the total exclusion volume. It is the total interstitial volume in the chromatographic system and the point in the chromatogram before which no polymer molecule can elute. V_t is the total permeation volume and represents the sum of the interstitial volume and the total pore volume. It is the point at which the smallest molecules in the sample mixture elute. All GPC separation takes place between V_0 and V_t. This retention volume domain is the selective permeation range.

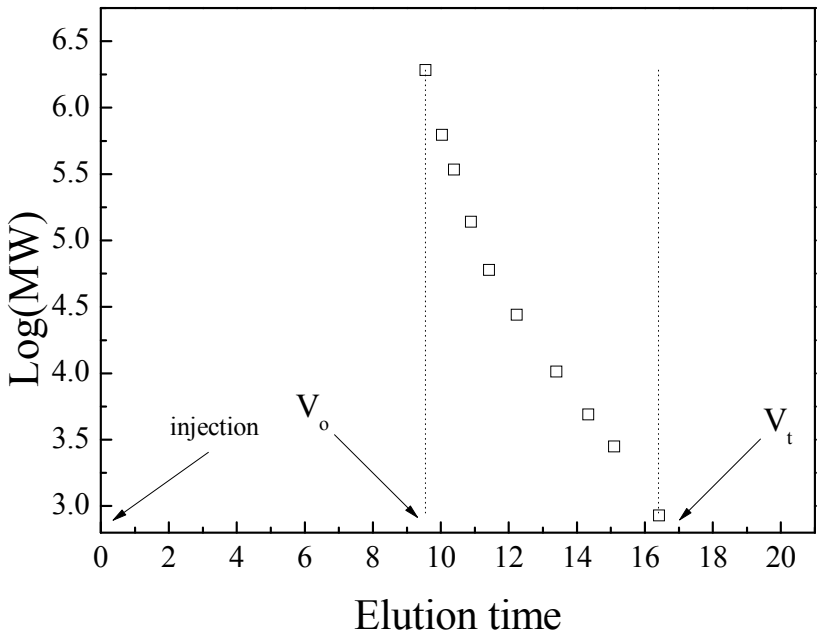

Figure 4. A semi logarithmic plot of molecular weight versus elution time for a series of PMMA standards.

2.2.1.3 Universal Calibration

Benoit and coworkers demonstrated that it is possible to use a set of narrow polymer standards of one chemical type to provide an absolute molecular weight calibration to a sample of a different chemical type [52, 59]. More analytically, this calibration considers the relationship between molecular weight, intrinsic viscosity, and hydrodynamic volume, the volume of a random, freely jointed polymer chain in solution. This relationship has been described by both the Einstein-Simha viscosity law for spherical particles in suspension,

$$[\eta] = C\frac{V_h}{M}$$

and the Flory-Fox equation for linear polymers in solution,

$$[\eta] = \Phi\frac{\left\langle R_g^2 \right\rangle^{3/2}}{M}$$

where [η] is the intrinsic viscosity, V_h is the hydrodynamic volume, $\left\langle R_g^2 \right\rangle^{3/2}$ is the root-mean-square radius of gyration of the polymer chain, and *C* and Φ are constants [61]. If either equation is multiplied by M, the molecular weight, the resulting product [η]×M is found proportional to the hydrodynamic volume. Benoit and coworkers plotted this product versus elution volume for a number of structurally different polymers investigated under identical GPC conditions and found that all points lay on the same calibration curve (**Figure 5**). This calibration was said to be "universal" for all the polymer types studied.

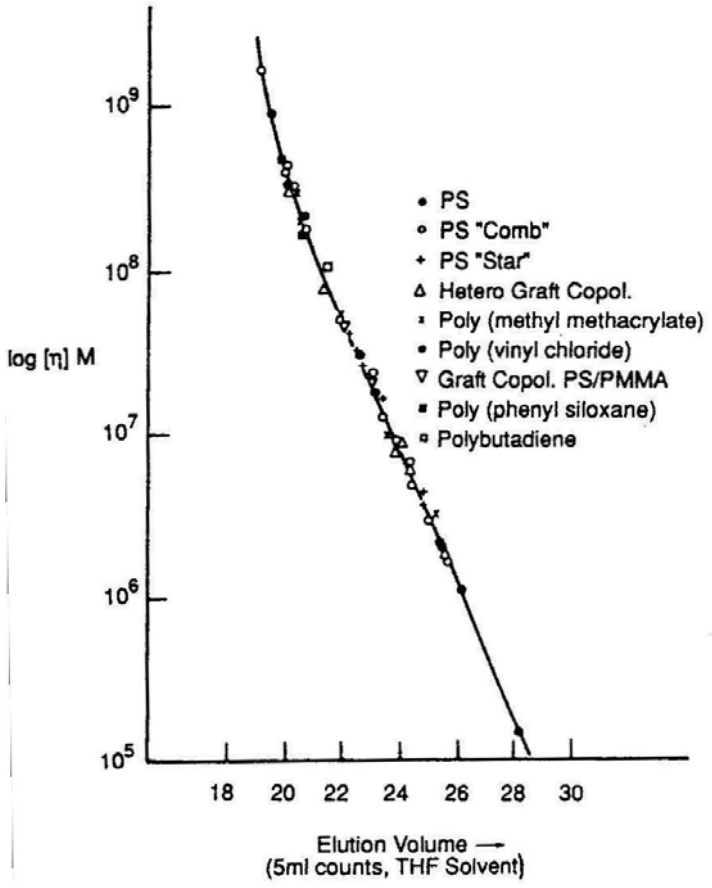

Figure 5. Universal calibration curve for various polymers [52].

In practice, one establishes the relationship

$$[\eta]_r M_r = [\eta]_s M_s$$

Where the subscripts "r" and "s" refer to reference (calibrant) and sample polymers respectively. Even if the intrinsic viscosities are known or can be measured for each standard, it is unlikely that the value of intrinsic viscosity would be known for each time slice in the molecular weight distribution of the sample polymer. Thus, the previous equation must be further modified to be more useful. This can be accomplished with the use of the Mark-Houwink equation

$$[\eta] = KM^{a}$$

where the coefficient K and exponent a are known as the Mark-Houwink constants. These constants are a function of both the polymer and its solvent environment (including temperature). If the constants are available from the literature or can be determined for the polymer sample using narrow fractions in the GPC mobile phase, then one can substitute the Mark-Houwink term for [η] into the previous equation to obtain:

$$\log(M_s) = \frac{1}{1+a_s}\log\frac{K_r}{K_s} + \frac{1+a_s}{1+a_r}\log M_r$$

which is an expression for the sample molecular weight in terms of the standard molecular weight and both sets of Mark-Houwink constants.

2.2.1.4 Gel Permeation Chromatography detectors

As it was mentioned above there are various types of detectors used in gel permeation chromatography. The most common by far is considered to be the differential refractive index (DRI) detector. DRI detects differences in refractive index between a moving stream and a static reference of mobile phase using a split optical cell. It responds well (at a moderate concentration level) to most polymeric samples, provided that they are different in refractive index from the mobile phase in which they are dissolved. DRI is considered a concentration detector because it is assumed that the response of the DRI is equally proportional to polymer concentration in all molecular weight regimes. There are also other kinds of detectors which are

characterized as molecular weight sensitive and determine absolute molecular weights. A common molecular weight detector is the one-line viscometer. All current instrument designs depend on the relationship between the pressure drop across a capillary through which the polymer solution must flow and the viscosity of the solution. This relationship is based on Poiseuille's law for laminar flow of incompressible fluids through capillaries:

$$\eta = \frac{\pi \Delta P r^4 t}{8 V l}$$

where η is the absolute viscosity, ΔP is the observed pressure drop, t is the efflux time, and r, l, and V are the radius, length, and volume of the capillary, respectively. In a capillary viscometer operating at ambient pressure, one can define the relative viscosity η_r as the ratio of the absolute viscosities of solution to solvent, which is equal to the ratio of their efflux times at low concentrations. Yet, when such a capillary is used as a GPC detector, the flow time is constant and the relative viscosity becomes

$$\eta_r = \frac{\eta}{\eta_o} = \frac{\Delta P}{\Delta P_o}$$

which is the ratio of the solution to solvent pressure drops. Because the intrinsic viscosity $[\eta]$ is defined as

$$[\eta] = \lim_{c \to 0} \frac{\ln \eta_r}{c}$$

combing the above equations the intrinsic viscosity is derived as

$$[\eta] = \frac{\ln \Delta P / \Delta P_o}{c}$$

provided that c is very small. Thus an on-line viscosity detector is capable of providing intrinsic viscosity distribution information directly.

Another mass sensitive detector which is commonly been used is the low angle laser light scattering (LALLS) which was originally developed by Kaye and Havelik [62]. The low angle light scattering detector not only senses the solutes as they are eluted from the column but can also provide an approximate value for their molecular weight. This type of detector is largely employed for sensing very high molecular weight compounds. The light is provided by a laser and the incident light beam is blocked, and the light that is scattered at a low angle to the incident light is measured by an appropriately placed sensor. In order to determine the molecular weight of the solute, the refractive index of the solution is also required and so a refractive index detector is usually placed in line with, and prior to, the light scattering detector. Employing calibrating substances, the molecular weight can be calculated from the concentration of the solute, the intensity of the scattered light and the refractive index of the solute using equations provided by light scattering theory [63, 64]

2.2.1.5 Experimental Setup

Figure 6 shows the gel permeation chromatography apparatus. The experiments were carried out using a Waters 150-CV Plus instrument together with four Styragel^{TM} columns. The porosity range was 10^5 to 500 Å. Three detectors, a Viscotec model TDA 300 triple detector with a differential refractometer, a differential viscometer and a low angle laser light scattering detector were used at 35 ^{o}C. The carrier solvent was THF at a flow rate of 1 mL min^{-1}. The solvent was degassed using a Viscotec model VE 7510 degasser. Data were collected and handled by Atlas Workstation and Cirrus GPC software. It should also be noted that GPC characterization of poly(2-(dimethylamino)ethyl methacrylate)s has been reported by several research groups to suffer, absorption of the polymer on the GPC columns [65, 66]. To overcome this problem GPC measurements in the present study were conducted in THF containing 2 v/v % triethylamine [66, 67].

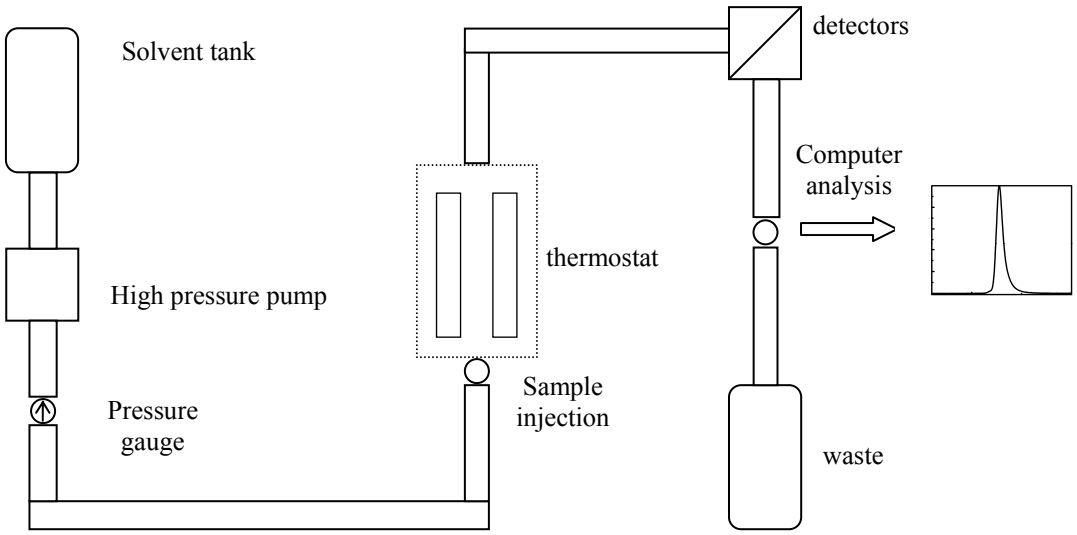

Figure 6. Experimental setup of Gel Permeation Chromatography

2.2.2 Nuclear Magnetic Resonance spectroscopy

Nuclear magnetic resonance (NMR) spectroscopy is the most effective and significant method for determining the structure and dynamics of polymer chains both in solution and in the solid state. Undoubtedly the widest application of NMR spectroscopy is in the field of structure determination. The identification of certain atoms or groups in a molecule as well as their position relative to each other can be obtained by one-, two-, and three-dimensional NMR. An enormous amount of information can be derived from a single spectrum, and in many cases this facilitates the determination of the chemical structure of a molecule.

2.2.2.1 Principles

The fundamental property of the atomic nucleus involved in this technique is the nuclear spin (I), which takes either even or odd values. A nucleus with nuclear spin I adopts 2I+1 nondegenerate spin orientations in a magnetic field. The energy of the i^{th} spin state (E_i) is directly proportional to the nucleus spin m_i and the magnetic field strength B_o:

$$E_i = -m_i \frac{\gamma h B_o}{2\pi}$$

In this equation h is Planck's constant, while γ is called the gyromagnetic ratio, a proportionality constant characteristic of the isotope being examined. The selection rule for the NMR transitions is that m_i can only change by one unit. Thus, the transition energy is given by:

$$\Delta E = \frac{\gamma h B_o}{2\pi}$$

Transition from the lower to the upper state is possible by absorption of radiation of the appropriate frequency. This radiation is in the radiofrequency region of the electromagnetic spectrum and its precise frequency can be calculated using the formula:

$$\nu = \frac{\gamma B_o}{2\pi}$$

In an NMR experiment either the field B_o or the frequency ν can be varied.

2.2.2.2 Theory of chemical shifts

The electron cloud surrounding each nucleus in a molecule serves to shield that nucleus from the external magnetic field. Thus, bare proton nucleus process appears at much higher frequency than a proton nucleus surrounded by electrons.

The external magnetic field B_o causes each electron pair surrounding the nucleus to circulate through its orbital in such a way as to generate an induced magnetic field (B_i) that opposes to the external field. Thus, while a bare proton experiences the full magnitude of the external field, the shielded nucleus experiences an effective field (B_{eff}) that is equal to the external field minus the induced field:

$$B_{eff} = B_o - B_i$$

Because the strength of the induced field is directly proportional to that of the external field, we can define a shielding constant σ that is a function of the exact molecular environment of the nucleus:

$$B_i = \sigma B_o$$

Combining the two last equations the following equations can be derived

$$B_{eff} = (1-\sigma) B_o$$

The above equation can be used to derive the resonance frequency

$$\nu = \frac{\gamma(1-\sigma) B_o}{2\pi}$$

Thus, the greater the shielding of the nucleus, the lower is its resonance frequency and the farther to the right it will appear in an NMR spectrum. Conversely, nuclei from which electron density has been withdrawn are said to be deshielded and appear towards the left of the spectrum.

2.2.2.3 The chemical shift scale

It is virtually impossible to measure absolute frequencies with the high degree of precision necessary in NMR, but it is possible to measure frequency differences very precisely. This is the reason why NMR signal frequencies are measured as the difference ($\Delta\nu_i$) between the precession frequency and the instrument's operating frequency:

$$\Delta\nu_i = \nu_i - \nu_o$$

In order to device a reproducible scale for the frequency axis of an NMR spectrum, we add in each sample a small amount of a standard internal reference compound that gives rise to a sharp signal somewhat apart from the other signals of interest. We

arbitrarily assign the reference signal the frequency value zero and measure frequency differences in hertz downfield or up field of the reference signal. As a result, the signal position is given by:

$$\delta\nu_i = \Delta\nu_i - \Delta\nu_{ref}$$

Another problem is that the spectroscopic data, when expressed as δν, will vary from one spectrometer to another if their operation frequency is different. This is because precessional frequencies, and their differences, are directly proportional to the field strength. In order to solve this problem, we define a new quantity called the chemical shift of a nucleus i (δ_i) by the equation:

$$\delta_i = \frac{10^6 \left(\Delta\nu_i - \Delta\nu_{reff}\right)}{\nu_o}$$

δ scale normalizes the frequency differences over the operating frequency. δ is expressed at part per million (ppm).

2.2.2.4 Experimental setup

The basic requirement for all high-resolution NMR spectrometers is a radiofrequency (RF) source and a magnetic field, both of which must be characterized by very high stability and homogeneity. The sample is placed in a probe, which is positioned between the poles of the magnet as shown in **Figure 7**

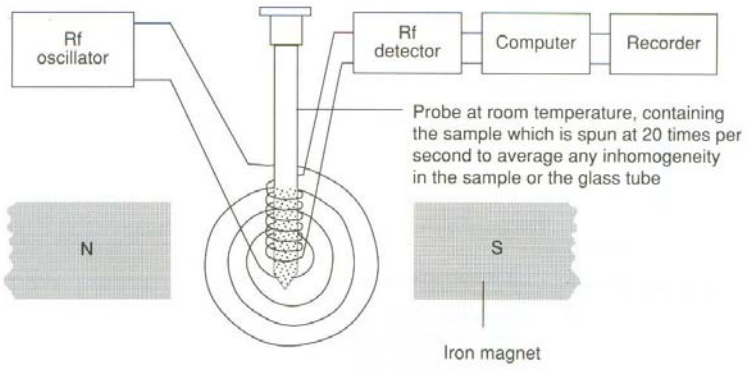

Figure 7. NMR spectrometer.

Either the magnetic field or the RF frequency is slowly varied. A radiofrequency detector is set at right angles to the radiofrequency transmitter inducing resonance, and a recorder charts the absorption of energy as a function of the applied field or frequency.

For the ^{1}H NMR experiments in this study deuterated cloroform ($CDCl_3$) was used as a solvent. The hyperbranched polymers were dissolved in $CDCl_3$ at a 2 wt% concentration. For all experiments a Bruker AMX-500 spectrometer was used.

2.2.3 Dilute Solution Viscosity of Polymers

Dilute solution viscometry is a technique used for the accurate quantitative measurement of the increase in viscosity of a polymer solution and allows determination of the intrinsic ability of a polymer to increase the viscosity of a particular solvent at a given temperature. This quantity provides information related to the size of the polymers in solution, including the effects of the chain dimensions of the polymer structure, molecular shape, degree of polymerization, and polymer-solvent interactions. Most commonly, dilute solution viscosity is used to estimate the molecular weight of a polymer, and involves the use of semi empirical equations that have to be established for each polymer-solvent-temperature system by analysis of polymer samples whose molecular weights are known.

Capillary flow measurement is the simplest experimental method for the determination of viscosity. A liquid drains or is forced through a dine-bore tube, and the viscosity is determined from the measured flow, applied pressure, and tube dimensions.

In this project an Ubbelohde glass capillary viscometer was used. The Ubbelohde viscometer is a u-shaped piece of glassware with a reservoir on one side and a measuring bulb with a capillary on the other. A liquid is introduced into the reservoir then sucked through the capillary and measuring bulb. The liquid is allowed to travel back through the measuring bulb and the time it takes for the liquid to pass through two calibrated marks is a measure of its viscosity.

In order to calculate the intrinsic viscosity of a polymer solution the specific viscosity η_{sp} must be measured first at several concentrations. Then the intrinsic viscosity can be obtained by extrapolating a plot of η_{sp}/c versus c to c = 0. The

linearity of the plot of η_{sp}/c versus c and the dependence of the slope of the linear plot on $[\eta]$, which is the intercept, has been described by a purely empirical equation by Huggins.

$$\eta_{sp}/c=[\eta]+k'[\eta]^2c$$

where k', is the Huggins constant. Another commonly used empirical equation is

$$\left(\ln[\eta]_{rel}\right)/c=[\eta]+k''[\eta]c$$

where k'' is the Kraemer constant, which is usually negative.

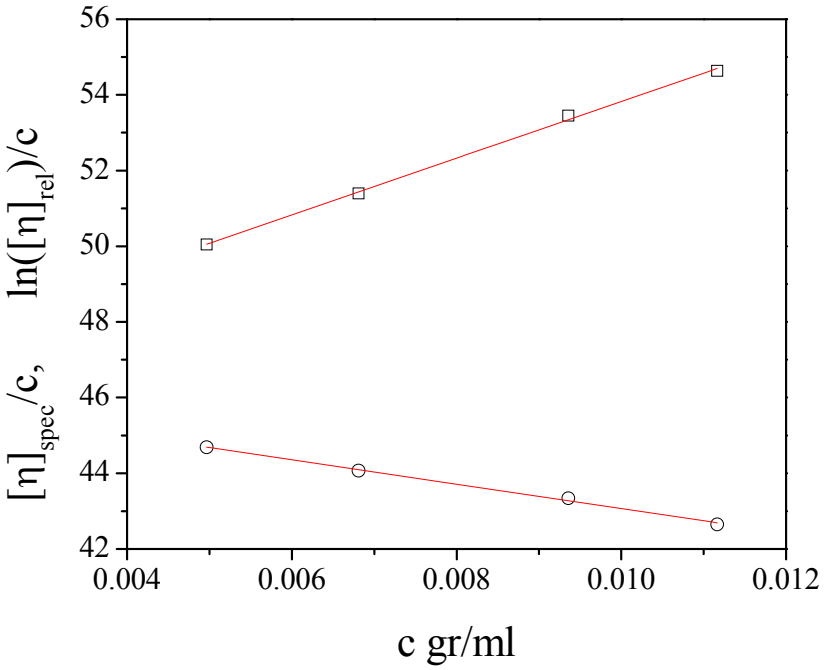

Figure 8. Typical plots of η_{sp}/c (-○-) and $\ln[\eta]_{rel}/c$ (- -) as a function of concentration for linear polystyrene in THF.

Flexible polymer chains expand with increasing solvent power of the medium leading to an increase in $[\eta]$ with increasing polymer solvation. For chains of a similar kind, varying in length (homologous series), the relationship between $[\eta]$ and molecular weight, M, may be represented by the Mark Houwink relationship. $[\eta] = KM^{\alpha}$ where K

and α are constants for a given polymer solvent-temperature system. The exponent a increases with the solvent power of the medium. Theory [68] predicts that it should lie in the range $0.2 < \alpha < 0.5$ for dendritic polymers, $0.5 < \alpha < 0.8$ for flexible chains, $0.8 < \alpha < 1.0$ for inherently stiff molecules (e.g., cellulose derivatives, DNA), and $1.0 < \alpha < 1.7$ for highly extended chains (e.g., polyelectrolytes in solutions of very low ionic strength, rods).In the present study hyperbranched polymers and linear PDMAEMA reference samples where characterised in several organic solvents by capillary viscosity measurements for the determination of the intrinsic viscosity using an Ubbelohde viscometer with internal dilution. The concentration range was 10^{-2} down to 10^{-3} gr/ml. The measurements took place at the National Hellenic Research Foundation under the supervision of Dr. S. Pispas

2.2.4 Potentiometric titrations

2.2.4.1 Titration curves

An acid-base titration involves the determination of the concentration of an acid or base in solution by its neutralization with a base or acid, respectively of known concentration. This allows the quantitative analysis of the concentration of an unknown acid or base solution. It makes use of the neutralization reaction that occurs between the acid and base. The titration curve for an acid-base titration is a plot of the solution pH against the volume of titrant added. Titration curves can be used to define the value of pH that signals the equivalent point, this is the point when the reaction is complete and all the analyte (acid or base) has reacted with the titrant (base or acid, respectively). The determination of the equivalent point is achieved by monitoring the pH changes during the titration. **Figure 9** shows the titration curve for a strong acid-strong base pair.

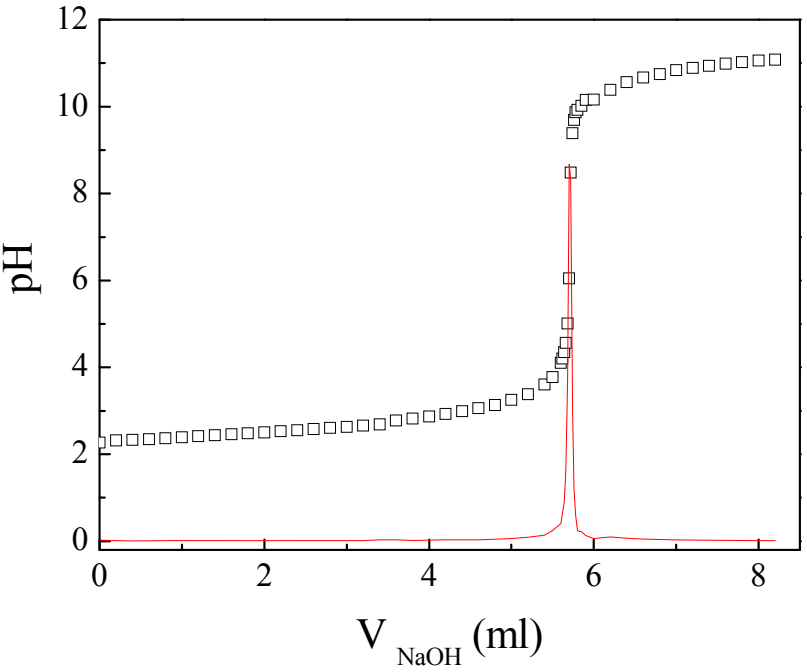

Figure 9. Titration curve of HCl with NaOH and its first derivative.

At the beginning, the solution has a low pH (pH~2) and increases slowly as the strong base is added. As the solution nears the point where all of the H^+ are neutralized, the pH rises sharply and then levels out again as the solution becomes more basic and more OH^- ions are added. The equivalent point occurs when the slope of the titration curve changes (see **Figure 9**) and can be calculated from the maximum of the first derivative of the data. In the above plot an equivalent point at pH 7 is obtained as expected from a strong acid-strong base pair.

The titration of a weak acid with a strong base is different from that of a strong acid/base titration, primarily in the beginning of the titration, i.e., before the equivalent point. Moreover, the equivalent point itself is shifted upward in pH. The reaction that occurs in the solution is

$$HA(aq) + OH^-(aq) \rightleftharpoons A^-(aq) + H_2O(l)$$

As base is added, a buffer solution forms and the pH does not change rapidly until all of the weak acid reacts with the base. Analysis of the titration curve provides a mean for determining the dissociation constant of the acid. The pK_a of the acid is equal to

the pH at the midpoint of the titration curve. This can be seen from the following equation, which describes the weak acid equilibrium

$$pH = pK_a + \log\left(\left[A^-\right]/\left[HA\right]\right)$$

Where [11] is the concentration of the basic form of the acid and [HA] is the concentration of the acid. At the midpoint, [11] = [HA] and the second term on the right side of the equation becomes zero allowing to determine the pK_a from the pH.

2.2.4.2 Degree of ionization

The degree of ionization, α, of a weak acid is defined as the ratio of the concentration of the ionized units divided by the total concentration of acid units in the solution. In accordance, the fraction of charged tertiary amine units of the hyperbranched polymers used in this study is defined as the degree of ionization of the polymer. Assuming that all of the protons from the added HCl protonate the amine groups the degree of protonation is defined as the net moles of HCl divided by the moles of the amine in the solution. This is expressed as:

$$\alpha = \frac{\left[\text{netHCl}\right]}{\left[\text{DMAEMA}\right]}$$

The effective pK_a value of the protonated tertiary amine units can be calculated from the previous equation at a degree of ionization α = 0.5 where $\left[\text{DMAEMA}^+\right]=\left[\text{DMAEMA}\right]$. Its value is obtained from the pH versus α curve shown in **Figure 10**.

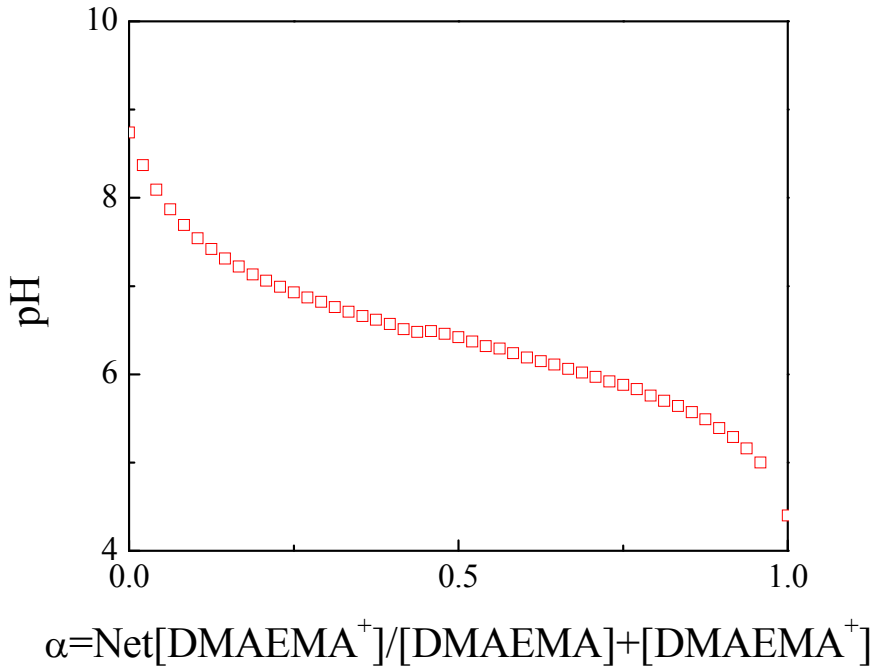

Figure 10. Solution pH versus degree of ionization of a hyperbranched PDMAEMA

Titration curves for the HBPs prepared in this work were obtained upon addition of base in a pre-dissolved polymer solution adjusted at pH 2. Small amounts of base (NaOH 0.1M) were added in the sample via a micropipette while the pH was monitored with a GLP 21 Crison pH meter. The rate of base addition depends on the pH range. Between pH 2 and 3 the amount of base added was 100 μL. In this range neutralization of the excess acid occurs. When all the excess protons in the solution are neutralized, further addition of base results in the deprotonation of the amine groups. Smaller amounts of base (20μL) were added in order to follow more accurately the deprotonation process. The pH increased slightly and a plateau was observed until the deprotonation of the amine groups was complete. Following the deprotonation of the amine groups an abrupt increase of the pH was observed due to the excess of base in the solution.

2.2.5 Light scattering

Light scattering occurs whenever a beam of light encounters matter. When there is no absorption, nuclei and electrons undergo induced vibrations in phase with

the incident light wave and act as sources of light that is propagated in all directions, aside from a polarization effect, with the same wavelength as the exciting beam. Light scattering accounts for many natural phenomena, including the colour of the sky and the rainbow. Lord Rayleigh [69, 70] developed the theoretical interpretation of light scattering from dilute gases. Einstein [71] and Smoluchowski [71-73] explained particle diffusion in liquid on the basis of local thermal fluctuations in the medium. Working from this basis, Debye [74, 75] extended the work to macromolecular solutions and showed a relationship between local fluctuations and osmotic pressure. Light scattering from solution allows the determination of the molecular parameters of the scattering particles and thermodynamic quantities [76-79].

In a light-scattering experiment the quantity that is measured is the total scattered intensity $I(q,t)$ at specific q (scattering wave vector), $q = \frac{4\pi n}{\lambda}\sin\left(\frac{\theta}{2}\right)$, which can be used to extract information on the static and dynamic properties of the system probed at a length scale of ~$2\pi/q$, where n is the refractive index of the medium, λ the wavelength of the laser and θ the angle between the incident beam and the scattered beam. **Figure 11** shows a sample's geometry where a beam of light is focused on a region of a fluid and is scattered into a detector. Polarizers and analyzers are used to define the polarization of the incident and scattered light beams, respectively.

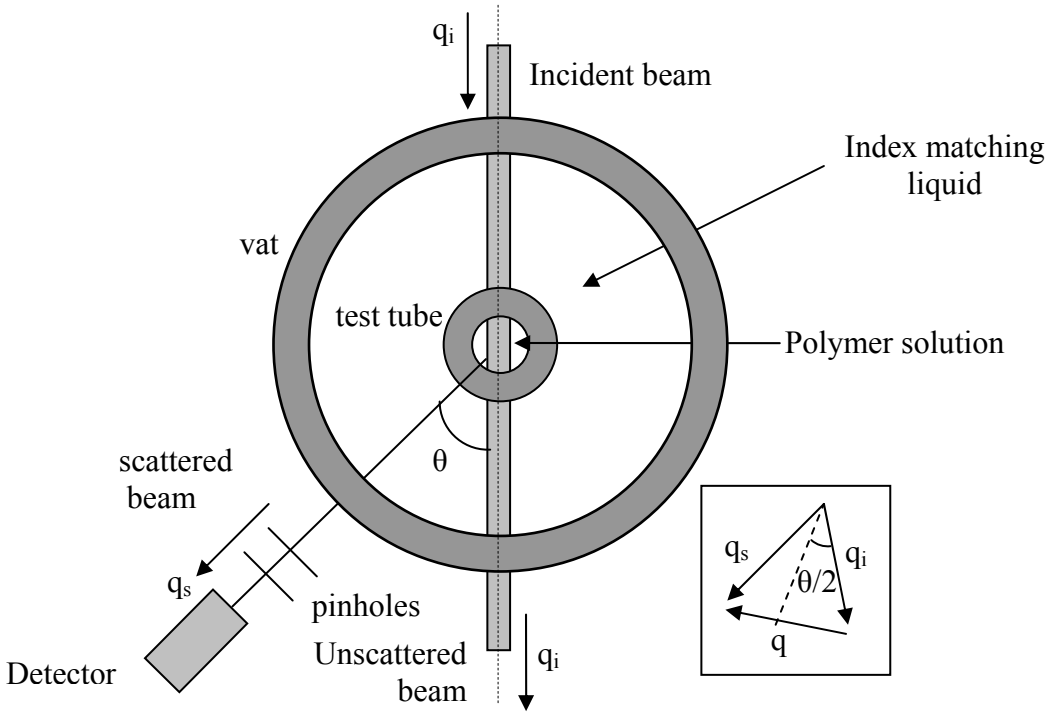

Figure 11. Top view of the geometry around the sample cell. The wave vector q_i of the incident beam changes to q_s when scattered. Two pinholes or two slits specify the scattering angle. The inset defines the scattering wave vector q.

2.2.5.1 Dynamic light Scattering

Particles in solution show a random motion (Brownian motion) caused by thermal density fluctuations. As a consequence of the temporal changes in interparticle positions and the corresponding temporal concentration fluctuations, the interference pattern and the resulting scattered intensity detected at a given scattering angle also change with time, reflecting the Brownian motion of the scattering particles. To quantitatively analyze the particle mobility by light scattering, it is helpful to express the scattering intensity fluctuations in terms of correlation functions.

In a photon correlation experiment the normalized autocorrelation function of the scattered intensity G(q,t), of the scattered intensity is measured

$$G(q,t)=\frac{\langle I(q,t)\cdot I(q,0)\rangle}{\langle I(q,0)\rangle^2}$$

where G(q,τ) is the autocorrelation function at a particular wave vector q and delay time τ, and I is the intensity. The quantity related with the dynamic response of the system is the autocorrelation function of the scattered field

$$g(q,t)=\frac{\left\langle E(q,t)E^{*}(q,0)\right\rangle}{\left\langle \left|E(q)^{2}\right|\right\rangle}$$

For Gaussian statistics the Siegert equation relates the autocorrelation of the scattered intensity function with the autocorrelation function of the scattered field as follows:

$$G(q,t) = 1 + f^{*}\left[g(q,t)\right]^{2} = 1 + f^{*}\left|C(q,t)\right|^{2}$$

where the parameter f* is a correction factor that depends on the geometry and alignment of the laser beam in the light scattering setup.

2.2.5.2 Analysis of the correlation function

Once the autocorrelation data have been generated, different mathematical approaches can be employed to determine from it the *z*-averaged translational diffusion coefficient.

For monodisperse samples the correlation function can be described with a simple exponential decay and can be fitted with a function of the form $C(q,t) = Ae^{-t/\tau}$, where A is analogous to the intensity and τ is the relaxation time. But in cases of polydisperse samples the correlation function is not a simple exponential decay. A way to analyze the autocorrelation function in this case is the Contin analysis. The autocorrelation function can be mathematically expressed as a sum of exponentials

$$C(q,t)=\int_{-\infty}^{\infty} L(\ln\tau)\exp(-t/\tau)\,d(\ln\tau)$$

Then the procedure to estimate G(Γ) from $C(q,t)$ is by inverse Laplace transformation. For this purpose a numerical computer program named Contin [8, 80,

81] is used which treats the normalized autocorrelation function as the sum of single exponential decays with fractions L(lnτ). **Figure 12** shows a typical example of the results obtained by applying the Contin method to a dilute solution of a hyperbranched PDMAEMA using acetone (9a) and THF (9b) as the solvent.

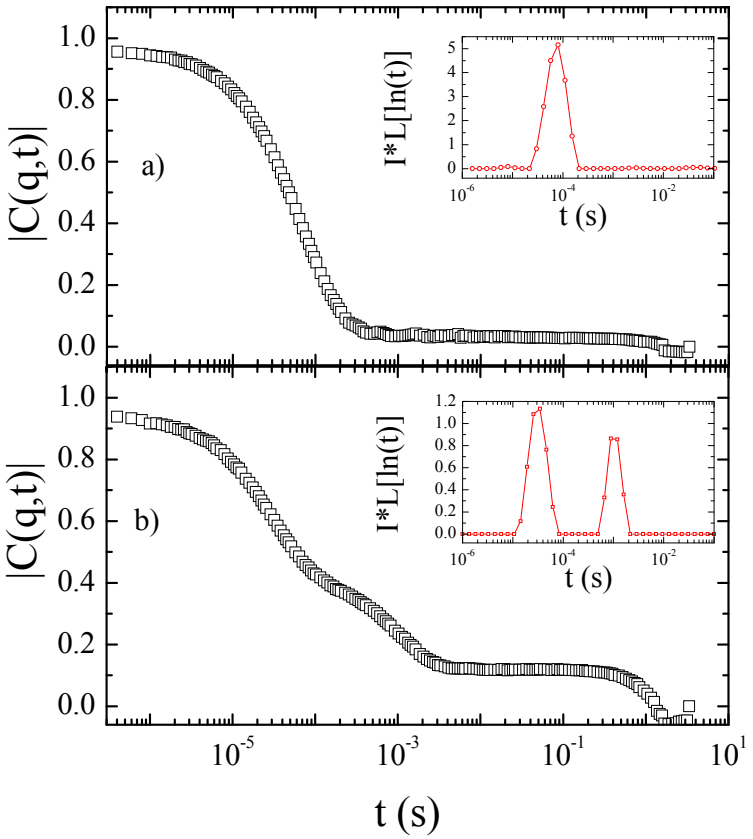

Figure 12. Autocorrelation function of hyperbranched PDMAEMA in acetone (a), and THF (b). The inset shows the distributions of relaxation times multiplied by the normalized intensity.

The rate for each angle is calculated from the equation

$$\Gamma = \frac{1}{\tau}$$

where τ is calculated from the Gaussian fit of the inverse Laplace as mentioned above. The rate Γ is related to q^2 via the equation

$$\Gamma = Dq^2$$

The linear fit of the data of Γ vs q^2 gives the value of the diffusion coefficient D at q^2 = 0. The diffusion coefficient and the hydrodynamic radius R_h are related by the Stokes-Einstein equation

$$R_h = \frac{K_B T}{6\pi\eta D}$$

where η is the viscosity of the solvent, K_B is the Boltzmann constant and T is the temperature of the sample.

All Dynamic Light Scattering (DLS) measurements were carried out using the Photon Correlation spectroscopy (PCS) technique. The auto-correlation function of the scattered intensity $C_{vv}(q,t) = \langle I(q,t) I(q,0) / |I(q,0)| \rangle^2$, in the polarized geometry was measured for scattering angles from 30° to 150°. The samples were initially prepared at c~0.4 wt% in THF and were filtered through 0.45 μm pore size filters into dust free light scattering cells (outer diameter 10-12 mm). After filtration they were allowed to equilibrate for an hour before being measured.

2.2.6 Rheology

Rheometry refers to a set of standard techniques that are used to experimentally determine rheological properties of materials (fluid or solid). The idea underpinning rheometry is to realize flows, where the stress and/or strain fields are known in advance, which makes it possible to deduce rheological properties from measurements of the flow properties. A rheometer is usually an engine, which can exert a torque/force on a material and accurately measures its response with time (or conversely, it can impose a strain and measures the resulting torque).

In a typical rheological experiment a sample, confined in a particular geometry, is subjected to a displacement and the resulting force is measured. An example is shown in **Figure 13** for the deformation called simple shear. The material is confined between two parallel plates, and if one surface is moved a distance dx then

the sample has been subjected to a strain, $\gamma = dx/dy$. The velocity of the plate $v_x = dx/dt$, and $d(dx/dy)/dt = \gamma$ is called the strain rate or shear rate. It takes the application of a force to accomplish the deformation, alternatively the material exerts a force on the moving plate. The total force will depend on the area of the plate in contact with the material and thus we consider the force per unit area, or stress, σ. There are several different kinds of deformation geometries, such as uniaxial elongation, biaxial elongation.

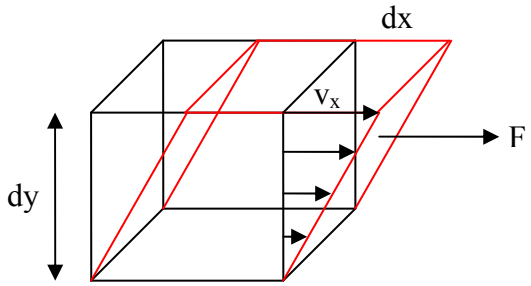

Figure 13. Illustration of simple shear flow between two parallel plates

The effect (shear strain τ) is quantified by the displacement per unit height and the rate (strain rate γ) is the velocity per unit height (V/H), where the height is the distance to a relatively unaffected position. The viscosity η is the tendency of the fluid to resist flow and is defined by

$$\eta = \frac{\text{shear stress}}{\text{shear rate}} (\text{Pa} \times \text{s})$$

In this kind of experiment a sinusoidal strain with angular frequency ω is applied to a sample in the simple shear geometry

$$\gamma(t) = \gamma_o \sin(\omega t)$$

The principle advantage of this technique is that the viscoelastic response of any material can be probed directly on different time scales $(1/\omega)$ of interest by simply varying the angular frequency ω. If the material studied is a perfectly elastic solid, then the stress in the sample will be related to the strain thought Hooke's Law

$$\sigma(\tau)=G\gamma(t)=G\gamma_o\sin(\omega t)$$

If the material being studied is a Newtonian liquid the stress in the liquid will be related to the shear rate thought Newton's Law

$$\sigma(t)=\eta\frac{d\gamma(t)}{dt}=\eta\gamma_o\omega\cos(\omega\tau)$$

The linear response of a viscoelastic material always has the stress oscillate at the same frequency as the applied strain, but the stress leads the strain by a phase angle δ

$$\sigma(t)=\sigma_o\sin(\omega t+\delta)$$

In general δ can be frequency dependent with any value in the range $0 \le \delta \le \pi/2$. Solids that obey Newton's Law have δ=0 at all frequencies, while liquids that obey Newton's Law have δ=π/2 at all frequencies. Since the stress is always a sinusoidal function with the same frequency as the strain we can separate the stress into two orthogonal functions that oscillate with the same frequency, one in-phase with the strain and the other out of phase, by π/2, with the strain.

$$\sigma(\tau)=\gamma_o\left[G'(\omega)\sin(\omega t)+G''(\omega)\cos(\omega t)\right]$$

The above equation defines $G'(\omega)$ as the storage modulus and $G''(\omega)$ as the loss modulus. The storage modulus represents storage of elastic energy, while the loss modulus represents the viscous dissipation of that energy. The ratio of storage and loss moduli is the tangent of the phase angle called the loss tangent.

$$\tan\delta=\frac{G''}{G'}$$

A material is viscoelastic if both G' and G" are significant and we can anticipate that when $G' \geq G''$ the material is solid like, and when $G'' \geq G'$ the material is liquid like. For the solid-like the storage modulus is much higher and G' is nearly frequency independent. For the liquid-like fluid the storage modulus is much lower than the loss modulus and it scales with the frequency as $G' \sim \omega^2$, the loss modulus scales with the frequency as $G'' \sim \omega$ (Maxwell model). The low frequency liquid-like region in which G' and G" obey these power law is called the terminal regime.

In the current project dynamic rheological measurements were performed with the use of a strain controlled rheometer in the parallel plate geometry (**Figure 14**) over a temperature range that allowed to study the rheological behavior of the hyperbranched polymers at the melt state. Initially the glass transitions temperature was determined via DSC for all polymers and was found around 18 ^{o}C. Samples were prepared for melt testing by vacuum molding. The samples were placed on a freshly cleaned 8 mm diameter aluminum disk and were placed in a vacuum oven at temperatures between 40 – 60 ^{o}C. Dynamic mechanical measurements were performed using a Rheometric Scientific Ares mechanical rheometer in the parallel plate geometry. The diameter of the plate was 8 mm with a gap spacing from 1 to 1.5 mm over a temperature range 50 – 90 ^{o}C. Experiments were performed under a dry nitrogen atmosphere. Dynamic strain sweeps were performed first in order to determine the regime of linear viscoelasticity followed by dynamic time sweep tests in order to ensure the equilibrium of the samples. Finally frequency sweeps tests were then constructed from 100 to 0.1 s^{-1} for each temperature using a strain corresponding to the linear regime. The time temperature superposition was successfully applied and produced master curves at a reference temperatures of T_{ref} = 60 ^{o}C.

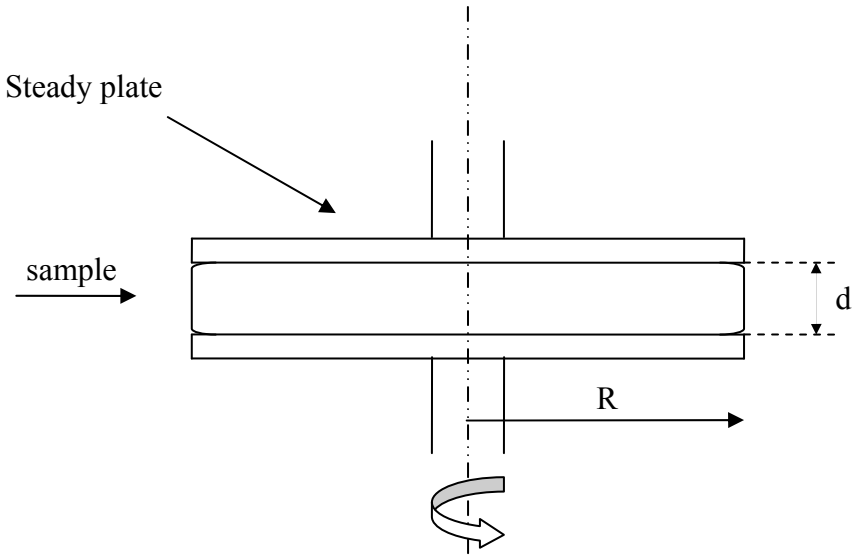

Figure 14. Parallel plate geometry

To model the dynamic shear viscoelasticity of the hyperbranched polymers the dynamic scaling model of Rubinstein et al. [82, 83] was used. This model, is based on the percolation theory and assumes a Rouse model for the polymer chains where hydrodynamic interactions are screened and the polymer chains are unentangled. In the dynamic scaling model of Rubinstein et al the contribution of a molecule with degree of polymerization N to the full complex modulus is obtained by the equation:

$$G^*(\omega) = \frac{d_R G_0}{2} \frac{i\omega}{1-(N_x/N_{char})^{\tau-2}} \times \left[\int_{\varepsilon_{char}}^{\varepsilon_x} \frac{(\varepsilon/\varepsilon_x)^{d_R(\tau-1)/2-1}}{i\omega+\varepsilon} \frac{d\varepsilon}{\varepsilon_x} - \left(\frac{N_x}{N_{char}}\right)^{\tau-2} \int_{\varepsilon_{char}}^{\varepsilon_x} \frac{(\varepsilon/\varepsilon_x)^{(d_R/2)-1}}{i\omega+\varepsilon} \frac{d\varepsilon}{\varepsilon_x} \right]$$

Where G_0 is the shear modulus due to the polymer strand, ε_{char} is the longest relaxation time of the polymer while ε_x is the slow rate cutoff associated with the spacer length between branch points $N_{x,}$ and d_R is the dimension of the relaxation rate spectrum and τ is the Fischer exponent which is calculated by the static scaling form of the number fraction of molar mass

$$n(M) \sim M^{-\tau} f\left(\frac{M}{M_{char}}\right)$$

Where $f(M/M_{char})$ f is a (exponential) cutoff function that cuts off the power law scaling at large mass scales M_{char}. Ficher 's exponent τ is associated with the structure of the polymer and has values $2 < \tau < 3$ indicating that the polymers are above the gel point (polymer gels), while for $1 < \tau < 2$ the polymers are below the gel point and the system is a mixture of branched polymers. In our system τ was found < 2 and assuming that $N_{char} \gg N_x$ the above equation was simplified to

$$G^*(\omega) = \frac{d_R G_0}{2} i\omega \left[\int_{\varepsilon_{char}}^{\varepsilon_x} \frac{(\varepsilon/\varepsilon_x)^{(d_R/2)-1}}{i\omega + \varepsilon} \frac{d\varepsilon}{\varepsilon_x} \right]$$

Chapter 3

Results and discussion

3.1 Synthesis of MTSHEMA

Nuclear magnetic resonance was used to confirm the successful synthesis and the purity of the MTSHEMA inimer. The ^{1}H NMR spectrum of MTSHEMA after synthesis is shown in **Figure 1**.

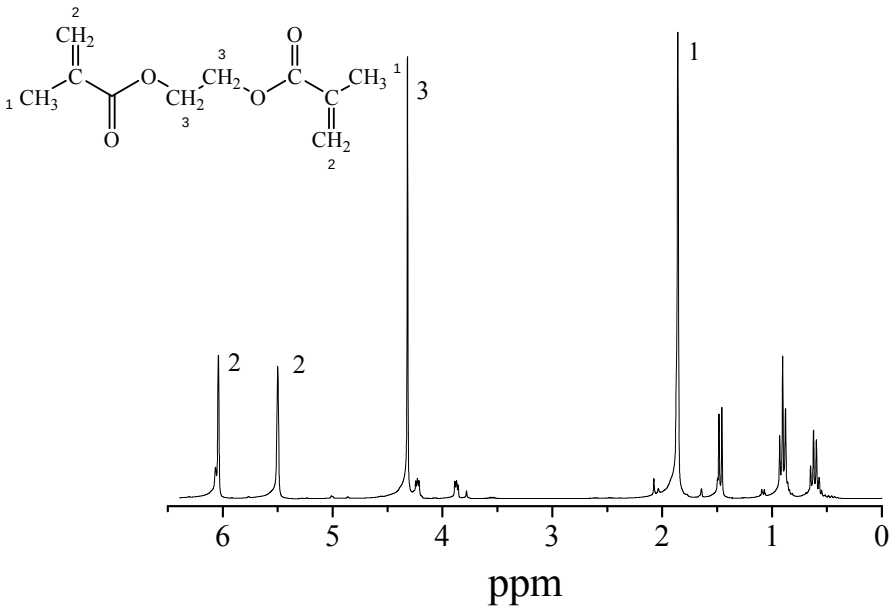

Figure 1. ^{1}H NMR spectrum of MTSHEMA after synthesis in $CDCl_3$

As seen in the above spectrum the peaks attributed to the residual EGDMA are quite intense. These are (500 MHz $CDCl_3$): δ = 1.93 (singlet, 6H, 1); 4.93 (singlet, 4H, 3); 5.5 (singlet, 1H, 2); 6.1 (singlet, 1H, 2). The less intense peaks at 0.5 - 1.5 ppm and 3.5 - 4.2 ppm are attributed to the MTSHEMA. The yield of the reaction was calculated at 76% by comparing the integrals of the peaks at 3.9 ppm attributed to the ethylene linkage protons of MTSHEMA and 4.93 ppm attributed to the ethylene protons of EGDMA.

The ^{1}H NMR spectrum of MTSHEMA after purification is shown in **Figure 2**.

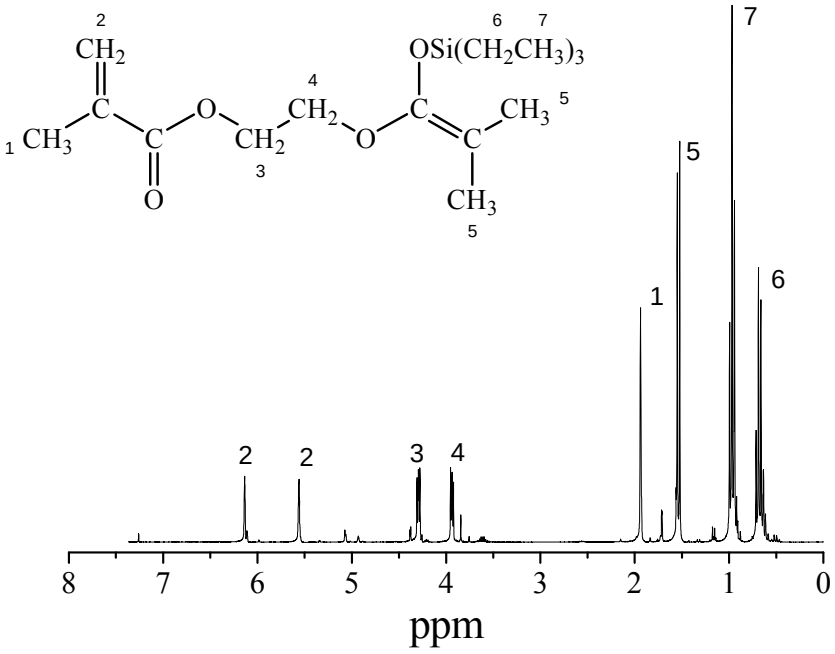

Figure 2. ^{1}H NMR spectrum of MTSHEMA after purification in $CDCl_3$.

The characteristics peaks of MTSHEMA are observed (500 MHz $CDCl_3$): δ = 0.65 (quartet, 6H, 6); 0.95 (triplet, 9H, 7); 1.55 (doublet, 6H, 5); 1.95 (single, 3H, 1); 3.9 and 4.3 (each triplet, each 2H, 3 and 4); 5.5 (singlet, 1H, 2); 6.1 (singlet, 1H, 2). The absence of any additional peaks in the spectrum verifies the purity of the inimer.

3.2 Homopolymerization of MTSHEMA

After its synthesis the polymerization of MTSHEMA was carried out in order to test the functionality of the inimer and prepare a PMTSHEMA hyperbranched polymer. The GPC trace of the PMTSHEMA homopolymer is shown in **Figure 3**

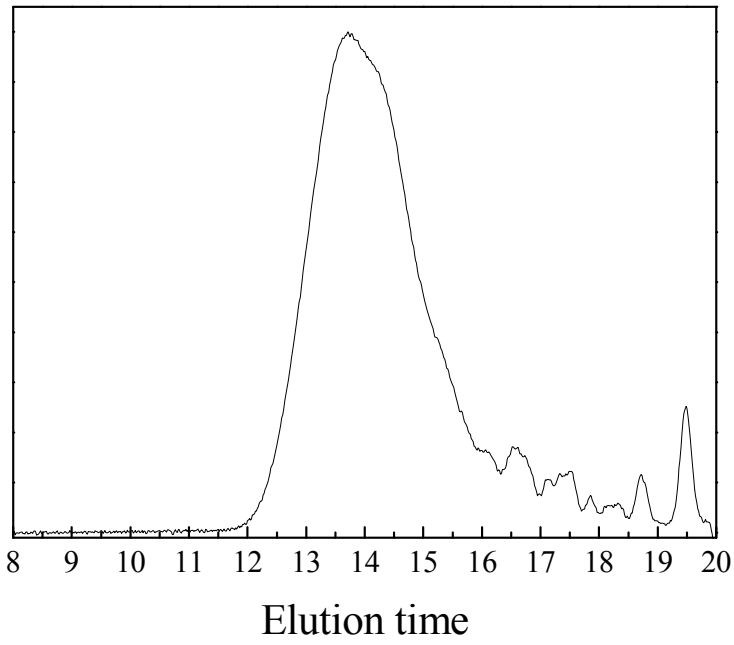

Figure 3. GPC trace of PMTSHEMA synthesized by SCVP.

The molecular weight distribution of PMTSHEMA is broad but unimodal, while the presence of shoulders at higher elution times (low molecular weights) is attributed to oligomers formed at the early stages of the polymerization [84]. The resulting polymer had a molecular weight M_n = 3,600 $gmol^{-1}$ and M_w/M_n = 2.4 (GPC, universal calibration). The molecular structure of PMTSHEMA was confirmed by ^1H NMR and is presented in **Figure 4**

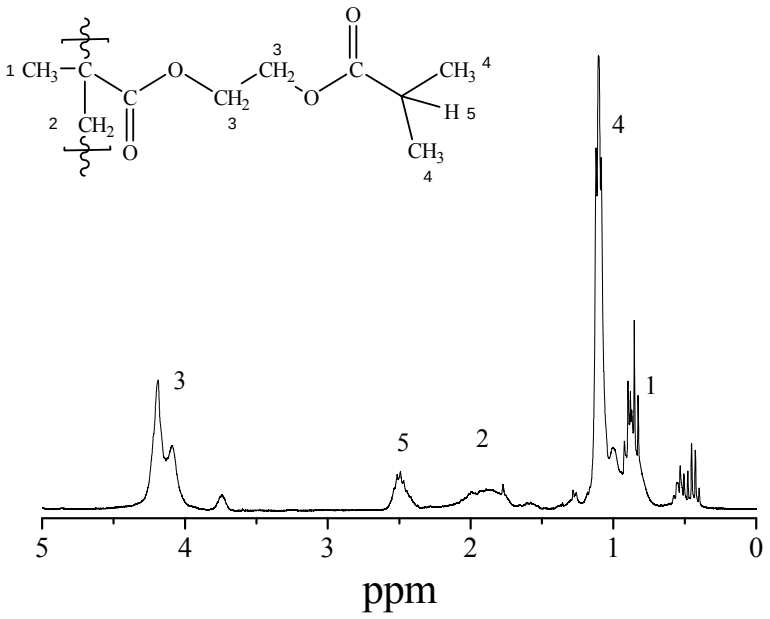

Figure 4. ^{1}H NMR spectrum of PMTSHEMA in $CDCl_3$

The ^{1}H NMR-spectrum of PMTSHEMA shows the following signals (300 MHz $CDCl_3$): δ = 0.85 (3H, 1); 1.1 (6H, 4); 1.9 (2H, 2); 2.4 (1H, 5); 4.1 (4H, 3); the sharp peaks at δ = 0.4-0.5 ppm, and 3.74 are due to the deactivated triethylsilyl acetal units with methanol. Furthermore, ^{1}H NMR analysis did not reveal any definite evidence of branching.

3.3 Copolymerization of MTSHEMA with DMAEMA

The general synthetic route to hyperbranched PDMAEMA is outline in **Figure 5**. The curved lines represent polymer chains. A^*, B^* and M* are active units, whereas a, b, and m are reacted ones. A and M stand for the vinyl groups of the inimer and monomer, respectively.

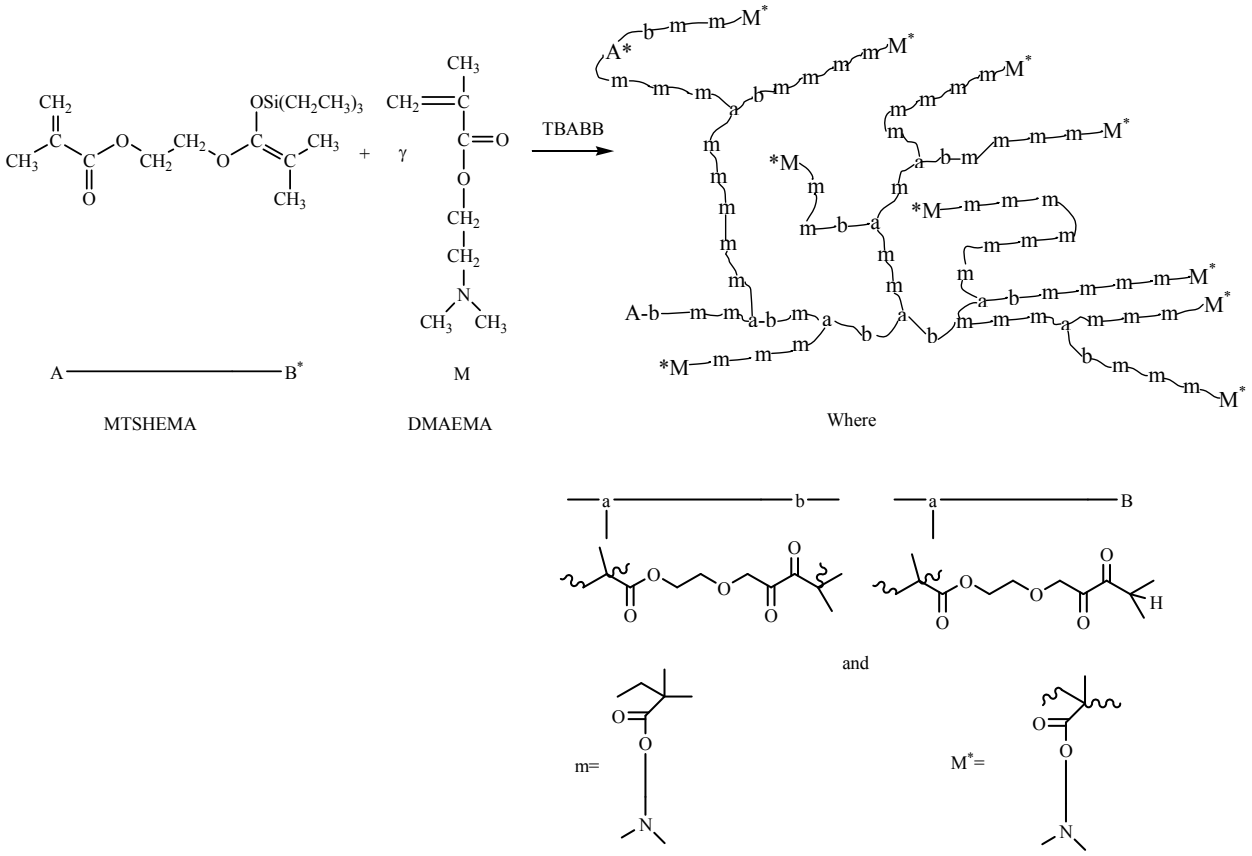

Figure 5. General route to hyperbranched PDMAEMA via self-condensing vinyl copolymerization

3.3.1 Self condensing vinyl copolymerization of MTSHEMA with DMAEMA at $c_{pol.}$ = 20 v/v %

The polymerization conversion and the composition of the HBP copolymers were determined by proton nuclear magnetic resonance (^{1}H NMR) spectroscopy. **Figure 6a** presents the ^{1}H NMR spectrum for PDMAEMA γ=11, $c_{pol.}$ = 20 vv %. The broad peaks at 0.7-1.5 ppm and 1.6-2.2 ppm are attributed to methyl and methylene group of the backbone, respectively. The strong peak at 2.2 ppm is attributed to the methyl protons geminal to the nitrogen atom. The peak at 2.5 ppm is assigned to the methylene group next to the nitrogen atom, while the peak at 4.1 ppm is attributed at the methylene protons next to the oxygen atom. The peaks due to the inimer are also observed. The signal at 3.8–4.4 ppm correspond at the ethylene linkage of the inimer which is overlapping with the peak of the oxymethylene protons of DMAEMA. The composition (ratio γ) of the HBP was calculated by ratioing the integrals of the peak

of the methylene group at 2.5 ppm due to DMAEMA to the signal of the ethylene glycol linkage of the inimer. The conversion of the polymerization was calculated by rationing the peak integrals of the methylene groups at 1.6 - 2.2 ppm due to PDMAEMA to the integrals of the vinyl signals at 5.5 - 6.1 ppm due to residual DMAEMA monomer.

The comonomer composition as described earlier is in good agreement with the comonomer composition in the feed for low γ ratio. However, for higher γ ratios (**Figure 6b)** the comonomer composition cannot be calculated by NMR because the signal of the peaks attributed to the inimer are very low and do not appear in the spectrum. For this reason, the comonomer composition or degree of branching can not be determined directly by NMR analysis. Therefore, other methods will be used to confirm the compact structure of the HBP polymers.

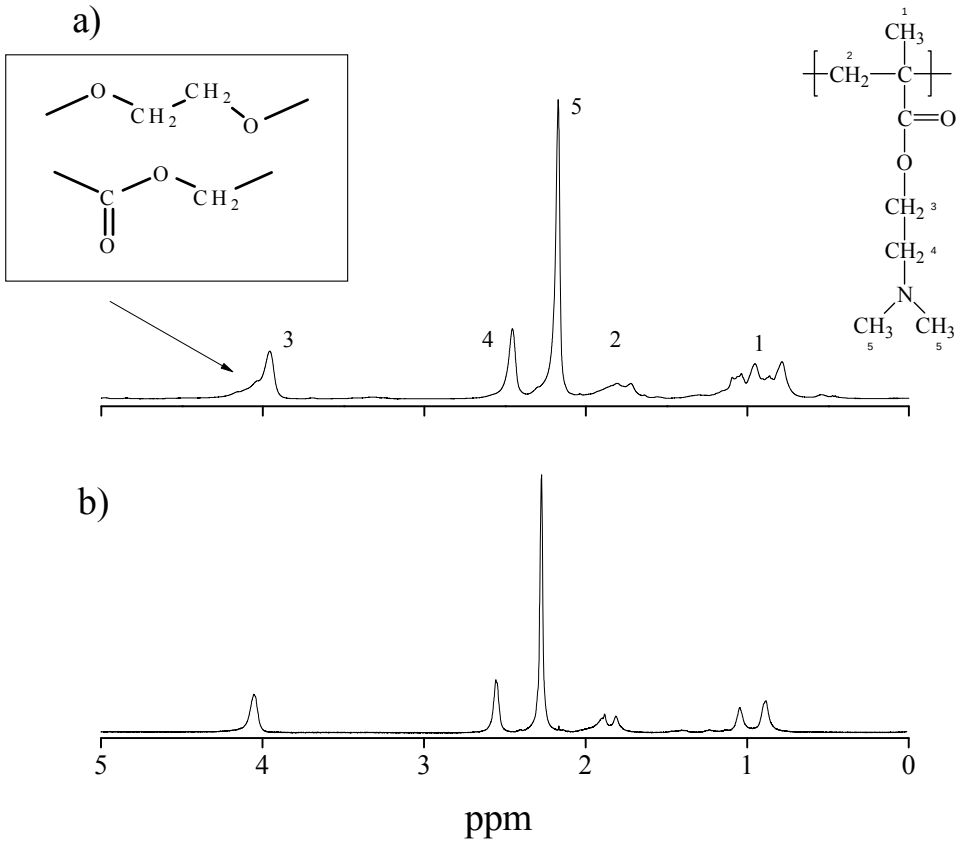

Figure 6. ^{1}H NMR spectra of hyperbranched PDMAEMA a) γ =11 for $c_{pol.}$=20 v/v % and b) γ =80 for $c_{pol.}$=20 v/v % in $CDCl_3$

The GPC traces of the HBP polymers obtained by the copolymerization of MTSHEMA with DMAEMA for different comonomer ratios γ at $c_{pol.}$ = 20 v/v % are shown in **Figure 7**.

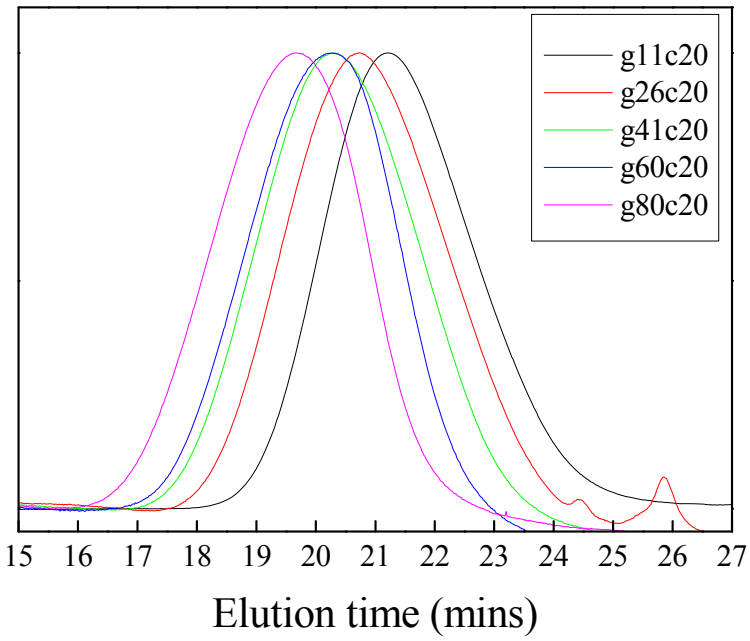

Figure 7. GPC traces of the hyperbranched copolymers of MTSHEMA with DMAEMA prepared at different comonomer ratios at $c_{pol.}$ = 20 v/v %

For all samples unimodal peaks were obtained of almost gaussian distribution. The distribution as a whole shifts to lower elution times when increasing the comonomer ratio γ and thus both the number and the weight-average molecular weights of the copolymers increase with γ, whereas the polydispersity index, M_w/M_n remains almost constant. Similar results were previously obtained for the SCVCP of tert-butyl acrylate with an acrylate inimer via ATRP [85] as well as SCVCP of methyl methacrylate using MTSHEMA as the inimer [28] and SCVCP of 2-(diethylamino)ethyl methacrylate with a methacrylate inimer [86]. The molecular weight of the polymers calculated by conventional GPC and the absolute molecular weight determined by the universal calibration are given in the following table.

Table 1. Molecular weights of the hyperbranched PDMAEMA polymers obtained at different comonomer ratios γ at $c_{pol.}$= 20 v/v %

sample	γ[a]	conversion[b]	M_n[c] (M_w/M_n)	M_n[d] (M_w/M_n)
g11c20	11	97	7,700 (1.6)	6,300 (1.8)
g26c20	26	97	13,000 (1.7)	31,000 (1.9)
g41c20	41	98	15,000 (1.7)	70,000 (2.0)
g60c20	60	99	20,000 (1.7)	97,000 (1.7)
g80c20	80	99	30,000 (1.6)	88,700 (1.9)

[a]γ=[DMAEMA]/[MTSHEMA], [b] Conversion of double blonds as determined by ^{1}H NMR, [c] Determined by GPC (RI detector) using THF as the eluent and linear PMMA standards, [d] Determined by GPC (viscosity detector)

The molecular weights determined by GPC using the universal calibration are higher than to the apparent molecular weights obtained by conventional GPC as expected for the branched polymer structures. The absolute number average molecular weights ranged between 6,300 and 88,700 $gmol^{-1}$, while the polydispersity remains constant at $M_w/M_n \approx 2$. The very high monomer conversion (> 98 %) observed for all γ ratios can be attributed to the low viscosity of the reaction medium due to the low molecular weight of the polymers in which the monomer can diffusive relatively freely.

It is also known that the solution and melt viscosities of branched macromolecules are lower than those of conventional linear polymers [89-91]. The low viscosity is due to the fact that the branched polymer chains are less entangled than the same molecular weight linear polymers due to their spherical shapes. The intrinsic viscosity versus the molecular weight for the branched polymers prepared in this study are shown schematically in **Figure 8**. The intrinsic viscosity versus molecular weight for linear PDMAEMA of the same range of molecular weights is also shown for comparison.

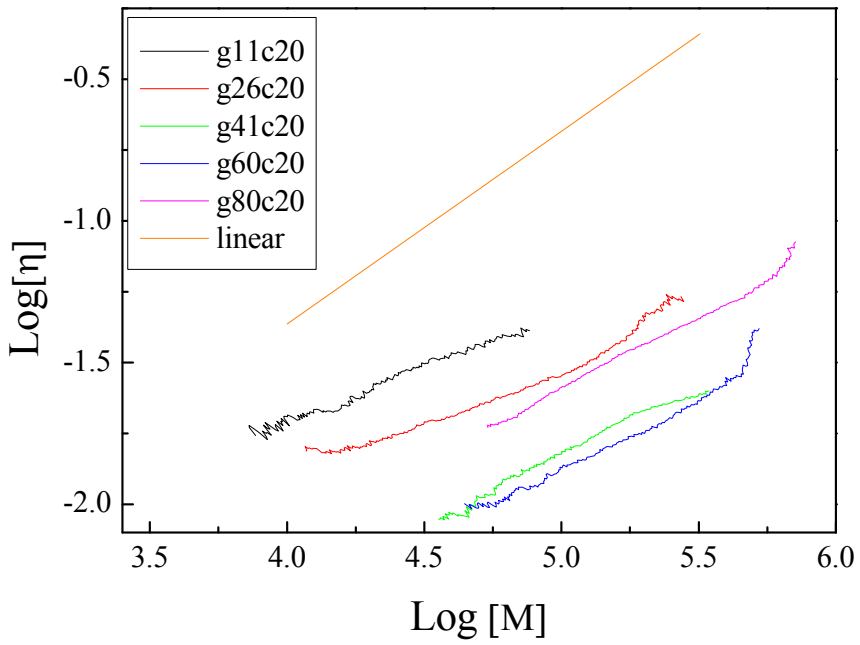

Figure 8. Mark-Houwink plot for the hyperbranched PDMAEMA polymers at different comonomer ratios and at $c_{pol.}$ = 20 v/v %. The respective plot for linear PDMAEMA is also shown for comparison.

As seen in **Figure 8** the viscosities of the branched polymers are significantly lower compared to those of linear PDMAEMA of the same range of molecular weights which suggests a highly compact structure for the branched polymers in solution. Besides, the Mark–Houwink exponent α of the branched polymers is significantly lower (α = 0.2-0.5) compared to that for the linear PDMAEMA (α = 0.6) consistent again with the compact structure of the HBPs. However, as seen in **Figure 8** the intrinsic viscosities of the branched polymers are not monotonous with the ratio γ. It would be expected that as γ increases (lower degree of branching) the intrinsic viscosity of the polymer would increase. It would also be expected, as other studies have shown [85, 86, 92], that the intrinsic viscosities should increase when increasing the molecular weight. This anomalous behavior will be investigated further using dilute viscometry measurements, in a section below.

Data from GPC-LALLs have also provided some additional information regarding the polymer structure [93]. The GPC elution time depends on the molecular weight of the branched polymers. Due to the compact structure of the hyperbranched polymers their elution times should be much higher compared to that of a linear

polymer of the same absolute molecular weight. Thus, comparison of the absolute molecular weights of the hyperbranched and linear PDMAEMA samples versus their elution time plots should reveal differences in the molecular structure, of the polymers attributed to the different degrees of branching. **Figure 9** shows the absolute molecular weights versus elution time for the hyperbranched PDMAEMAs and a linear polymer. Indeed the elution times for the branched polymers are different from those of the linear analogues thus confirming differences in the polymer structure. These results support the conclusion that the synthesized polymers are highly branched because the logM versus elution time plots lie significantly above that for the linear PDMAEMA. Note that as discussed above the traces of the branched PDMAEMAs do not follow a monotonous trend with the comonomer ratio γ.

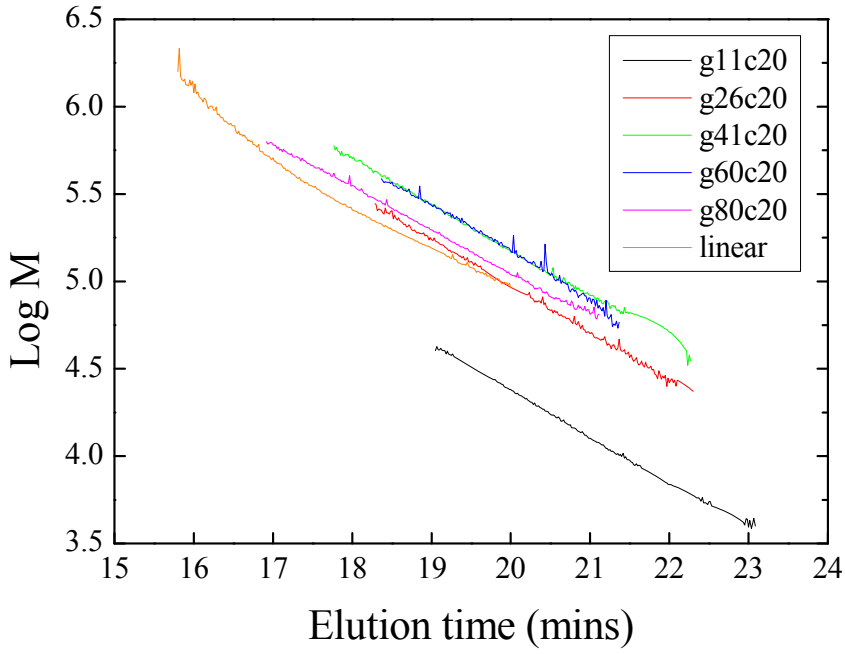

Figure 9. Semi logarithmic plot of the absolute molecular weight versus elution time for the hyperbranched and a linear PDMAEMA

3.3.2 Self condensing vinyl copolymerization of MTSHEMA with DMAEMA at $c_{pol.}$ = 80 v/v %

In order to investigate the influence of the monomer concentration in the polymerization reaction on the branching and the molecular weights of the polymers, polymerizations where performed for the same γ ratios at an initial monomer concentration $c_{pol.}$ = 80 v/v %. The GPC traces of the hyperbranched PDMAEMAs prepared at $c_{pol.}$= 80 v/v % are presented in **Figure 10**.

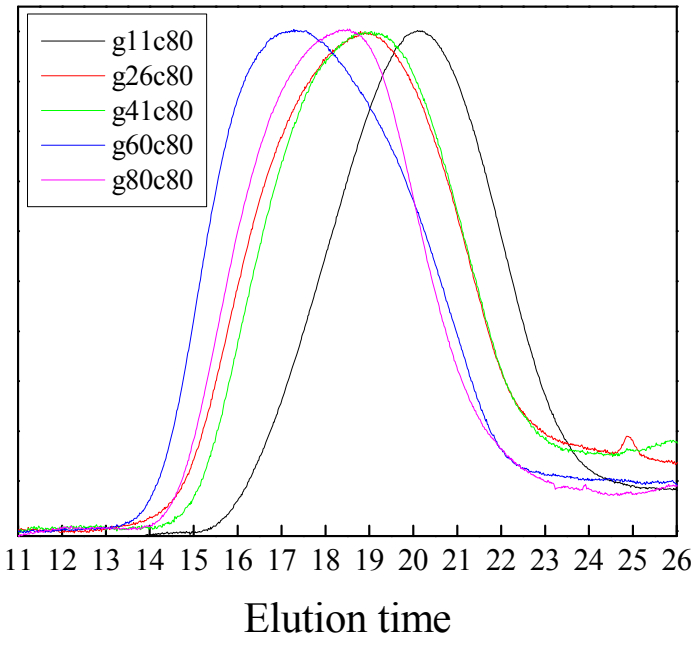

Figure 10. GPC traces of the hyperbranched PDMAEMA polymers prepared at different comonomer ratios γ at $c_{pol.}$ = 80 v/v %

In this case the polymers elute at elution times suggesting higher molecular weight polymers. Moreover, the peak does not shift monotonously to lower elution times as the ratio γ increases as was discussed above for $c_{pol.}$= 20 v/v %. The molecular weights calculated by the conventional and universal calibration are given in **Table 2**.

Table 2. Molecular weights of the hyperbranched PDMAEMAs prepared at different comonomer ratios γ at $c_{pol.}$= 80 v/v %

sample	γ[a]	conversion[b] (%)	M_n[c] (M_w/M_n)	M_n[d] (M_w/M_n)
g11c80	11	97	24,000 (2.7)	42,000(2.9)
g26c80	26	97	59,000 (3.9)	65,000(6.6)
g41c80	41	98	52,000 (2.9)	81,000(3.4)
g60c80	60	99	65,000 (3,2)	146,003(4.6)
g80c80	80	99	70,000 (2.8)	121,000(4.5)

[a]γ=[DMAEMA]/[MTSHEMA], [b] Conversion of double blonds as determined by ^{1}H NMR, [c] Determined by GPC (RI detector) using THF as the eluent and linear PMMA standards [d] Determined by GPC (viscosity detector)

For $c_{pol.}$= 80 v/v % the absolute number average molecular weights were higher than those obtained at $c_{pol.}$= 20 v/v % and increased from 42,000 to 146,000 gmol^{-1} with increasing the ratio γ. Also higher polydispersities were calculated which are attributed to the slower monomer diffusion in the concentrated reaction medium. Almost complete polymerization conversion (> 97 %) was detected via ^{1}H NMR. **Figure 11** shows the intrinsic viscosities of the hyperbranched PDMAEMAs. In all cases the viscosity of the HBPs are lower compared to that of linear PDMAEMA as expected, however, they do not follow a monotonous trend with the polymer molecular weight and the ratio γ.

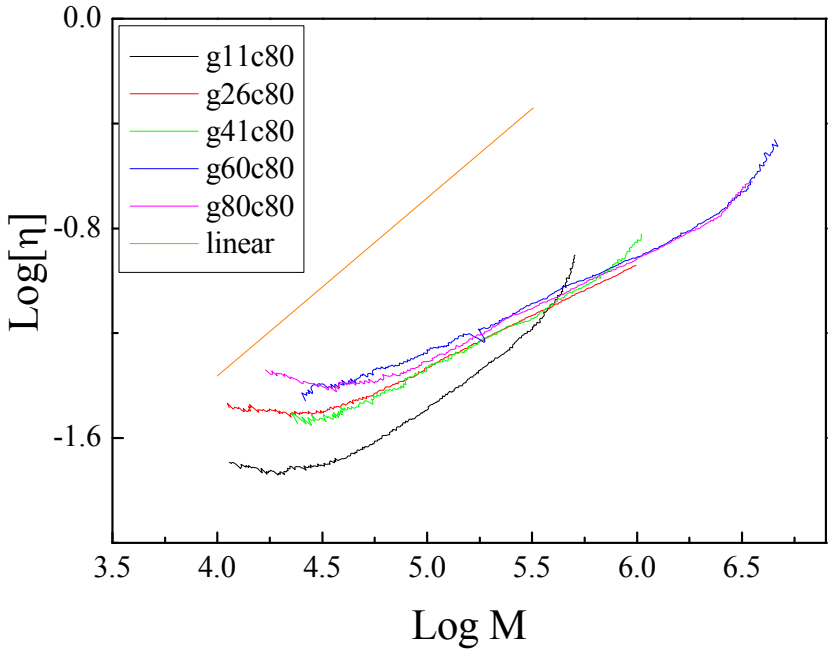

Figure 11. Mark-Houwink plot for the hyperbranched PDMAEMA polymers at different comonomer ratios and at $c_{pol.}$ = 80 v/v %. The respective plot for a linear PDMAEMA is also shown for comparison.

The Mark–Houwink exponent α of the branched polymers at $c_{pol.}$ = 80 v/v % is significantly lower (α = 0.2-0.5) compared to that for the linear PDMAEMA (α = 0.6) consistent again with the compact structure of the HBPs. As discussed above for the branched polymer prepared at c = 20 % the absolute molecular weight versus elution time curves for the branched polymers lie significantly above the one for linear PDMAEMA as seen in **Figure 12** suggesting that the synthesized polymers possess a branched structure.

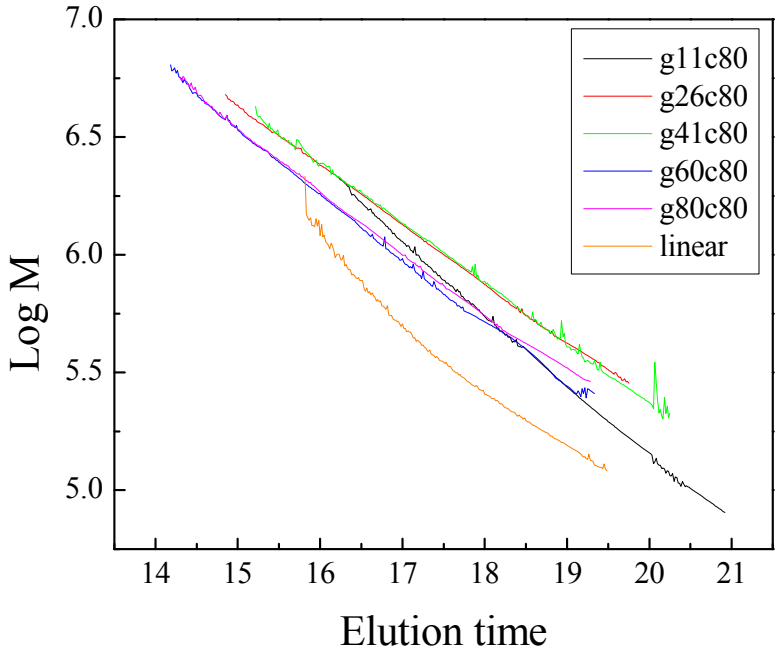

Figure 12. Semi logarithmic plot of the molecular weight vs elution time for the hyperbranched and linear PDMAEMA ($c_{pol.}$ =80 v/v %).

3.3.3 Self condensing vinyl copolymerization of MTSHEMA with DMAEMA in the bulk

Finally the SCVCP of MTSHEMA with DMAEMA in the absence of solvent was studied.

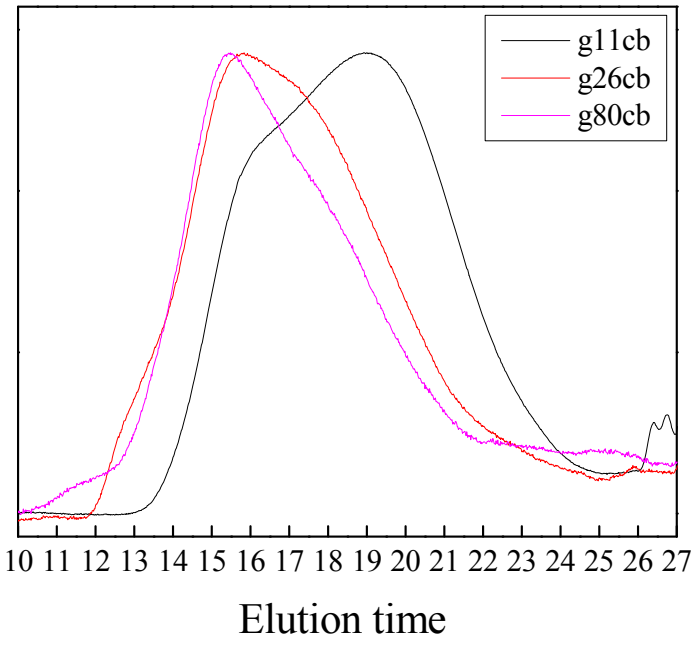

Figure 13. GPC traces of the hyperbranched copolymers of MTSHEMA with DMAEMA prepared in the bulk at different comonomer ratios

The GPC traces (**Figure 13**) of the hyperbranched copolymers prepared in bulk at different comonomer ratios γ show very broad almost bimodal distributions which are shifted to lower elution times in comparison to those obtained for the hyperbranched PDMAEMA 's synthesized at $c_{pol.}$ = 20 v/v % and $c_{pol.}$ = 80 v/v % suggesting non-uniform reaction kinetics possibly due to diffusion limitations at the later stages of the polymerization. It should also be noted that the conversion of the polymerizations as calculated by ^{1}H NMR were very low (8 - 10 %) (**Table 3**) verifying the slow monomer diffusion.

Table 3. Molecular weights of the hyperbranched PDMAEMA polymers obtained at different comonomer ratios γ, in the bulk

sample	γ^{a}	conversion^{b} (%)	$M_n{}^{c}$ (M_w/M_n)
g11b	11	8	43,000 (9.29)
g26b	26	9	146,000(19.56)
g80b	80	10	650,000 (9.12)

[a] γ=[DMAEMA]/[MTSHEMA] [b] Conversion of double blonds as determined by ^{1}H NMR [c] Determined by GPC (viscosity detector)

For the polymerizations in the bulk the absolute number molecular weights of the hyperbranched PDAMEMAs were higher than those obtained for the copolymers at $c_{pol.}$= 20 v/v % and $c_{pol.}$= 80 v/v % and range from 43,000 to 650,000 gmol^{-1} when increasing the ratio γ. The high polydispersities observed for the polymers prepared in the bulk are attributed to the absence of a polymerization solvent. In the early stage of the reactions the monomer plays the role of the solvent. However, as the monomer is consumed and the polymer molecular weight increases the viscosity of the reaction medium increases resulting in slow diffusion rates and thus very high polydispersities and low monomer conversion as discussed above. In other words for the polymer synthesized in the bulk the diffusion of monomer to growing polymer end becomes very slow already at low monomer conversions [94, 95].

3.4 Self condensing vinyl copolymerization of MTSHEMA with DMAEMA in the presence of a monofunctional initiator

Theoretical and experimental work [28, 96] has reported that the presence of an f-functional initiator, $G_{f,}$ which contains only initiating B* moieties, should further increase the control exerted over the molecular weight distribution and leads to polymers with narrower molecular weight distributions and higher degrees of branching if the AB* monomer is added slowly (semibatch conditions). We thus prepared a series of hyperbranched PDMAEMA polymers using MTSHMEA inimer, DMAEMA monomer and MTS as a common monofunctional GTP initiator.

μ is defined as the comonomer-to-initiator ratio and is equal to:

$$\mu = \frac{M_0 + I_0}{G_0}$$

Where, M_0, I_0 and G_0 represent the initial concentration of monomer, inimer and monofunctional initiator, respectively. **Figure 14** shows the GPC traces of the three

hyperbranched PDMAEMA polymers prepared at different ratios μ and a constant ratio γ = 26

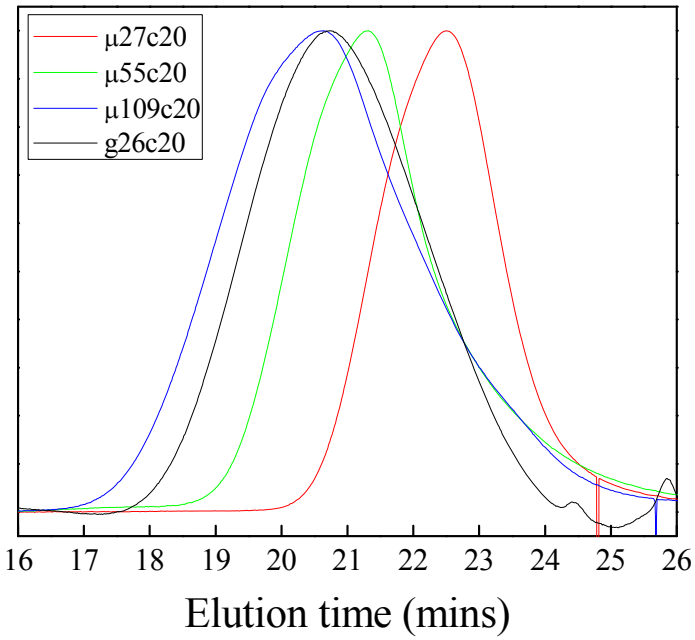

Figure 14. GPC traces of the hyperbranched PDAMEMA polymers prepared at different ratios of comonomer to initiator and a constant comonomer ratio γ =26. The trace for γ=26 in the absence of added monofunctional initiator is also shown for comparison.

The elution times shift to lower values for higher μ ratios suggesting an increase of the molecular weight (**Table 4**) when increasing the ratio μ. Moreover, for low μ ratios the molecular weight distribution is significantly lower while it becomes broader when μ increases. Compared to γ = 26 in the absence of monofunctional initiator the use of the initiator permitted a better control over the molecular weight distribution, in particular for low μ ratios, in agreement with the literature.

Table 4. Molecular weights of hyperbranched polymers for different comonomers/initiator ratios μ at a constant comonomer ratio γ = 26

sample	μ^a	$M_n{}^b$ (M_w/M_n)	$M_n{}^c$ (M_w/M_n)
μ27c20	27	4,500 (1.4)	6,400 (1.3)

μ55c20	55	8,800 (1.8)	10,000 (1.7)
μ109c20	109	11,500 (2.4)	12,000 (2.2)

[a] $\mu = \frac{M_0 + I_0}{G_0}$, [b] GPC Conventional, [c] GPC universal calibration

The absolute number average molecular weights range from 6,400 to 12,000 $gmol^{-1}$ which are comparable with the number average molecular weight calculated from the convetional GPC indicating a less branched structure. The polydispersity index increases systematically from 1.3 to 2.2 when increasing the ratio μ.

3.5 Synthesis of hyperstar polymers

The synthetic route to hyperstar polymers comprising a hyperbranched PDMAEMA core and linear –OH functioanalized precursor chains in the shell is outlined in **Figure 15**

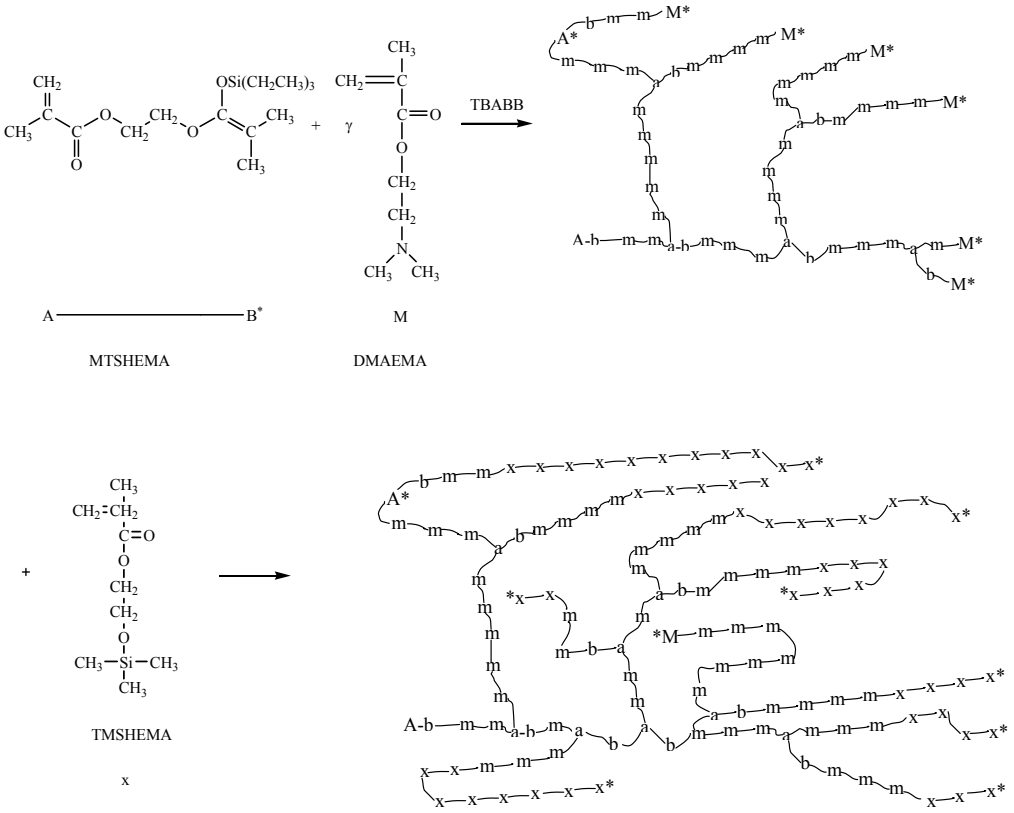

Figure 15. General synthetic route for the preparation of hyperstar polymers via self-condensing vinyl copolymerization

The curved lines represent polymer chains. A^*, B^* and M* are active units, whereas a, b, and m are reacted sites belonging to the MTSHEMA inimer and the DMAEMA monomer, respectively, whereas x stands for the reacted monomer of TMSHEMA and x* for the active TMSHEMA chain ends. The GPC traces of the hyperstar polymers prepared using two different ratio γ for the synthesis of the hyperbranched core are presented in **Figure 16**.

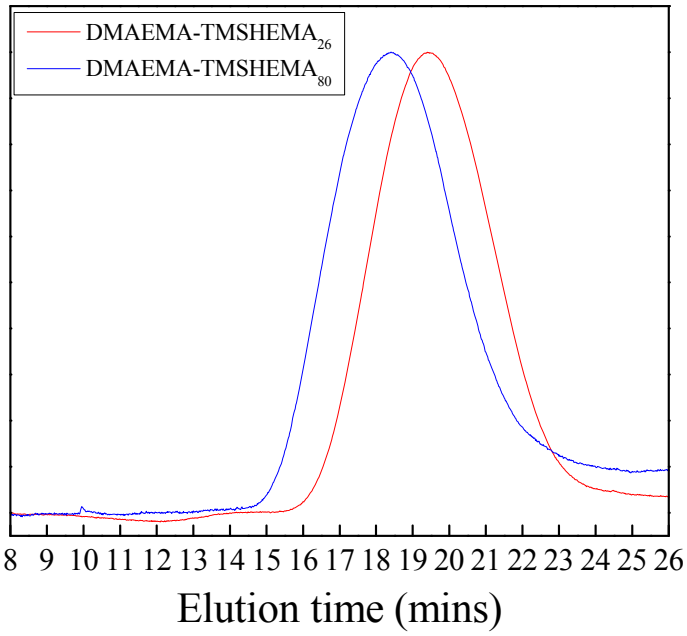

Figure 16. GPC traces of the hyperstar PDMAEMA core - TMSHEMA-shell for different ratios of the precursor γ

As seen in **Figure 16** the peak maximum of the hyperstar polymers is shifted to lower elution times increasing the ratio γ of the PDMAEMA precursors. The molecular weights of the hyperstar polymers calculated from the GPC data by conventional and universal calibration are shown in **Table 5**.

Table 5. Molecular weights of the PDMAEMA-core TMSHEMA-shell hyperstar polymers prepared from hyperbranched cores of different comonomer ratios γ

Sample	M_n [a] (M_w/M_n)	M_n [b] (M_w/M_n)
PDMAEMA-TMSHEMA$_{26}$	36,000 (2.9)	68,000 (1.7)
PDMAEMA-TMSHEMA$_{80}$	68,000 (2.1)	310,000 (1.7)

[a] Determined by GPC (RI detector) using THF as the eluent and linear PMMA standards [b] Determined by GPC (viscosity detector)

The molecular weights calculated using the universal calibration were significantly higher compared to those obtained from the conventional calibration which is consistent with the branched structure of the polymers. The absolute number average molecular weights were found 68,000 and 310,000 gmol^{-1}, respectively while the polydispersity was high and similar for the two polymers. The measured intrinsic viscosities plotted against the molecular weights of the polymers gave the Mark-Houwink plots shown in **Figure 17.**

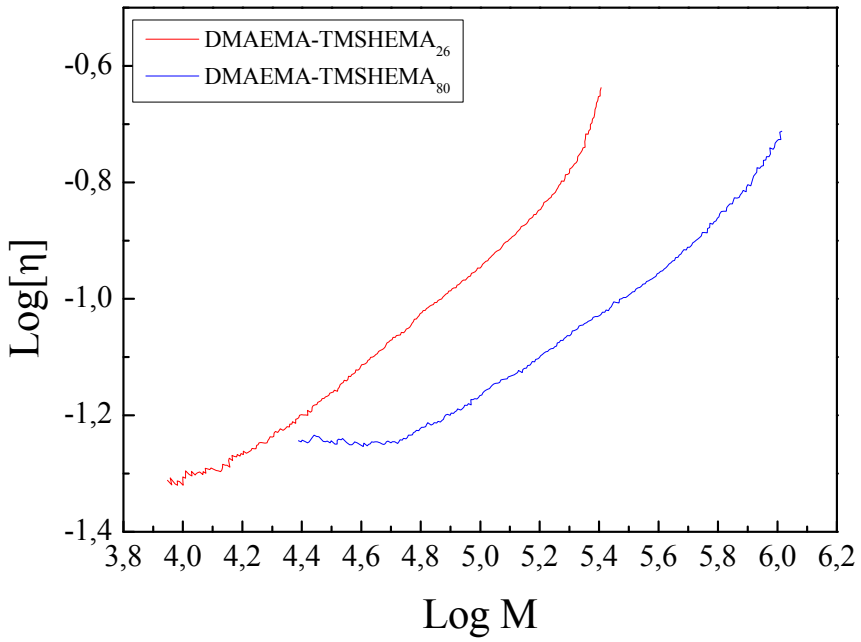

Figure 17. Mark-Houwink plot of the hyperstar DMAEMA-core TMSHEMA-shell hyperstar copolymers

The branched polymer structure is corroborated by the low Mark-Houwink exponent α ~0.35 calculated for both hyperstar polymers.

3.6 Characterization in organic solvents

3.6.1 Dynamic light scattering (DLS)

Next, the HBPs were characterized by DLS in organic media to investigate the effect of the solvent on the polymer state in solution. **Figure 18** shows characteristic autocorrelation functions of the scattered intensity for g41c20 at different scattering angles and c = 0.4 wt % in THF.

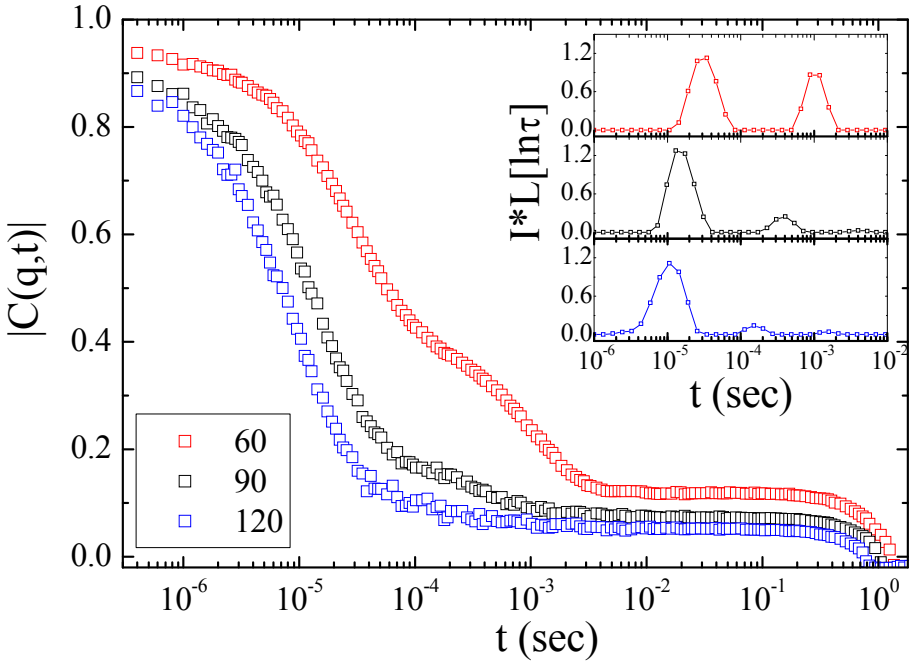

Figure 18. Intensity autocorrelation functions for g41c20 in THF c = 0.4 wt % and scattering angles 60º (□), 90º (□) and 120º (□). Inset: distribution of relaxation times multiplied by the total scattering intensity (normalized to that of toluene).

From the analysis of the autocorrelation functions two processes are clearly observed. The first process with a hydrodynamic radius R_{h1}= 4 nm (fast process) is attributed to the HBP polymer, while the second process with a hydrodynamic radius of R_{h2} = 80

nm (slow process) is attributed to the formation of polymer aggregates in the solvent medium. From the q-dependence of the intensity a radius of gyration of R_g ~ 96 nm was calculated for the slow process. Similar results were obtained for all the HBPs in THF suggesting polymer aggregation in the medium. DLS measurements were also performed at c = 0.4 wt % in acetone which is more polar solvent compared to THF. **Figure 19** shows the autocorrelation functions for g41c20 in acetone, c = 0.4 wt % at different scattering angles.

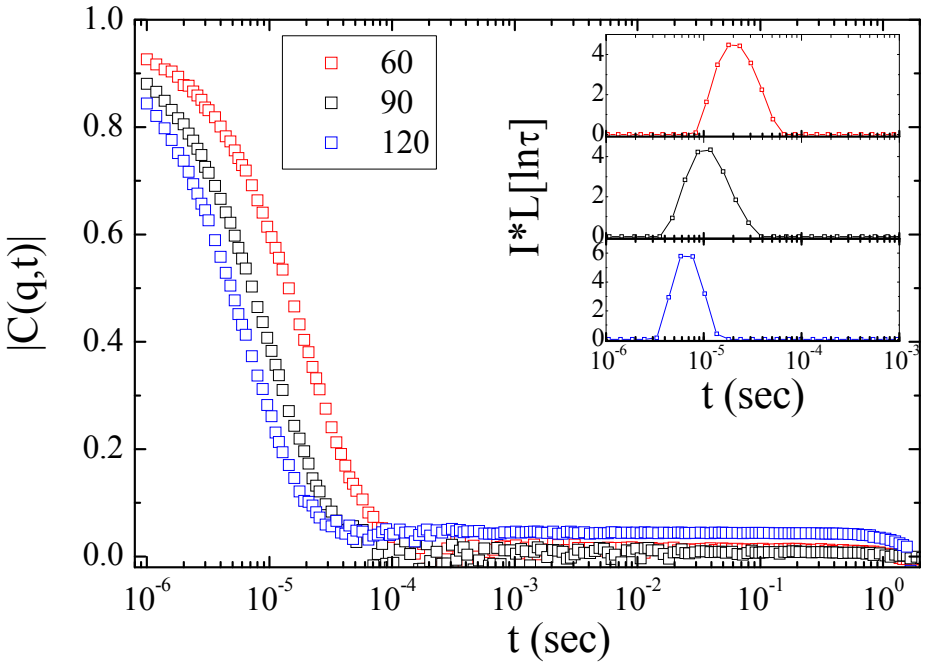

Figure 19. Intensity autocorrelation functions for g41c20 in acetone, c = 0.4 wt % for scattering angles 60º (□), 90º (□) and 120º (□). Inset: distribution of relaxation times multiplied by the total scattering intensity (normalized to that of toluene).

In this case a single process dominates the autocorrelation functions which corresponds to a hydrodynamic radius R_h= 4 nm. The presence of a single process was also verified for all the hyperbranched PDMAEMAs in acetone.

Table 6 summarizes the DLS results in acetone for hyperbranched PDMAEMAs preapared at $c_{pol.}$ = 20 v/v %.

Table 6. Absolute molecular weights (in THF) and hydrodynamic radii in acetone of the hyperbranched PDMAEMAs copolymers prepared at c = 20 v/v %

Sample	M_n(gr/mol) [a]	R_h (nm)
g11c20	6,300	2.6
g26c20	31,000	3.5
g41c20	70,000	4.0
g60c20	97,000	5.0
g80c20	88,700	5.0

[a] Determined by GPC (viscosity detector)

The hydrodynamic radii of the hyperbranched PDMAEMAs (**Table 6**) increase systematically from 2.6 nm to 5 nm when increasing the γ ratio. This is attributed to both the increase of the polymer molecular weight (calculated by GPC) and the decrease of the degree of branching as γ increases.

Table 7 presents the hydrodynamic radii in acetone obtained by DLS for the hyperbranched PDMAEMA prepared at $c_{pol.}$ = 80 v/v %.

Table 7. Absolute molecular weights (in THF) and hydrodynamic radii in acetone of the hyperbranched PDMAEMA copolymers prepared at c = 80 v/v %

Sample	M_n(gr/mol) [a]	R_h (nm)
g11c80	42,000	7.8
g26c80	65,000	15.5
g41c80	81,000	15.8
g60c80	146,003	15.0
g80c80	121,000	12.0

[a] Determined by GPC (viscosity detector)

Similarly, DLS results in acetone gave a single process for the HBPs prepared at $c_{pol.}$ = 80 v/v %. The R_h is again found to increase from 7.8 nm to 15.8 nm for g11c80 to g41c80 while for g60c80 and g80c80 it decreases to 15.0 and 12 nm respectively. It is noted that the R_h values for the polymers prepared at $c_{pol.}$ = 80 v/v % are always higher than these obtained for the polymers prepared at $c_{pol.}$ = 20 v/v % at the same ratio. This is consistent with the GPC results which showed higher molecular weights for the polymers prepared at c = 80 v/v % compared to those prepared at $c_{pol.}$ = 20 v/v % (**Table 6,7**).

3.6.2 Capillary viscosity measurements

In order to investigate further the unusual solution viscosity behavior of the hyperbranched PDMAEMAs (see **Figure 8, 11** and the relative discussion in the text), the effect of the apparent molar mass of the polymer on its specific solution viscosity in THF was investigated for the hyperbranched PDMAEMAs as a function of polymer concentration via capillary viscosity measurements.

Figure 20 shows a reduced viscosity for g80c20 in the concentration range from 10^{-3} to 10^{-2} gr/ml in THF.

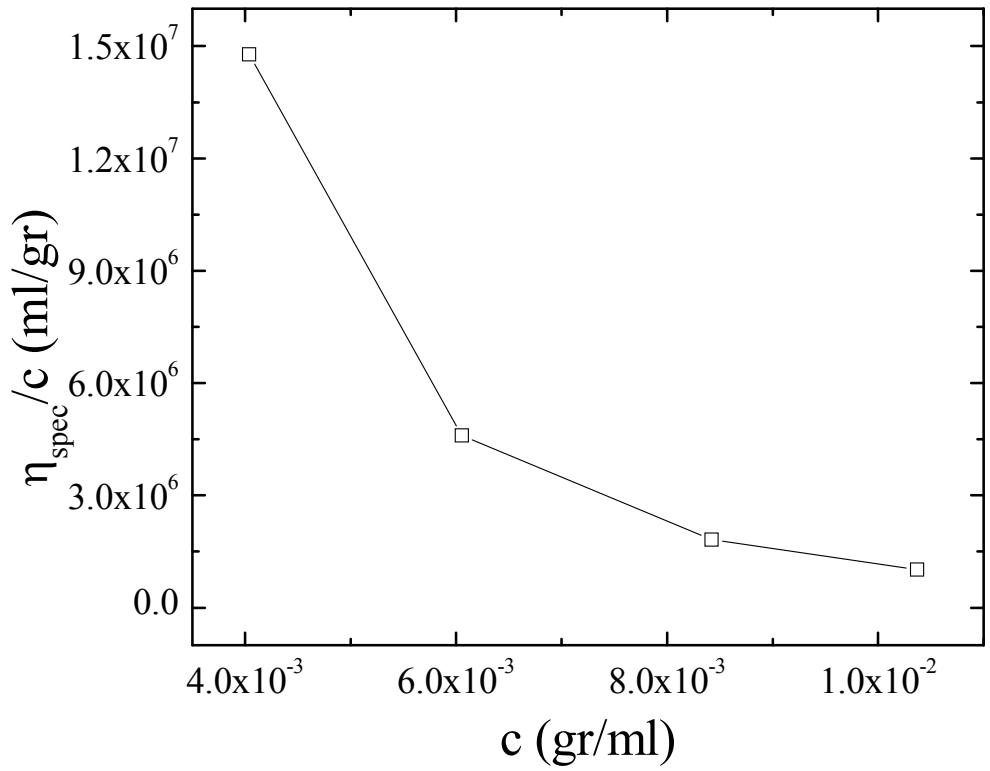

Figure 20. Reduced viscosity versus polymer concentration for g80c20

In THF PDMAEMA is not charged and thus we anticipated to use the Huggins and Krammer equations to determine the intrinsic viscosity of the polymer. In contrast, the reduced viscosity profile (see **Figure 20**) showed a polyelectrolyte behavior characterized by a sharp increase of the reduced viscosity in the low concentration

range [78, 97]. These curves could not be extrapolated to zero concentration in order to determine the intrinsic viscosity of the polymer. A similar behavior was also found in other organic solvents such as acetone, DMF, and acenotonitrile. Previous studies have investigated highly charged quaternized PDMAEMA homopolymers via capillary viscosity measurements in water and have shown a similar behavior [60, 98]. In these studies the polyelectrolyte behavior was attributed to the strong polyelectrolyte effect which causes the expansion of the polymeric chain due to the enhanced dissociation of the ionizable groups at lower polymer concentration. These studies concluded that at low polymer concentration the intramolecular repulsive interactions between the ionized groups are stronger and spread all along the chain. However in the case of the neutral PDMAEMA in organic media investigated herein the polyelectrolyte-like behavior evident in the solution viscosity measurements, cannot be explained and further investigation is required to reveal possible polymer-solvent interactions and their dependence on the polymer concentration, the polymer molecular weight and the polarity of the solvent.

3.7 Characterization in aqueous solution

3.7.1 pH responsive behaviour of the hyperbranched PDMAEMA copolymers

Titration curves were constructed in order to examine the response of the hyperbranched PDMAEMA polymers to pH changes and investigate their behaviour in acidic and basic environment. DMAEMA is an ionisable monomer possessing a tertiary amine unit which behaves as a weak base and participates in a weak acid-base equilibrium upon changing the solution pH. The deprotonation of $PDMAEMA^+$ upon the addition of base is illustrated in **Figure 21**.

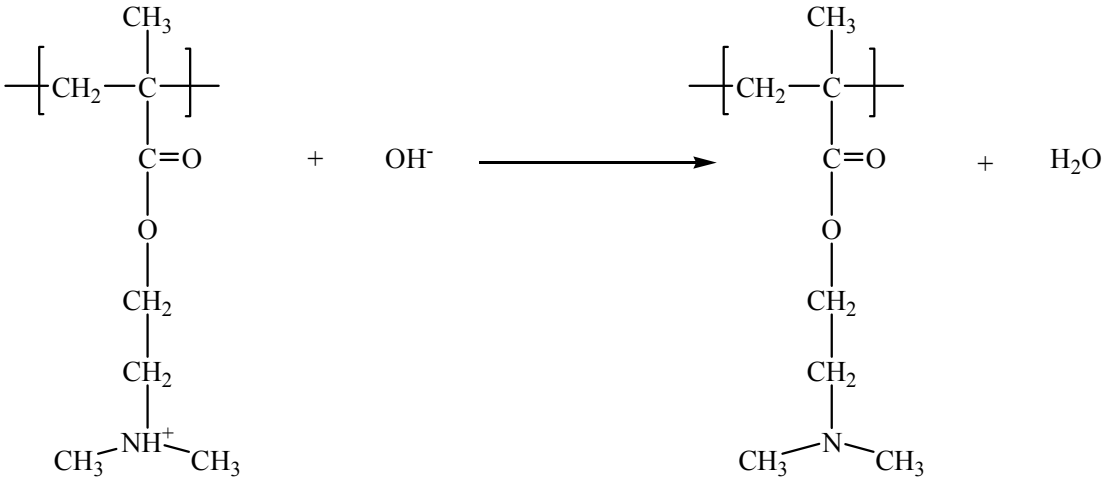

Figure 21. Deprotonation of PDMAEMA$^+$ upon the addition of base

At low pH the polymer is fully ionized and water soluble, while upon increasing the solution pH the PDMAEMA$^+$ units become deprotonated. This reversible ionization process results in the appearance of a plateau in the titration curve of PDMAEMA which is located at a pH range between 4 and 8 (the effective pK_a of PDMAEMA$^+$) originating from the buffer in capacity of the weak polyelectrolyte. This is shown clearly in **Figure 22**. The base added at the beginning of the titration (pH < 3) neutralizes the excess acid in the solution. However, at pH around 3, the addition of base causes a rapid increase of the pH to a value of ~ 5. At this point further addition of base results in the deprotonation of the amine groups and the slight increase of the pH (plateau region). Finally, when the PDMAEMA units have become fully deprotonated an abrupt increase of the solution pH is observed due to the excess base added in the solution.

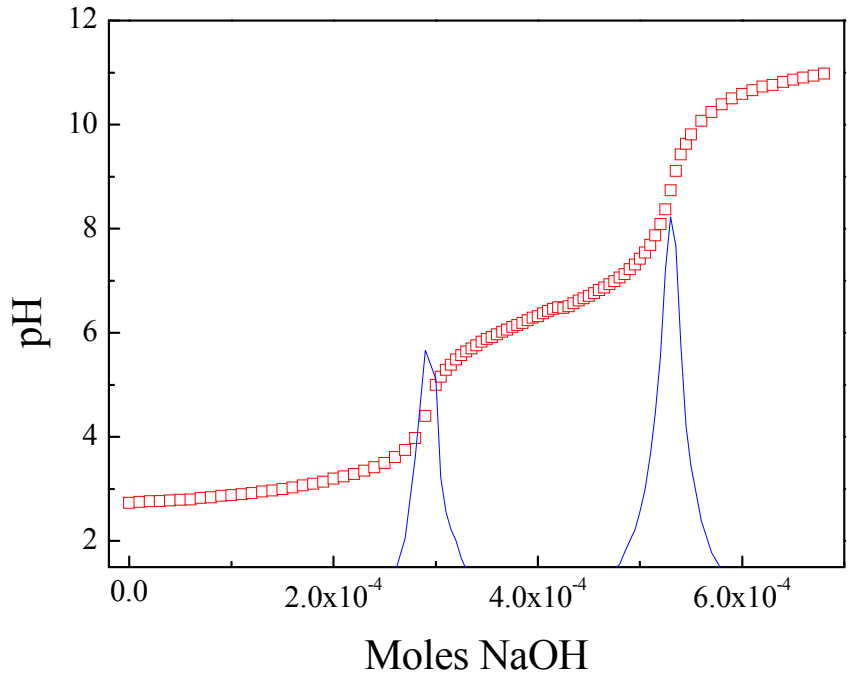

Figure 22. Titration curve for g11c80 at c = 0.1 wt %. The blue line is the first derivative of the titration data

As discussed in Chapter 2 the degree of ionization is defined as the ratio of the concentration of the ionized monomer repeat units divided by the concentration of the total monomer repeat units in the solution. For PDMAEMA the degree of ionization/protonation is expressed as

$$\alpha = \frac{\left[\mathrm{DMAEMA^+}\right]}{[\mathrm{DMAEMA}] + [\mathrm{DMAEMA^+}]}$$

Where $\left[\mathrm{DMAEMA^+}\right]$ is the concentration of protonated DMAEMA repeat units and [DMAEMA] is the concentration of deprotonated DMAEMA repeat units. The effective pK_a value of the protonated tertiary amine units is defined by the equation

$$\mathrm{pH} = \mathrm{pK}_{\alpha} + \log\frac{[\mathrm{DMAEMA^+}]}{[\mathrm{DMAEMA}]}$$

At the midpoint of the plateau region the concentration of $\left[\mathrm{DMAEMA}^{+}\right]$ is equal to the concentration of [DMAEMA] and the second term of the above equation becomes zero allowing the determination of the pK_a value. Practically, the pK_a value can be determined by a diagram of the solution pH versus the degree of protonation (α) at $\alpha=\frac{1}{2}$.

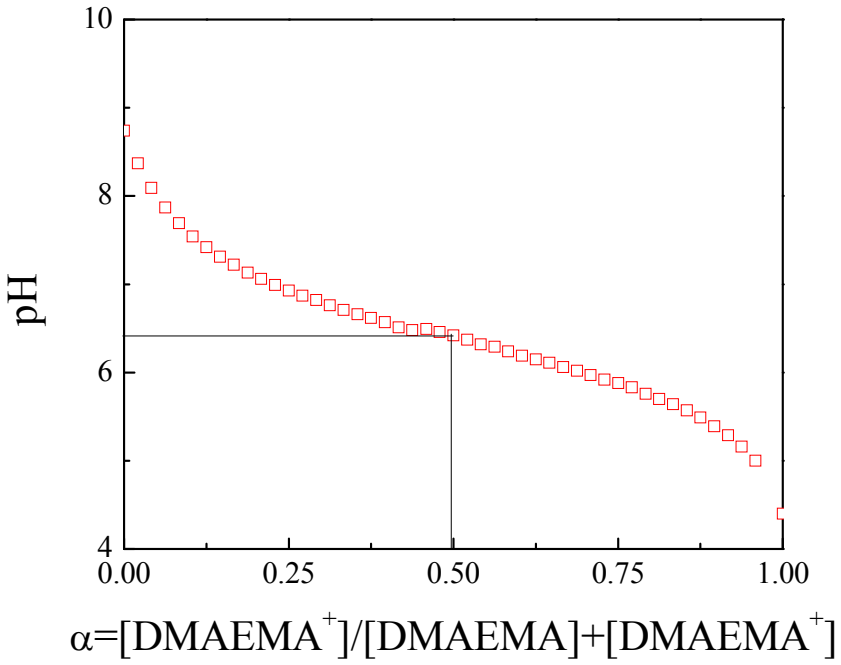

Figure 23. Solution pH versus degree of ionization for g11c80

Figure 23 shows the solution pH as a function of the degree of protonation in the range $0 < \alpha < 1$ for the hyperbranched g11c80 polymer. α approximates the degree of protonation assuming that all of the H^+ from the added HCl protonate the amine groups. The small change of the pH as a function of α is attributed to the buffering capacity of the polymer at this pH region. The effective pK_a of the polymer was calculated quite accurately from this plot as the pH of the polymer solution at a degree of ionization $\alpha = 0.5$ and was found 6.4. The pK_a values for all hypervranched PDMAEMA polymers prepared at c = 80 v/v % are listed in **Table 8**. Similar pK_a values were found for all polymers suggesting that the value pK_a is not affected by the ratio γ and thus the degree of branching of the polymer (At least in the range of the ratios γ investigated in the present study). In addition, the pK_a of DMAEMA monomer

is 8.5 and that of a linear PDMAEMA polymer is about 7.5 [99-101] suggesting that the branched polymer structure, has an effect on the ionization constant of the tertiary amino groups and hinders the ionization of the DMAEMA units.

Table 8. Effective pK_a values for the hyperbranched PDMAEMA polymers prepared at $c_{pol.}$= 80 v/v %

Sample	Effective pK_a
g11c80	6.4
g26c80	6.5
g41c80	6.2
g60c80	6.4
g80c80	6.4

3.7.2 Temperature responsive behaviour of the hyperbranched PDMAEMA copolymers

The temperature responsive behaviour of the hyperbranched PDMAEMAs was investigated by measuring the hydrodynamic size of the polymers as a function of solution temperature in aqueous media. **Figure 24** shows the autocorrelation functions for g80c20 at c= 0.4 wt % in water at different scattering angles and T = 20 ^{o}C.

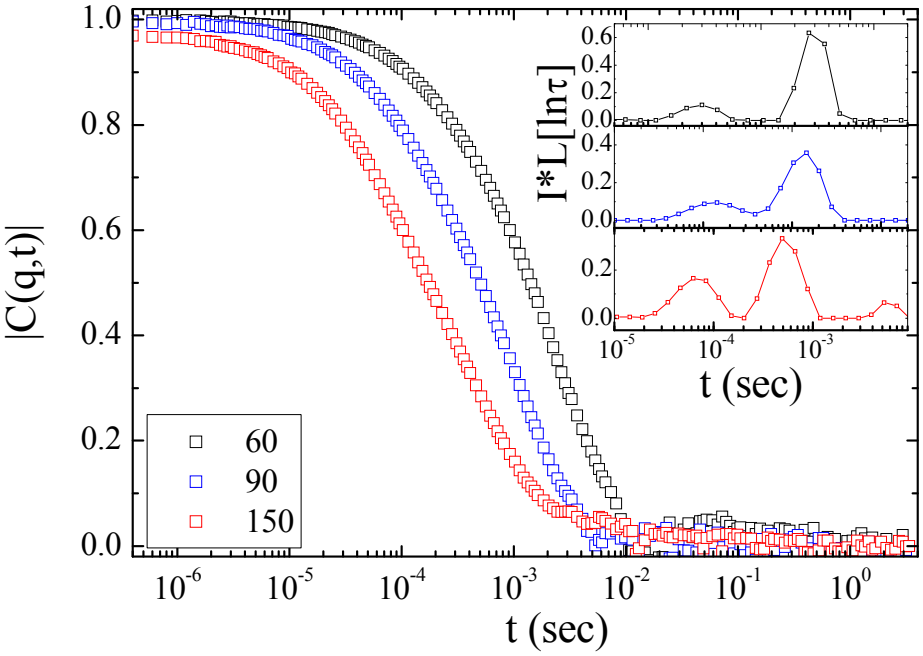

Figure 24. Intensity autocorrelation functions for g80c20 at c = 0.4 wt % in water and T = 20 °C for scattering angles 60° (□), 90° (□) and 150° (□). Inset: distribution of relaxation times multiplied by the total scattering intensity (normalized to that of toluene).

From the analysis of the autocorrelation functions two processes were found. The first process with a hydrodynamic radius R_{h1} = 11 nm (fast process) is attributed to the hyperbranched polymer, while the second process with a hydrodynamic radius of R_{h2} = 106 nm (slow process) is attributed to the formation of aggregates similar to the results discussed above in THF. Note that in water the size of the polymer is twice that found in acetone. This may me attributed that water is a better solvent than acetone for the polymer. **Figure 25** shows hydrodynamic size for g41c20 as a function of solution temperature.

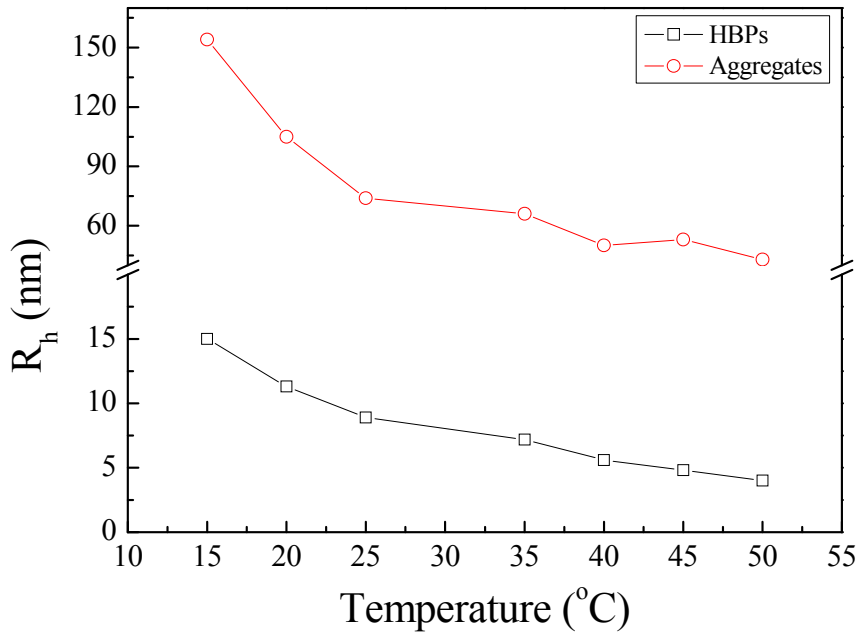

Figure 25. Hydrodynamic radius versus temperature of g41c20 at c = 0.1 w/w %.

As seen in **Figure 25** a pronounced drop of the hydrodynamic radius for both the HBP and the polymer aggregates is formed in the temperature range between 15 and 50 ^{o}C. The temperature increases the HBP gradually shrinks from $R_{h.}$ = 15 nm to 4 nm and the aggregates from $R_{h.}$ = 154 nm to 43 nm. This behaviour was attributed to the temperature sensitivity of PDMAEMA. At lower temperatures, the HBP is hydrophilic and water is a good solvent. As the temperature increases, the polymer-solvent interactions become unfavourable and the molecules collapse in the aqueous solution. At much higher temperatures (>40 ^{o}C) the hydrophobic polymer interactions dominate and macroscopic phase separation (precipitation) occurs.

3.8 Viscoelastic properties

The frequency dependences of G' and G" were presented as master curves superimposed on the frequency sweeps measured at various temperatures. Temperature dependences of the shift factors were, for all samples (linear and branched) in a good agreement with the WLF relation

$$\log(a_T) = C_1(T - T_{ref}) / \left[C_2 + (T - T_{ref})\right]$$

With parameters $C_1 \approx 8.2$ and $C_2 \approx 85$ °C at $T_{ref} = 60$ °C. **Figure 26** presents the dynamic viscoelastic properties (moduli) of linear PDMAEMA with molecular weight $M_n = 22.000$ gmol^{-1} at $T_{ref} = 60$ °C.

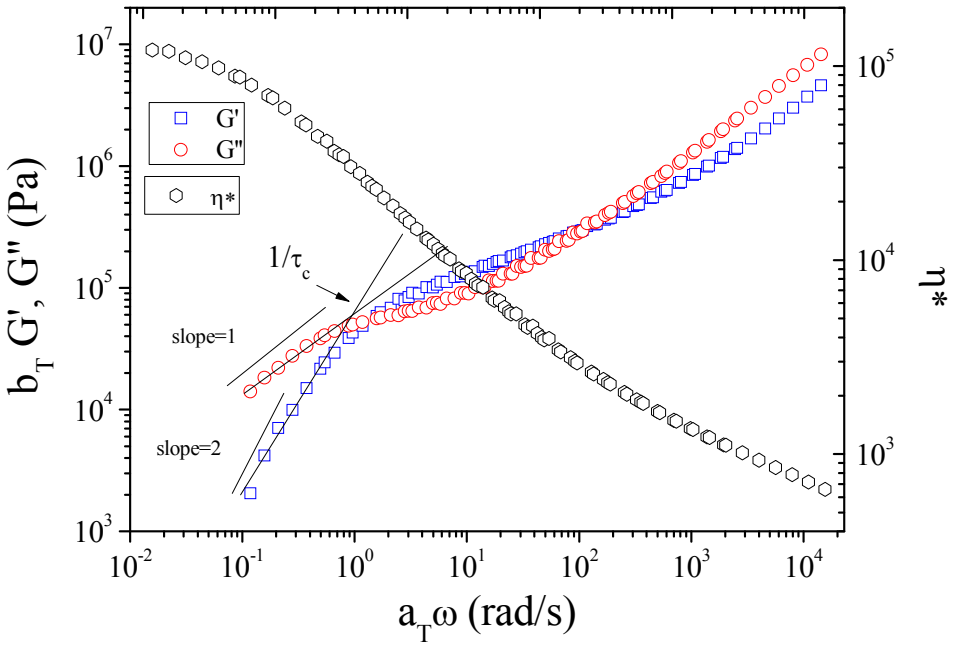

Figure 26. Storage and loss moduli G' (□) and G" (○), respectively, and complex viscosity of linear PDMAEMA M_n =22,000 gmol^{-1} as a function of shear frequency at a reference temperature of $T_{ref} = 60$ °C.

For the linear polymers the dependences in **Figure 26** indicate a chain relaxation process at low frequencies, which separates the rubbery plateau corresponding to the frequency range of internal relaxations of entangled chains from the chain flow regime. The longest relaxation time τ_c can be determined as the intersection of the G' and G" dependences (indicate by the solid lines) extrapolated from the low frequency range, where they reach the characteristics slopes 1 and 2 according to the scaling relationships $G' \approx \omega^2$ and $G'' \approx \omega^1$, respectively.

The entanglement molecular weight is calculated using Graessley – Fetters definition $M_e = (4/5)\rho RT/G_N^0$ where the plateau modulus G_N^0 was obtained from the frequency at which the loss tangent tanδ (tanδ = G"/G') is minimum

$G_N^0 = G'(\omega)_{\tan\delta_{min}}$ .The entanglement molecular weight for PDMAEMA from **Figure 26** was calculated M_e=14,000 $gmol^{-1}$.

The range of dynamic response of the hyperbranched polymers prepared at $c_{pol.}$ = 20 vv % is demonstrated in **Figures 27-30** which show the dynamic spectra for all samples. **Figure 27** presents the results for the sample of the lowest molecular weight, g26c20.

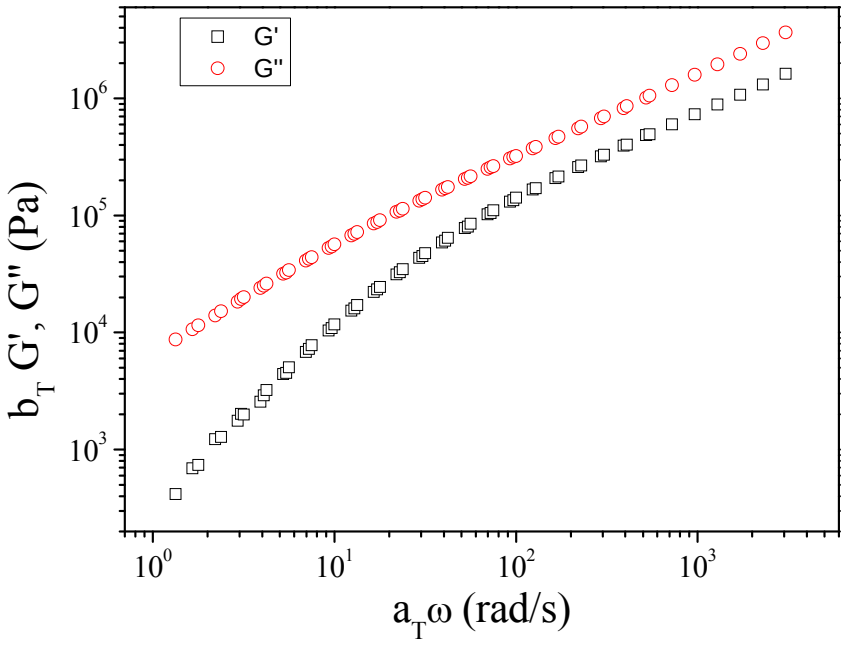

Figure 27. Dynamic spectra for sample g26c20 referenced to T = 60 °C

The dynamic storage modulus, G' is always lower than the loss modulus, G''. Such behaviour is characteristic of unentangled polymer chains. G' and G'' rise in parallel over two decades of frequency. The corresponding power-law exponents are 0.67 for G' and 0.69 for G''. This behaviour is referred as Zimm like with the slope predicted by the Zimm model to be 2/3, which is very close to the experimental value of 0.67. In the low-frequency region, a deviation from the terminal scaling is observed that is G'' ~ 0.94 and G' ~1.61. This terminal scaling behaviour has been also observed in rheological studies of other dendritic polymers [28, 102] as was attributed to very slow relaxation modes of the materials.

Figure 28 presents the dynamic spectra for g41c20.

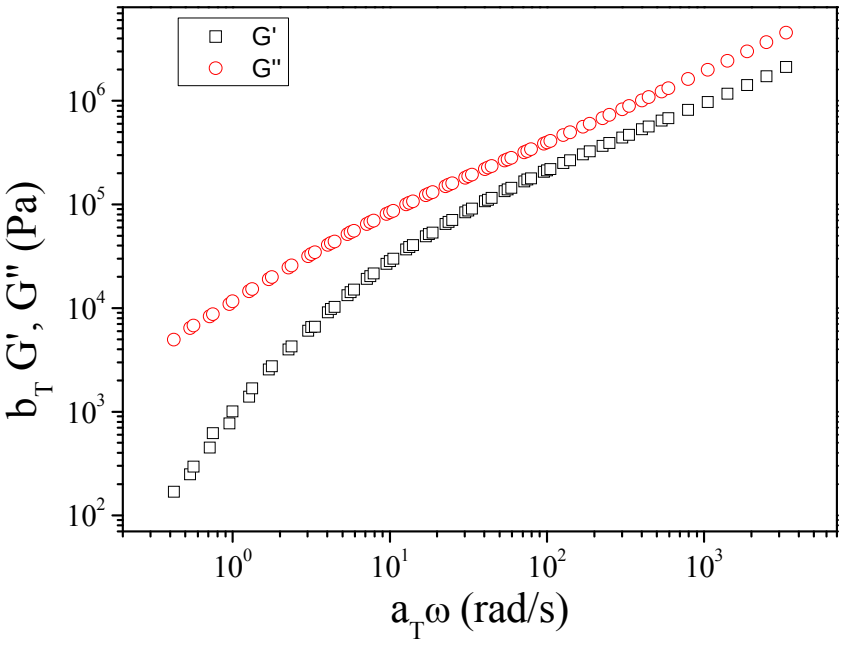

Figure 28. Dynamic spectra for sample g41c20 referenced to T = 60 °C

The dynamic spectra of g41c20 show a similar dynamic behavior to those for g26c20. In the medium frequency regime the corresponding power-law exponents are 0.66 for G' and 0.71 for G'', while at the terminal zone at low frequencies the characteristics slopes of 1 for G'' and 2 for G' are reached according to the scaling relationships $G' \propto \omega^2$ and $G'' \propto \omega^1$, respectively.

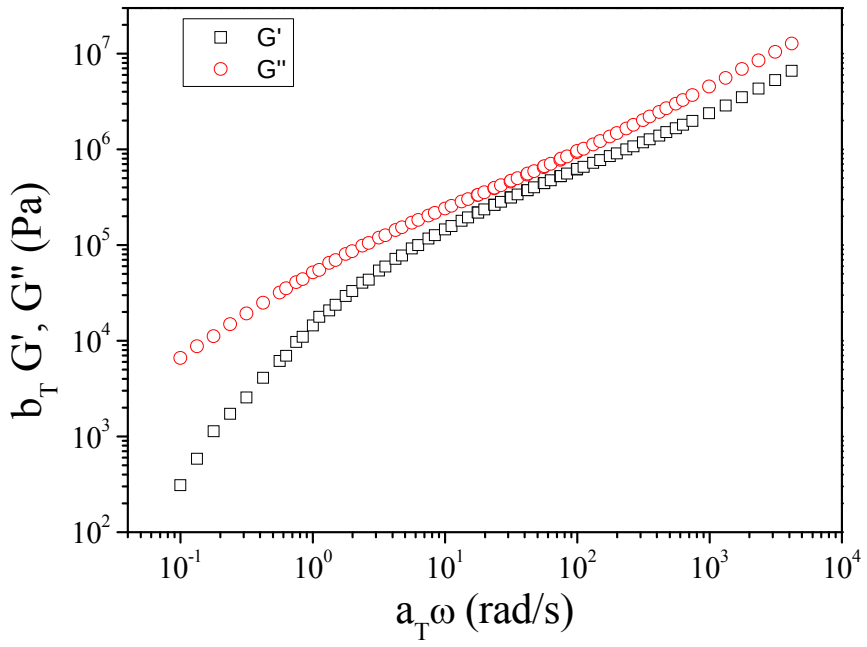

Figure 29. Dynamic spectra for sample g60c20 referenced to T = 60 ^oC

Figure 29 presents the dynamic moduli of g60c20. Again the dynamic storage modulus, G' is lower than the loss modulus, while G' and G" rise for more than 3 decades of frequency range in a nearly parallel fashion. In the medium frequency regime the power-law exponents are 0.66 for G' and 0.69 for G". Similarly, **Figure 30**, the dynamic spectra of g80c20 show. G' and G" modulis curves which rise parallel without crossing each other for 3 decades at frequency range with a characteristic slope of 0.69 for G' and G". The terminal zone at small frequencies has been reached with the characteristics slopes of 1 for G" and 2 for G'. Interestingly, in all cases the absence of a true rubbery plateau suggests that these materials are essentially unentangled despite having molecular weights significantly above the M_e for linear PDMAEMA. The apparent absence of such entanglements is attributed to the highly branched architecture of the polymers. The experimental power laws in the high frequencies for G' and G" were found to be in good agreement with the theory which predicts $G' \sim G'' \sim \omega^{0.66}$ [82, 83]. Moreover, while G' and G" rise in parallel in high frequencies for all samples, when the ratio γ increases the two curves approach each other suggesting that the average molecular weight between crosslinks increases with the ratio γ.

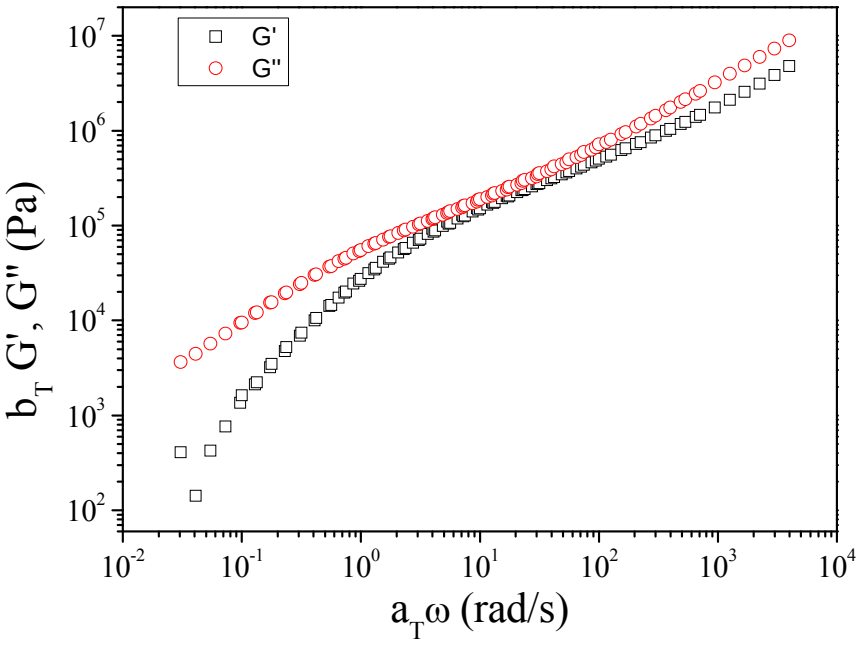

Figure 30. Dynamic spectra for sample g80c20 referenced to T = 60 ^oC

The results from the dynamic spectra for all samples are summarized in **Table 9**

Table 9. Characterization of the hyperbranched PDMAEMA prepared at $c_{pol.}$=20 v/v % by viscoelastic spectroscopy

sample	M_n	t_c(sec)[b]	G' & G" slopes[c]		η_o (Pas)[d]
g26c20	31,000	0.07	0.67	0.69	34,000
g41c20	70,000	0.44	0.66	0.71	60,000
g60c20	97,000	1.16	0.66	0.69	370,000
g80c20	88,700	2.17	0.69	0.69	700,000

[a] GPC universal calibration, [b] longest relaxation time, [c] slopes in the high frequency range, [d] zero shear viscosity calculated by the carreau viscosity model

The longest relaxation times increase from 0.07 to 2.17 sec while the zero shear viscosity increase from 34,000 to 700,000 Pas as the ratio γ increases. In **Figure 31**, the complex viscosity data are plotted against the frequency for all the hyperbranched

polymers and a linear PDMAEMA sample (Mn = 22,000 $gmol^{-1}$).

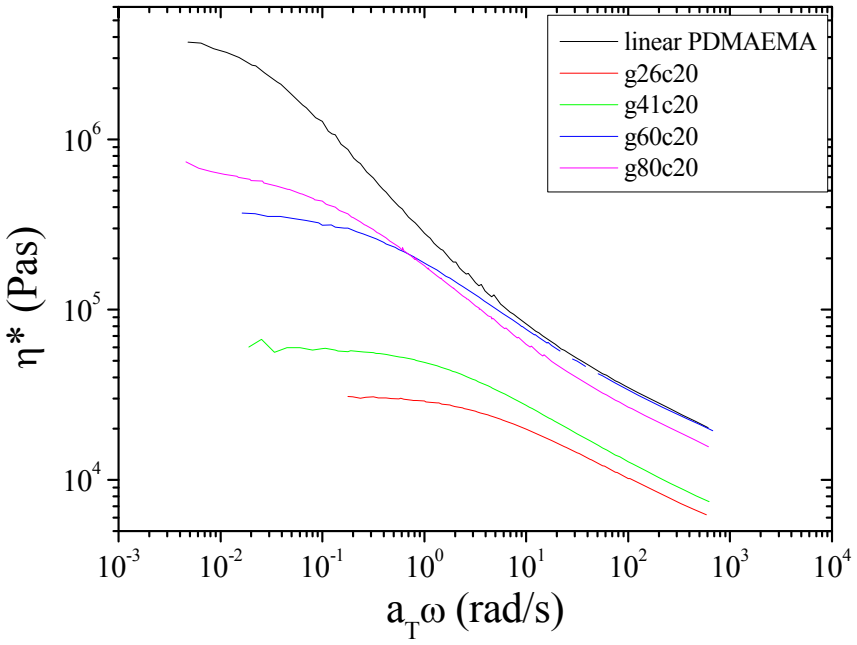

Figure 31. Complex viscosities as a function of frequency for the hyperbranched PDMAEMA copolymers prepared at c_{pol} = 20 v/v % at different comonomer ratios γ. The respective plot for a linear PDMAEMA is also shown for comparison.

As expected the complex viscosities increase with the ratio γ but always remain lower than that of linear PDMAEMA (M_n = 22,000 $gmol^{-1}$) due to the compact structure of the branched polymers. The increase of the complex viscosities follow the increase of the polymer molecular weight.

The dynamic scaling model of Rubinstein et al. [82, 83] was used to model the dynamic shear viscoelasticity of the hyperbranched polymers. Size exclusion chromatography was used to determinate of the number density of molecules n(M). Assuming that each elution time Vi corresponds to a single molar mass, the number of molecules $n(M_i)$ of molecular weight M_i is given by

$$n(M_i) = -\frac{M_o}{2.303(M_i)^2}\frac{c_i}{\sum_0^i c_i}\frac{dV_i}{d\log(M_i)}$$

Where c is the area under the DRI chromatograph and c_i/c is the weight fraction of polymer in the ith retention volume, V_i, and the derivative $dV_i/d\log(M_i)$ is obtained

from the GPC (Log(M) vs V) calibration curve. The number density of molecules using a simple exponential cut off for f, is calculated as

$$n(M) \approx M^{-\tau} \exp\left(-M/M_{char}\right)$$

Which allows the determination of the exponent τ and the largest characteristic molecular weight, $M_{char.}$ **Figure 32** illustrates the number density function for g26c20.

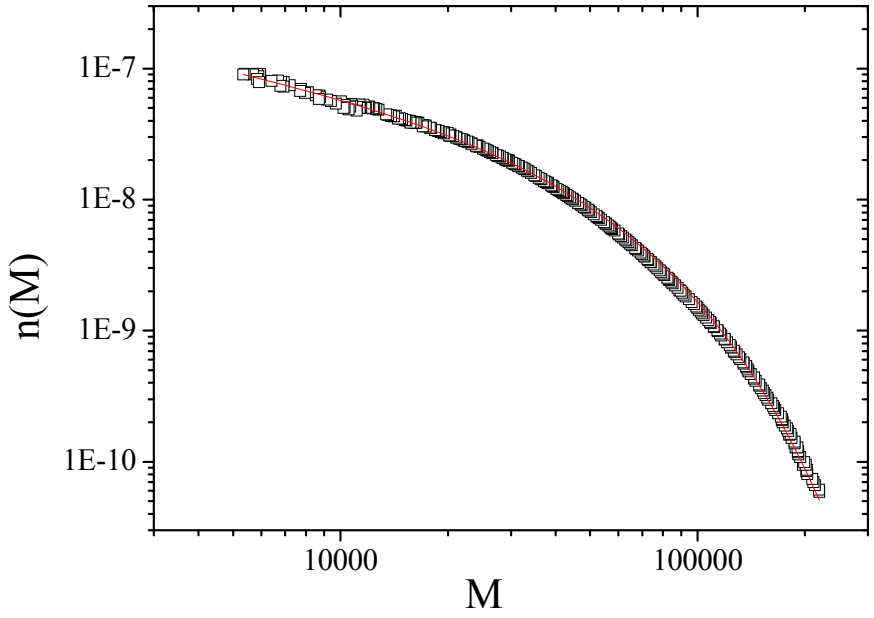

Figure 32. Molar mass distribution obtained for g26c20 from GPC in combination with a viscosity detector. The solid line represents the fit to the data using the equation for the number density of molecules.

The fitted values of M_{char} and τ using the fitting procedure discussed above were calculated for all the samples prepared at $c_{pol.}$ = 20 v/v % and are given in **Table 10**.

Table 10. Number density parameters for the hyperbranched PDMAEMA copolymers at $c_{pol.}$ = 20 v/v %

sample	τ	M_n	M_{char}
g26c20	1.59	31,000	88,500
g41c20	1.72	70,000	182,000
g60c20	1.75	97,000	265,000
γ80c20	1.71	88,700	264,000

The Fischer exponent for all samples was calculated at ~1.7 indicating that the polymers are below the gel point and have a branched structure. The results also agree with the scaling relationship $M_{char} \propto M_w$ thus establishing that the obtained values of M_{char} are reasonable. The above calculated parameters were used to fit the experimental data. The parameters related to the length between two branching points $\varepsilon_{x,}$ and the shear modulus $G_{0,}$ where calculated numerically. Normally, these parameters are used as adjustable parameters when the model is fitted to the experimental data, but in our case due to the complex solution of the model the fitting of the data was not possible.

Figure 33 presents the master curves with model fits for all samples.

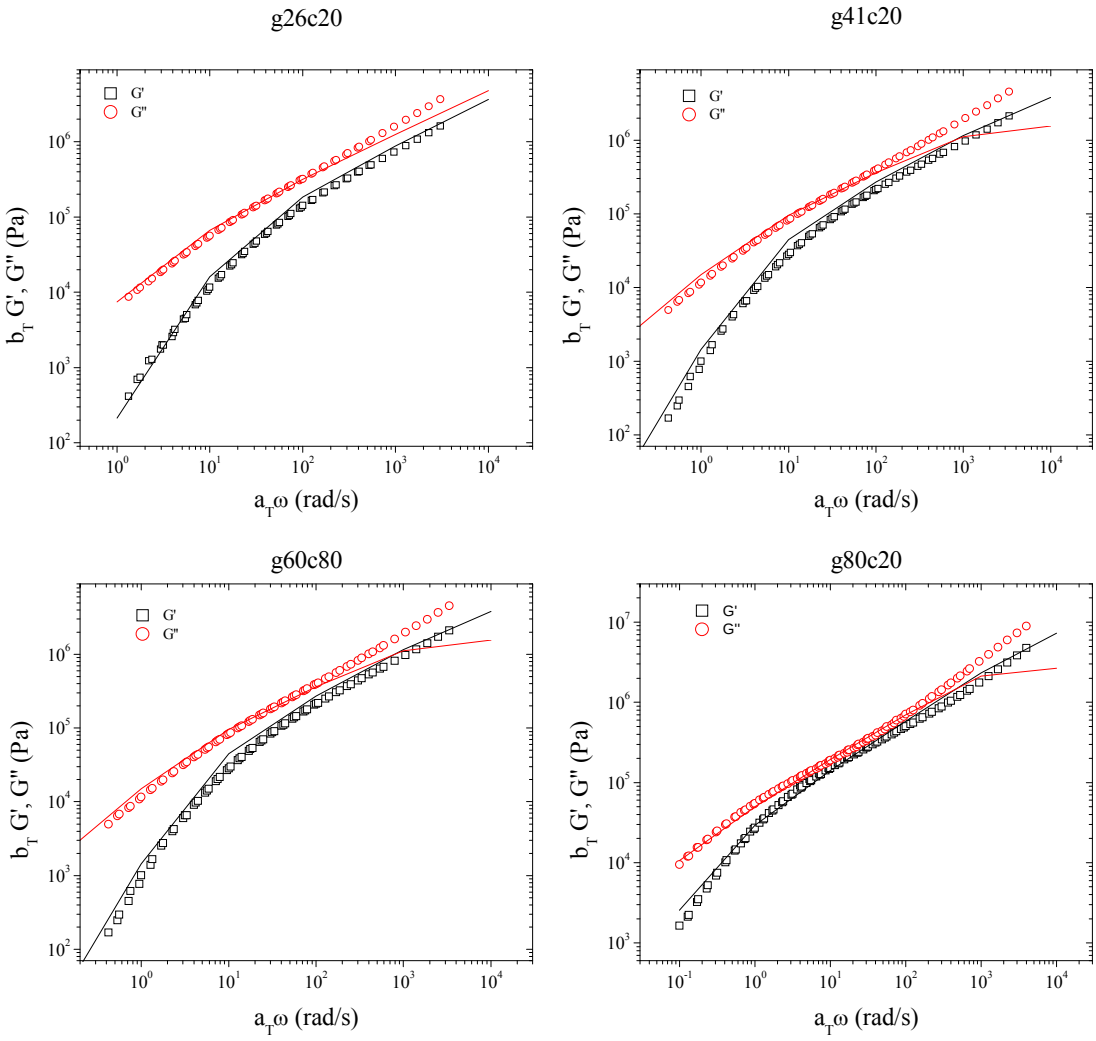

Figure 33. Storage and loss modulus against frequency for all samples. The symbols represent the experimental data points while the lines are the model fits to the data.

At high frequencies the response is not well predicted as seen in **Figure 33**. In the low frequencies there is reasonable agreement between theory and experiment. The best fit of the model to the experimental data could provide useful information about the number of monomers in a polymer strand between the crosslinks and could allow the determination of the degree of branching. This should be the aim of the future work of this study in order to complete the rheological characterization of these materials in the melt.

Chapter 4

Conclusions

Hyperbranched PDMAEMA copolymers of various molecular weights and degrees of branching were synthesized by SCVCP combined with group transfer polymerization. The copolymerization of the inimer MTSHEMA with DMAEMA as a comonomer at different monomer/inimer ratios led to hyperbranched copolymers. The Mark-Houwink exponents, for the hyperbranched copolymers were determined and suggested a dramatic decrease of the solution viscosity for the branched polymer structures. Addition of a monofunctional initiator, MTS, resulted in a decrease of polymer molecular weight, and a narrower molecular weight distribution compared to those obtained in the absence of initiator. Moreover, higher molecular weights and broader molecular weight distributions were obtained as the monomer concentration of the polymerization increased. Finally, the addition of a second monomer TMSHEMA, to a living hyperbranched DMAEMA precursor yielded a densely packed hyperstar structure as revealed by the corresponding Mark-Houwink plots. Capillary viscosity measurements revealed a polyelectrolyte behavior, characterized by a sharp increase of the reduced viscosity at low polymer concentration for all polymers. The pK_a 's were determined by potentiometric titration curves and were found to be lower than that of a linear PDMAEMA homopolymer, however they were not affected by the ratio γ. The hydrodynamic radii of the HBPs were determined in organic media by DLS increased monotonously with the polymer molecular weight, while the presence of polymer aggregates were found in certain solvents i.e. THF. The LSCT of the hyperbranched PDMAEMAs were determined by DLS and was found in the range 15 to 50 ^{o}C. The dynamic rheology spectra of the hyperbranched polymers in the melt revealed the absence of a rubbery plateau for all samples which indicates the lack of chains entanglements. This was attributed to the highly branched structure of the polymers. The parallel scaling of G' and G" in the intermediate frequency regime was found for all samples and was found to be less separated as the ratio γ increased which led to the assumption that the molecular weight of the strands between the crosslinks increased with γ. The complex viscosities of the hyperbranched polymers were found to be lower compared to those of a linear

analogue, due of the compact structure of the hyperbranched polymers. Also the complex viscosities were found to increase with the ratio γ, this led to the assumption that the conformation of the hyperbranched polymers in solution is affected by the polymer-solvent and polymer-polymer interactions which can not be fully characterized. Finally, the rheological data at low and intermediate frequencies could be modeled using a dynamic scaling theory based on the Rouse model which would provide useful information fort the branched polymer structure.

References

1. Frechet, J.M., *Functional polymers and dendrimers: reactivity, molecular architecture, and interfacial energy*. 1994. p. 1710-1715.
2. Gao, C.Yan, D., *Hyperbranched polymers: From synthesis to applications.* Progress in Polymer Science (Oxford), 2004. **29**(3): p. 183-275.
3. Jikei, M.Kakimoto, M., *Hyperbranched polymers: a promising new class of materials.* Progress in Polymer Science, 2001. **26**(8): p. 1233-1285.
4. Tomalia, D.A.Dvornic, P.R., *What promise for dendrimers?* Nature, 1994. **372**(6507): p. 617-618.
5. Roovers, J., *Encyclopedia of Polymer Science and Engineering*, ed. Wiley. Vol. 2. 1985, New York.
6. Bywater, S., *preparation and properties of star-branched polymers.* Advances in Polymer Science, 1979(30): p. 89-116.
7. Mark, J.E., *Physical Properties of Polymers* ed. 2nd. 1993, Washington, D.C: American Chemical Society.
8. Flory, P.J., *Principles of Polymer Chemistry*. 1953, New York: Cornell University Press.
9. Tomalia, D.A., Baker, H., Dewald, J., Hall, M., Kallos, G., Martin, S., Roeck, J., Ryder, J.Smith, P., *Dendritic macromolecules: Synthesis of starburst dendrimers.* Macromolecules, 1986. **19**(9): p. 2466-2468.
10. Tomalia, D.A., Baker, H., Dewald, J., Hall, M., Kallos, G., Martin, S., Roeck, J., Ryder, J.Smith, P., *A new class of polymers: Starburst-dendritic macromolecules.* Polymer Journal, 2002. **34**(5 2): p. 132-147.
11. Dusek, K., Duskova-Smrckova, M.Voit, B., *Highly-branched off-stoichiometric functional polymers as polymer networks precursors.* Polymer, 2005. **46**(12): p. 4265-4282.
12. Voit, B., *New developments in hyperbranched polymers.* Journal of Polymer Science, Part A: Polymer Chemistry, 2000. **38**(14): p. 2505-2525.
13. Voit, B., *Hyperbranched polymers - All problems solved after 15 years of research?* Journal of Polymer Science, Part A: Polymer Chemistry, 2005. **43**(13): p. 2679-2699.

14. Yoon, K.Son, D.Y., *Syntheses of hyperbranched poly(carbosilarylenes).* Macromolecules, 1999. **32**(16): p. 5210-5216.
15. Miravet, J.F.Frechet, J.M.J., *New hyperbranched poly(siloxysilanes): Variation of the branching pattern and end-functionalization.* Macromolecules, 1998. **31**(11): p. 3461-3468.
16. Dusek, K., Somvarsky, J., Smrckova, M., Simonsick Jr, W.J.Wilczek, L., *Role of cyclization in the degree-of-polymerization distribution of hyperbranched polymers: Modelling and experiments.* Polymer Bulletin, 1999. **42**(4): p. 489-496.
17. Suzuki, M., Ii, A.Saegusa, T., *Multibranching polymerization: Palladium-catalyzed ring-opening polymerization of cyclic carbamate to produce hyperbranched dendritic polyamine.* Macromolecules, 1992. **25**(25): p. 7071-7072.
18. Huber, T., Bohme, F., Komber, H., Kronek, J., Luston, J., Voigt, D.Voit, B., *New hyperbranched poly(ether amide)s via nucleophilic ring opening of 2-oxazoline-containing monomers.* Macromolecular Chemistry and Physics, 1999. **200**(1): p. 126-133.
19. Bednarek, M., Biedron, T., Helinski, J., Kaluzynski, K., Kubisa, P.Penczek, S., *Branched polyether with multiple primary hydroxyl groups: Polymerization of 3-ethyl-3-hydroxymethyloxetane.* Macromolecular Rapid Communications, 1999. **20**(7): p. 369-372.
20. Magnusson, H., Malmstrem, E.Hult, A., *Synthesis of hyperbranched aliphatic polyethers via cationic ring-opening polymerization of 3-ethyl-3-(hydroxymethyl)oxetane.* Macromolecular Rapid Communications, 1999. **20**(8): p. 453-457.
21. Liu, M., Vladimirov, N.Frechet, J.M.J., *A new approach to hyperbranched polymers by ring-opening polymerization of an AB monomer: 4-(2-Hydroxyethyl)-e-caprolactone.* Macromolecules, 1999. **32**(20): p. 6881-6884.
22. Frechet, J.M.J., Henmi, M., Gitsov, I., Aoshima, S., Leduc, M.R.Grubbs, R.B., *Self-condensing vinyl polymerization: An approach to dendritic materials.* Science, 1995. **269**(5227): p. 1080-1083.
23. Flory, P.J., *Molecular Size Distribution in Three Dimensional Polymers. VI. Branched Polymers Containing A—R—B_{f-1} Type Units.* Journal of the American Chemical Society, 1952. **74**(11): p. 2718-2723.

24. Hawker, C.J., Frechet, J.M.J., Grubbs, R.B.Dao, J., *Preparation of Hyperbranched and Star Polymers by a "Living", Self-Condensing Free Radical Polymerization.* Journal of the American Chemical Society, 1995. **117**(43): p. 10763-10764.
25. Gaynor, S.G., Edelman, S.Matyjaszewski, K., *Synthesis of Branched and Hyperbranched Polystyrenes.* Macromolecules, 1996. **29**(3): p. 1079-1081.
26. Krzysztof, M., Jeffrey, P.Scott, G.G., *Preparation of hyperbranched polyacrylates by atom transfer radical polymerization, 4. The use of zero-valent copper*. 1998. p. 665-670.
27. Matyjaszewski, K., Gaynor, S.G., Kulfan, A.Podwika, M., *Preparation of Hyperbranched Polyacrylates by Atom Transfer Radical Polymerization. 1. Acrylic AB* Monomers in "Living" Radical Polymerizations.* Macromolecules, 1997. **30**(17): p. 5192-5194.
28. Simon, P.F.W.Muller, A.H.E., *Synthesis of Hyperbranched and Highly Branched Methacrylates by Self-Condensing Group Transfer Copolymerization.* Macromolecules, 2001. **34**(18): p. 6206-6213.
29. Webster, O.W., *Living polymerization methods.* Science, 1991. **251**(4996): p. 887-893.
30. Webster, O.W., *Discovery and commercialization of group transfer polymerization.* Journal of Polymer Science, Part A: Polymer Chemistry, 2000. **38**(16): p. 2855-2860.
31. Webster, O.W., *Group transfer polymerization: Mechanism and comparison with other methods for controlled polymerization of acrylic monomers*, in *Advances in Polymer Science*. 2004. p. 1-34.
32. Webster, O.W., *Group Transfer Polymerization: A Critical Review of Its Mechanism and Comparison with Other Methods for Controlled Polymerization of Acrylic Monomers*, in *New Synthetic Methods*. 2004. p. 257-266.
33. Webster, O.W., Hertler, W.R., Sogah, D.Y., Farnham, W.B.RajanBabu, T.V. *group tranfer polymerization - addition polymerization with organosilicon iniators*. in *American Chemical Society, Polymer Preprints, Division of Polymer Chemistry*. 1983. Washington, DC, USA: ACS, Div of Polymer Chemistry.

34. Webster, O.W., Hertler, W.R., Sogah, D.Y., Farnham, W.B.RajanBabu, T.V., *Group-transfer polymerization. 1. A new concept for addition polymerization with organosilicon initiators.* Journal of the American Chemical Society, 1983. **105**(17): p. 5706-5708.
35. Cosulich, M.E., Russo, S., Pasquale, S.Mariani, A., *Performance evaluation of hyperbranched aramids as potential supports for protein immobilization.* Polymer, 2000. **41**(13): p. 4951-4956.
36. Kim, Y.H.Webster, O.W., *Hyperbranched polyphenylenes.* Macromolecules, 1992. **25**(21): p. 5561-5572.
37. Massa, D.J., Shriner, K.A., Turner, S.R.Voit, B.I., *Novel blends of hyperbranched polyesters and linear polymers.* Macromolecules, 1995. **28**(9): p. 3214-3220.
38. Schmaljohann, D., Potschke, P., Hassler, R., Voit, B.I., Froehling, P.E., Mostert, B.Loontjens, J.A., *Blends of amphiphilic, hyperbranched polyesters and different polyolefins.* Macromolecules, 1999. **32**(19): p. 6333-6339.
39. Eva, M., Mats, J.Anders, H., *The effect of terminal alkyl chains on hyperbranched polyesters based on 2,2-bis(hydroxymethyl)propionic acid*. 1996. p. 3199-3207.
40. Karthaus, O., Ijiro, K., Shimomura, M., Hellmann, J.Irie, M., *Monomolecular Layers of Diarylethene-Containing Dendrimers.* Langmuir, 1996. **12**(26): p. 6714-6716.
41. Sheiko, S.S., Muzafarov, A.M., Winkler, R.G., Getmanova, E.V., Eckert, G.Reineker, P., *Contact Angle Microscopy on a Carbosilane Dendrimer with Hydroxyl End Groups: Method for Mesoscopic Characterization of the Surface Structure.* Langmuir, 1997. **13**(15): p. 4172-4181.
42. Bar, G., Rubin, S., Cutts, R.W., Taylor, T.N.Zawodzinski, T.A., *Dendrimer-Modified Silicon Oxide Surfaces as Platforms for the Deposition of Gold and Silver Colloid Monolayers:β€‰ Preparation Method, Characterization, and Correlation between Microstructure and Optical Properties.* Langmuir, 1996. **12**(5): p. 1172-1179.
43. Takashi, S.Takehisa, M., *Synthesis and photochemical surface fixation of hydroxylated cascade molecules*. 1997. p. 137-142.
44. Takada, K., Diaz, D.J., Abruna, H.D., Cuadrado, I., Casado, C., Alonso, B., Moran, M.Losada, J., *Redox-Active Ferrocenyl Dendrimers: Thermodynamics*

and Kinetics of Adsorption, In-Situ Electrochemical Quartz Crystal Microbalance Study of the Redox Process and Tapping Mode AFM Imaging. Journal of the American Chemical Society, 1997. **119**(44): p. 10763-10773.

45. Mueller, A., Kowalewski, T.Wooley, K.L., *Synthesis, Characterization, and Derivatization of Hyperbranched Polyfluorinated Polymers.* Macromolecules, 1998. **31**(3): p. 776-786.
46. Aoki, A., Ghosh, P.Crooks, R.M., *Micrometer-Scale Patterning of Multiple Dyes on Hyperbranched Polymer Thin Films Using Photoacid-Based Lithography*. Langmuir, 1999. **15**(22): p. 7418-7421.
47. Lackowski, W.M., Franchina, J.G., Bergbreiter, D.E.Crooks, R.M., *An Atomic Force Microscopy Study of the Surface Morphology of Hyperbranched Poly(acrylic acid) Thin Films*. 1999. p. 1368-1371.
48. Yates, C.R.Hayes, W., *Synthesis and applications of hyperbranched polymers.* European Polymer Journal, 2004. **40**(7): p. 1257-1281.
49. Lange, J., Stenroos, E., Johansson, M.Malmström, E., *Barrier coatings for flexible packaging based on hyperbranched resins.* Polymer, 2001. **42**(17): p. 7403-7410.
50. Dicker, I.B., Cohen, G.M., Farnham, W.B., Hertler, W.R., Laganis, E.D.Sogah, D.Y., *Oxyanions catalyze group-transfer polymerization to give living polymers.* Macromolecules, 1990. **23**(18): p. 4034-4041.
51. Ojima, I., Kumagai, M.Nagai, Y., *Hydrosilylation of a,β-unsaturated nitriles and esters catalyzed by tris (triphenylphosphine)chlororhodium.* Journal of Organometallic Chemistry, 1976. **111**(1): p. 43-60.
52. Grubisic, Z., Rempp, P.Benoit, H., *A universal calibration for gel permeation chromatography.* J. Polym. Sci., Polym. Lett, 1967. **5**(9): p. 753-759.
53. Sanayei, R.A., Pang, S.Rudin, A., *A new approach to establishing universal calibration curves for size exclusion chromatography.* Polymer, 1993. **34**(11): p. 2320-2323.
54. Sanayei, R.A., Suddaby, K.G., Rudin, A.O'Driscoll, K.F. *Novel method of data interpretation in SEC-viscometry analysis*. in *Polymeric Materials Science and Engineering, Proceedings of the ACS Division of Polymeric Materials Science and Engineering*. 1993.
55. Billmeyer, F.W., *Textbook of Polymer Science*. 3 ed. 1984, New York: Wiley.
56. Hiemenz, P.C., *Polymer Chemistry: The Basic Concepts*. 1984.

57. Porath, J.Flodin, P., *Gel Filtration: A method for desalting and group separation.* Nature, 1959. **183**(4676): p. 1657-1659.
58. Moore, J.C., *Gel permeation chromatography. I. A new method for molecular weight distribution of high polymers*. 1964. p. 835-843.
59. Benoit, H., Grubisic, Z., Rempp, P., Decker, D.Zilliox, J.G., J. Chim. Phys., 1966. **63**.
60. Shim, Y.-H., Bougard, F., Coulembier, O., Lazzaroni, R.Dubois, P., *Synthesis and characterization of original 2-(dimethylamino)ethyl methacrylate/poly(ethyleneglycol) star-copolymers.* European Polymer Journal, 2008. **44**(11): p. 3715-3723.
61. Tanford, C., *Physical Chemistry of Macromolecules*. 1961, New York: John Wiley & Sons.
62. Kaye, W., *Low angle laser light scattering-particle measurement.* Journal of Colloid And Interface Science, 1973. **44**(2): p. 384-386.
63. Jordan, R.C., J. Liquid Chromatogr., 1980. **3**(3): p. 439-463.
64. McConnell, M.L., Am. Lab., 1978. **10**(5).
65. Baines, F.L., Billingham, N.C.Armes, S.P., *Synthesis and Solution Properties of Water-Soluble Hydrophilic-Hydrophobic Block Copolymers.* Macromolecules, 1996. **29**(10): p. 3416-3420.
66. Creutz, S., Teyssie, P.Jerome, R., *Living Anionic Homopolymerization and Block Copolymerization of (Dimethylamino)ethyl Methacrylate.* Macromolecules, 1997. **30**(1): p. 6-9.
67. Zeng, F., Shen, Y., Zhu, S.Pelton, R., *Synthesis and Characterization of Comb-Branched Polyelectrolytes. 1. Preparation of Cationic Macromonomer of 2-(Dimethylamino)ethyl Methacrylate by Atom Transfer Radical Polymerization.* Macromolecules, 2000. **33**(5): p. 1628-1635.
68. Muthukumar, M., *Dynamics of polymeric fractals*. 1985, AIP. p. 3161-3168.
69. Rayleigh, L., Philos. Mag., 1871. **41**(4).
70. Rayleigh, L., Philos. Mag., 1881. **12**(5).
71. Einstein, A., Ann. Phys., 1910. **33**.
72. Smoluchowski, M., Ann. Phys., 1908. **33**.
73. Smoluchowski, M., Philos. Mag., 1912. **23**(6).
74. Debye, P., *Light scattering in solutions.* Journal of Applied Physics, 1944. **15**(4): p. 338-342.

75. Debye, P., *The Collected Papers of P. Debye*. 1954, New York: Wiley-Inter science.
76. Berne, B.Pecora, R., *Dynamic Light Scattering,*. 1976, New York: Wiley Interscience Pupblications.
77. D. Mclntyre, F.G., *Light Scattering from Dilute Polymer Solutions*. 1964, New York: Gordon and Breach.
78. Huggins, M.L., *The Viscosity of Dilute Solutions of Long-Chain Molecules. IV. Dependence on Concentration.* Journal of the American Chemical Society, 1942. **64**(11): p. 2716-2718.
79. Schmitz, K.S., *Dynamic Light Scattering by Macromolecules*. 1990, London: Academic Press.
80. Provencher, S.W., *CONTIN: A general purpose constrained regularization program for inverting noisy linear algebraic and integral equations.* Computer Physics Communications, 1982. **27**(3): p. 229-242.
81. Provencher, S.W., *A constrained regularization method for inverting data represented by linear algebraic or integral equations.* Computer Physics Communications, 1982. **27**(3): p. 213-227.
82. Rubinstein, M.Colby, R.H., *Polymer Physics*. 2003: Oxford University Press.
83. Rubinstein, M., Colby, R.H.Gillmor, J.R. *Dynamic scaling for polymer gelation*. in *American Chemical Society, Polymer Preprints, Division of Polymer Chemistry*. 1989.
84. Simon, P.F.W., Radke, W.Müller, A.H.E., *Hyperbranched methacrylates by self-condensing group transfer polymerization.* Macromolecular Rapid Communications, 1997. **18**(9): p. 865-873.
85. Mori, H., Seng, D.C., Lechner, H., Zhang, M.Muller, A.H.E., *Synthesis and Characterization of Branched Polyelectrolytes. 1. Preparation of Hyperbranched Poly(acrylic acid) via Self-Condensing Atom Transfer Radical Copolymerization.* Macromolecules, 2002. **35**(25): p. 9270-9281.
86. Mori, H., Walther, A., Andre, X., Lanzendorfer, M.G.Muller, A.H.E., *Synthesis of Highly Branched Cationic Polyelectrolytes via Self-Condensing Atom Transfer Radical Copolymerization with 2-(Diethylamino)ethyl Methacrylate.* Macromolecules, 2004. **37**(6): p. 2054-2066.

87. Bütün, V., Armes, S.P.Billingham, N.C., *Synthesis and aqueous solution properties of near-monodisperse tertiary amine methacrylate homopolymers and diblock copolymers.* Polymer, 2001. **42**(14): p. 5993-6008.

88. Lee, A.S., Gast, A.P., Butun, V.Armes, S.P., *Characterizing the Structure of pH Dependent Polyelectrolyte Block Copolymer Micelles.* Macromolecules, 1999. **32**(13): p. 4302-4310.

89. Mourey, T.H., Turner, S.R., Rubinstein, M., Frechet, J.M.J., Hawker, C.J.Wooley, K.L., *Unique behavior of dendritic macromolecules: Intrinsic viscosity of polyether dendrimers.* Macromolecules, 1992. **25**(9): p. 2401-2406.

90. Turner, S.R., Voit, B.I.Mourey, T.H., *All-aromatic hyperbranched polyesters with phenol and acetate end groups: Synthesis and characterization.* Macromolecules, 1993. **26**(17): p. 4617-4623.

91. Turner, S.R., Walter, F., Voit, B.I.Mourey, T.H., *Hyperbranched Aromatic Polyesters with Carboxylic Acid Terminal Groups.* Macromolecules, 1994. **27**(6): p. 1611-1616.

92. Simon, P.F.W., Muller, A.H.E.Pakula, T., *Characterization of Highly Branched Poly(methyl methacrylate) by Solution Viscosity and Viscoelastic Spectroscopy.* Macromolecules, 2001. **34**(6): p. 1677-1684.

93. Podzimek, S.Vlcek, T., *Characterization of branched polymers by SEC coupled with a multiangle light scattering detector. II. Data processing and interpretation*. 2001. p. 454-460.

94. Rempp, P.Merril, E., *Polymer synthesis*, ed. 2nd. 1991: Basel: Huthig & Wepf.

95. Yamasaki, E.N.Patrickios, C.S., *Group transfer polymerization in the bulk: linear polymers and randomly cross-linked networks.* European Polymer Journal, 2003. **39**(3): p. 609-616.

96. Litvinenko, G.I.Muller, A.H.E., *Molecular Weight Averages and Degree of Branching in Self-Condensing Vinyl Copolymerization in the Presence of Multifunctional Initiators.* Macromolecules, 2002. **35**(12): p. 4577-4583.

97. Hara, M., *Polyelectrolytes (Science & Technology)*, ed. edition. 1992: CRC Press.

98. Ydens, I., Moins, S., Degıe, P.Dubois, P., *Solution properties of well-defined 2-(dimethylamino)ethyl methacrylate-based (co)polymers: A viscometric approach.* European Polymer Journal, 2005. **41**(7): p. 1502-1509.

99. Patrickios, C.S., Hertler, W.R., Abbott, N.L.Hatton, T.A., *Diblock, ABC triblock, and random methacrylic polyampholytes: synthesis by group transfer polymerization and solution behavior*. Macromolecules, 1994. **27**(4): p. 930-937.

100. Simmons, M.R., Yamasaki, E.N.Patrickios, C.S., *Cationic homopolymer model networks and star polymers: synthesis by group transfer polymerization and characterization of the aqueous degree of swelling*. Polymer, 2000. **41**(24): p. 8523-8529.

101. Simmons, M.R., Yamasaki, E.N.Patrickios, C.S., *Cationic Amphiphilic Model Networks: Synthesis by Group Transfer Polymerization and Characterization of the Degree of Swelling*. Macromolecules, 2000. **33**(8): p. 3176-3179.

102. Semen, B.K., Rangaramanujam, M.K., Jeff, J.C., Shivshankar, V.Gaddam, N.B., *Unusual contributions of molecular architecture to rheology and flow birefringence in hyperbranched polystyrene melts*. 2001. p. 2562-2571.